FUNGIBLE PARAMETER CONTOURS AND CONFIDENCE REGIONS IN STRUCTURAL EQUATION MODELS

Jolynn Pek

A dissertation submitted to the faculty of the University of North Carolina in partial fulfillment of the requirements for the degree of Doctor of Philosophy in the Department of Psychology of

Chapel Hill
2012

Approved by:

Daniel J. Bauer

Kenneth A. Bollen

Robert C. MacCallum

Keith Payne

David Thissen

ABSTRACT

JOLYNN PEK: Fungible Parameter Contours and Confidence Regions in
Structural Equation Models
(Under the direction of Robert C. MacCallum)

There are at least two kinds of uncertainty associated with parameter estimates when
statistical models are fit to sample data. The first kind of uncertainty is typically con-
veyed by confidence regions which provide a plausible range of values for population
parameters of interest. The second kind of uncertainty involves a sensitivity analysis
(Cook, 1986) with respect to model fit. Here, contours representing alternative so-
lutions for parameter estimates that are almost as good as the optimal estimates in
terms of model fit are obtained. Contours of these slightly suboptimal parameter val-
ues have been termed fungible weights or contours (Waller, 2008; Waller & Jones, 2009;
MacCallum, Browne & Lee, 2009). Although distinct from each other, confidence re-
gions and fungible contours communicate parameter uncertainty and are both com-
puted from the likelihood function. Given these commonalities, we set out to clarify
the relationship between confidence regions and fungible parameter contours by accom-
plishing three objectives.

First, we show that confidence regions and fungible parameter contours are an-
alytically related when both types of parameter uncertainty are unified under a gen-
eral perturbation framework. Second, we carried out a simulation study that confirms
the distinction between confidence regions and fungible parameter contours. Although
the magnitude of correlations among measured variables have an impact on these two
kinds of parameter uncertainty, confidence regions are primarily determined by sample
size while fungible parameter contours are determined primarily by model fit and, to a

much smaller extent, sampling variability. Third, we implemented a new computational procedure for obtaining confidence regions and fungible parameter contours associated with focal parameters by the profile likelihood method, which takes account of nuisance parameters. We conclude with directions for future research and end with a discussion of what applied researchers may gain from examining these two distinct kinds of parameter uncertainty.

To Mother

ACKNOWLEDGEMENTS

The dissertation would not have been possible without the help and support of the many kind people that surround me. First and foremost, I would like to thank my advisor, Bud MacCallum, for his nurturing encouragement and keen insight. Thank you for teaching me patience and perseverance, being an intellectual sounding board and an aspiration. I am also grateful to my committee members Dave Thissen, Ken Bollen, Keith Payne and Dan Bauer whose invaluable feedback and input challenged me to strengthen the work in terms of implementation and practical significance. Many thanks are due to the people who are the L. L. Thurstone Psychometric Laboratory for continuing in the culture of intellectual curiosity, collaborative support and camaraderie that provided an ideal environment for this work. Finally, I would like to thank my family for being there, always understanding and supportive.

TABLE OF CONTENTS

LIST OF TABLES

LIST OF FIGURES

Figure

Chapter 1

INTRODUCTION

A major goal of statistical modelling is to obtain parameter estimates that summarize regularity inherent in the data at hand. Such parameter estimates allow researchers to describe, understand, explain and predict complicated phenomena. Yet, parameter estimates carry different kinds of uncertainty which should be taken into account when these estimates are to be rigorously interpreted or applied.

One kind of uncertainty, due to sampling variability, is typically conveyed by confidence intervals or regions. Parameter estimates are only point estimates that are our best guess as to what the population parameter values truly are. With repeated sampling using replicate experiments or observations, a distribution of these point estimates may be empirically obtained. Without such replicate observations, assumptions regarding the distribution of these point estimates are made in order to construct confidence regions. Confidence regions provide a plausible range of values for the population parameters of interest. A confidence interval is constructed for a single parameter whereas a confidence region is constructed for more than one parameter. For example, a 95% confidence region denotes the range of parameter estimates which are expected to capture the true population value 95% of the time over repeated sampling. Stated differently, confidence regions convey how much statistical variation is inherent in the parameter estimates. Tight confidence regions communicate small sampling variability and little uncertainty or high precision in parameter estimates. With small sampling variability, parameter estimates obtained from another sample from the same population will not differ appreciably from the original estimates. Hence, tight confidence

regions promote cross-validation. Clearly, strong scientific conclusions require small sampling variability (Green, 1977).

A second kind of uncertainty associated with parameter estimates may be investigated via a sensitivity analysis (Cook, 1986). Sensitivity analysis involves introducing practically insignificant changes to modelling conditions and assessing their effects on study results. One form of sensitivity analysis examines the relationship between parameter estimates and model fit. Specifically, parameter uncertainty is investigated with respect to small perturbations introduced to model fit. Given a slightly suboptimal model fit, alternative solutions for parameter estimates may be obtained. Such alternative parameter values have been called exchangeable or "fungible" in that each set is associated with the same suboptimal model fit (Waller, 2008; Waller & Jones 2009). When a single parameter is involved, two fungible values are obtained. When more than one parameter is concerned, an infinite number of alternative solutions may be obtained. Uncertainty is couched as the degree of variation across different combinations of parameter values that give practically the same, albeit slightly worse, model fit as the unique optimal solution. Stated differently, fungible parameter contours convey information on parameter variation, given a slightly suboptimal model fit. If the size of parameter values change radically under a minute perturbation to model fit, such parameter values provide a weak basis for scientific conclusions.

The objective of computing fungible parameter values is to determine whether parameter variation, under a practically insignificant change to model fit, is tolerable. Stated differently, the goal of such a sensitivity analysis is to ensure that parameter estimates are robust to a minute change in model fit. Fungible parameter values in linear regression models have been studied by Waller (2008) and Waller and Jones (2009), building upon the work regarding the study of parameter sensitivity (Green, 1977; Wainer, 1976, 1978; Rozeboom, 1979; Koopman, 1988; Dana & Dawes, 2004). More recently, the study of fungible parameter values was extended to the more general frame-

work of structural equation models (SEMs) of which linear regression is a special case (MacCallum, Browne, & Lee, 2009). Indeed, the developments by these researchers are generalizable to virtually any statistical model.

Both tight confidence regions and tight fungible parameter contours promote strong scientific conclusions. Under maximum likelihood (ML) estimation, confidence regions or bounds and fungible contours are both based on the likelihood function which carries information regarding uncertainty associated with parameter estimates. While these two kinds of parameter uncertainty are distinct, these commonalities raise a need for clarification regarding the relationship between confidence regions and fungible contours. As such, there are three objectives of the study. First, we will examine the analytical relationship between confidence regions and fungible contours in the context of SEMs. Second, we propose to develop computational methods to obtain likelihood-based confidence regions and fungible parameter contours for more than one parameter. Third, an investigation is conducted on how these two kinds of uncertainty are influenced by aspects of the data and model. The following is an overview of the study.

To begin, conceptual definitions of confidence regions and fungible contours in SEM are provided to facilitate the development of analytical relationships between these two kinds of parameter uncertainty. First, we will review the SEM and ML estimation of model parameters. The theoretical construction of likelihood-based confidence intervals and regions is then described, followed by the analogous construction of fungible parameter values. This theoretical overview is followed by a brief review of existing computational methods to estimating likelihood-based confidence intervals, and then a description of the method used by MacCallum, Browne and Lee (2009) to compute fungible parameter values. Finally, a general theoretical framework for understanding these two kinds of uncertainty is laid out. It is noted that this framework is a generalization of the work of MacCallum, Browne and Lee (2009) in obtaining fungible

parameter values. Under this general theoretical framework, we will establish conditions under which confidence regions and fungible parameter contours are numerically identical, and summarize the similarities and differences between confidence regions and fungible contours.

Practical issues concerning the estimation of confidence regions and fungible contours are also discussed. In particular, computational difficulties arise when the number of parameters involved in computations is not small. Typically, analysts are interested in a small number of focal parameters and treat the remaining non-focal parameters as nuisance parameters. We will review several approaches to dealing with nuisance parameters and focus on the estimated likelihood and profile likelihood methods to address the presence of nuisance parameters. We will then describe a root finding algorithm (Brent, 1973) to obtaining confidence regions and fungible parameter contours from both the estimated likelihood and the profile likelihood. An empirical example based on published data (Schmitt, Branscombe, Kobrynowicz, & Owen, 2002) is used to demonstrate this computational method as well as illustrate the relationship between confidence regions and fungible parameter contours.

Next, we explore conditions and factors which influence the size of confidence regions and fungible contours with simulated data. Specifically, the effect of sample size, magnitude of correlations among the measured variables, and model fit are examined. Additionally, we examine two different perturbation schemes for obtaining fungible parameter contours. For this simulation, computations are generally carried out on the profile likelihood. However, for comparison, confidence regions and fungible parameter contours will also be obtained from the empirical likelihood in targeted study cells. Finally, we end with a discussion on the properties and behavior of these two kinds of uncertainty associated with parameter estimates, comment on the advantage of basing computations on the profile likelihood, and suggest future directions for research.

4

1.1 Structural Equation Models and Maximum Likelihood Estimation

To set the framework and establish notation, we first review the structural equation model (SEM) and maximum likelihood (ML) estimation of these model parameters. Structural equation models are multi-parameter models involving a hypothesized network of directional and non-directional relationships among sets of measured and latent variables (MVs and LVs). The $p \times p$ population covariance matrix of the MVs is typically denoted by $\boldsymbol{\Sigma}$ and the model implied $k \times 1$ vector of parameters is denoted by $\boldsymbol{\theta}$. We will focus on covariance structure models, although our developments may be extended to model mean structures. The SEM is simply expressed as $\boldsymbol{\Sigma} = \boldsymbol{\Sigma}(\boldsymbol{\theta})$, implying that the population covariance matrix for the MVs is a function of the model parameters. Parameter estimates $\hat{\boldsymbol{\theta}}$ are computationally obtained by minimizing the discrepancy between the model implied population matrix $\boldsymbol{\Sigma}(\boldsymbol{\theta})$ and the sample covariance matrix $\mathbf{S}$.

There are many discrepancy functions for obtaining SEM parameter estimates such as the generalized least squares (GLS) and the asymptotically distribution free (ADF; Browne, 1984) approaches. However, the method of ML is the most commonly used technique. The multivariate normal likelihood function $L(\boldsymbol{\theta})$ to be maximized is defined by the specified model parameters $\boldsymbol{\theta}$ and the data at hand. Note that $L(\boldsymbol{\theta})$ is a nonlinear expression of $\boldsymbol{\Sigma}(\boldsymbol{\theta})$. In practice, a monotonic transformation of the multivariate normal likelihood function $L(\boldsymbol{\theta})$, known as the ML discrepancy function F, is optimized to obtain $\hat{\boldsymbol{\theta}}$. Maximizing $L(\boldsymbol{\theta})$ is equivalent to minimizing F. The ML discrepancy function is

$$F(\boldsymbol{\Sigma}, \mathbf{S}) = \ln|\mathbf{S}| + \text{tr}(\mathbf{S}\boldsymbol{\Sigma}^{-1}) - \ln|\boldsymbol{\Sigma}| - p \tag{1}$$

where p is the number of MVs and $\text{tr}(.)$ denotes the trace function which is the sum of the diagonal elements of a square matrix.

The estimated sample discrepancy function is given by $\hat{F} = F(\mathbf{\Sigma}(\hat{\boldsymbol{\theta}}), \mathbf{S})$. Multiplying $\hat{F}$ by $(N-1)$, where N is the sample size, obtains the goodness-of-fit test statistic under the Wishart distribution (Browne & Arminger, 1995). This test statistic

$$T = (N-1)\hat{F} \tag{2}$$

asymptotically follows a χ^2 distribution with $p(p+1)/2 - k$ degrees of freedom under the null hypothesis that the model implied covariance matrix $\mathbf{\Sigma}(\boldsymbol{\theta})$ is no different from the population covariance matrix $\mathbf{\Sigma}$. Recall that k is the total number of parameters estimated under the specified model. This goodness-of-fit test statistic is also known as a likelihood ratio test (LRT) as this statistic compares the likelihoods of the specified model against the saturated model or the model which perfectly reconstructs the data (Bollen, 1989).

1.2   Constructing Confidence Regions and Fungible Contours

1.2.1   Likelihood-Based Confidence Regions

A useful supplement to ML point estimates is a confidence region, which conveys the sampling variability that underlies parameter estimates. Besides likelihood-based confidence regions, there exist other approaches to constructing confidence regions such as the standard Wald approach. Suppose that a confidence interval for a single parameter is desired. Wald-type confidence intervals are constructed using the formula: estimate $\pm$ percentile $\times$ standard error of estimate. Here, the percentile is determined by some chosen confidence or error rate α and a reference distribution such as the normal distribution. Wald-type confidence intervals, however, perform poorly when the distribution of the parameter estimate is markedly skewed or if the estimated standard error is inaccurate (Stryhn & Christensen, 2003).

Another alternative to constructing confidence regions is based on the Score

statistic or Lagrange Multiplier test. Score-type confidence regions are constructed using the same formula as Wald-type confidence regions. While the percentile for both the Wald-type and Score-type confidence regions are the same, the estimate and standard error of the estimate for the Score approach are distinct from the Wald method. In particular, Wald-type standard errors are obtained from the second derivatives of the likelihood function (or Hessian matrix) while Score-type standard errors are computed from the first derivatives of the likelihood function (or Gradient matrix). Score-type confidence regions suffer the same shortcomings as Wald-type confidence regions as these two approaches are based on quadratic approximations to the log-likelihood (Meeker & Escobar, 1995). Perfect conformity of the log-likelihood to the quadratic form is rare in SEMs (Neale & Miller, 1997). Therefore, we will investigate likelihood-based confidence regions here.

Likelihood-based confidence intervals are constructed by inverting a certain type of LRT as described below. Suppose a likelihood-based confidence region for the $k \times 1$ vector of parameter estimates is desired. The null hypothesis tested by the LRT is $H_0 : \boldsymbol{\theta} = \boldsymbol{\theta}_0$ where $\boldsymbol{\theta}_0$ is a $k \times 1$ vector of population parameter values determined by the null hypothesis. Formally, this LRT is defined as

$$G^2 = 2[l(\hat{\boldsymbol{\theta}}) - l(\boldsymbol{\theta}_0)] \tag{3}$$

where $l(\hat{\boldsymbol{\theta}})$ is the log-likelihood associated with the $k \times 1$ vector of ML estimates and $l(\boldsymbol{\theta}_0)$ is the log-likelihood associated with the $k \times 1$ vector of parameter values determined by the null hypothesis. The test statistic G^2 is asymptotically distributed as χ^2 with k degrees of freedom under the null hypothesis.

To construct a $100(1 - \alpha)\%$ confidence region, the LRT in Equation 3 is inverted. In particular, the confidence region is constructed such that values of $\boldsymbol{\theta}_0$ are found to be associated with a non-significant G^2 at some desired error rate α. There-

fore, the likelihood-based confidence region is determined by solving for values of $\boldsymbol{\theta}_0$ which satisfy the inequality

$$G^2 \leq \chi^2_{1-\alpha,k}. \tag{4}$$

In this vein, the bounds or limits to likelihood-based confidence regions are obtained by solving for values of $\boldsymbol{\theta}_0$ such that Equation 4 is an equality or $G^2 = \chi^2_{1-\alpha,k}$. Note that when the null hypothesis is false, the appropriate statistic approximately follows a noncentral χ^2 distribution with k degrees of freedom and a noncentrality parameter λ that depends on the alternative hypothesis that is taken to be true. Although confidence regions may be constructed using the noncentral χ^2 distribution, when the null hypothesis is not true, implementation of this approach would require the user to specify some value of λ reflecting the degree of model misfit in the population. As this task could be problematic in practice, we will focus on inverting the LRT based on the central χ^2 distribution in the current project.

Suppose now that a likelihood-based confidence region for a focal subset of the vector of parameters is desired. Let the parameter vector be partitioned into focal parameters and nuisance parameters as $\boldsymbol{\theta} = (\boldsymbol{\theta}_f, \boldsymbol{\theta}_n)'$. It follows from the general case that the null hypothesis tested by the LRT on focal parameters is $H_0 : \boldsymbol{\theta}_f = \boldsymbol{\theta}_{0f}$ where $\boldsymbol{\theta}_{0f}$ is a $k_f \times 1$ vector of parameter values specified under the null hypothesis. The associated LRT statistic is

$$G^2 = 2[l(\hat{\boldsymbol{\theta}}) - l(\tilde{\boldsymbol{\theta}}_n, \boldsymbol{\theta}_{0f})]$$

where $l(\hat{\boldsymbol{\theta}})$ remains the log-likelihood value associated with the ML estimates $\hat{\boldsymbol{\theta}} = (\hat{\boldsymbol{\theta}}_f, \hat{\boldsymbol{\theta}}_n)'$ and $l(\tilde{\boldsymbol{\theta}}_n, \boldsymbol{\theta}_{0f})$ is the joint log-likelihood associated with the ML nuisance parameter estimates $\tilde{\boldsymbol{\theta}}_n$ and the $k_f \times 1$ vector of population focal parameters under the null $\boldsymbol{\theta}_{0f}$. Note that $\hat{\boldsymbol{\theta}}_n$ is distinct from $\tilde{\boldsymbol{\theta}}_n$ as $\hat{\boldsymbol{\theta}}_n$ is estimated jointly with $\hat{\boldsymbol{\theta}}_f$ while $\tilde{\boldsymbol{\theta}}_n$ is estimated while holding $\boldsymbol{\theta}_{0f}$ fixed under the null hypothesis. This G^2 follows an asymptotic χ^2 distribution with k_f degrees of freedom under the stated null hypoth-

esis. Compared to the general case, values of $\boldsymbol{\theta}_{0f}$ are obtained in place of values of $\boldsymbol{\theta}_0$ so as to obtain confidence regions for a vector of focal parameters.

1.2.2 Fungible Parameter Contours

Fungible parameter values in SEM are obtained from applying a perturbation to the sample value discrepancy function $\hat{F}$, and then computing parameter values that are associated with the perturbed value of model fit (MacCallum, Browne & Lee, 2009). The magnitude of the perturbation to apply remains subjective and will be the responsibility of the investigator. However, perturbations should be small to the extent that the suboptimal model fit is practically no different than the fit of the optimal solution. Let $\hat{F}^*$ denote the perturbed sample value discrepancy function. It is important to apply a perturbation which may be understood on a meaningful metric. For instance, the perturbed $\hat{F}^*$ may be determined by adding some small percentage of $\hat{F}$ to the sample discrepancy value. Under such a perturbation scheme, a perturbation of 5% of $\hat{F}$ would result in $\hat{F}^* = 1.05\hat{F}$.

MacCallum, Browne and Lee (2009) have suggested the use of perturbations based on the root mean squared error of approximation (RMSEA; Browne & Cudeck, 1993; Steiger & Lind, 1980) as this index has a scale understood in terms of model fit. The RMSEA is defined in the population as

$$\epsilon = \sqrt{F_0/df} \tag{5}$$

where F_0 is the discrepancy due to model error in the population and $df = p(p + 1)/2 - k$ is the model degrees of freedom. The population RMSEA is a measure of discrepancy per degree of freedom for the model. Extending Equation 5 to a sample gives the sample RMSEA, which corrects for the bias in $\hat{F}$ as an estimator of F_0 (Browne &

Cudeck, 1993). Specifically, the sample RMSEA is a nonlinear function of $\hat{F}$ given by

$$\hat{\epsilon} = \sqrt{\max(\frac{\hat{F}}{df} - \frac{1}{N-1}, 0)} \tag{6}$$

where max(.) is the maximum operator. The sample RMSEA may be similarly interpreted as a measure of the discrepancy per degree of freedom for the model, and a value of RMSEA ≤ 0.05 is conventionally viewed as indicating a close fit of the model in relation to the degrees of freedom. In this vein, a perturbed value of the RMSEA may be expressed as

$$\epsilon^* = \hat{\epsilon} + \tilde{\epsilon} \tag{7}$$

where $\tilde{\epsilon}$ denotes the perturbation to the optimal RMSEA. For computations, $\hat{F}^*$ may be obtained from ϵ^* via Equation 7. Specifically, $\hat{F}^* = df((\hat{\epsilon} + \tilde{\epsilon})^2 + \frac{1}{N-1})$ when RMSEA $\neq 0$.

Fungible parameter values, denoted by the vector $\hat{\boldsymbol{\theta}}^*$, are obtained by solving the following equation

$$F(\boldsymbol{\Sigma}(\hat{\boldsymbol{\theta}}^*), \mathbf{S}) = \hat{F}^*$$

or

$$F(\boldsymbol{\Sigma}(\hat{\boldsymbol{\theta}}^*), \mathbf{S}) - \hat{F}^* = 0. \tag{8}$$

Here, $\mathbf{S}$, $\hat{F}^*$ and $\hat{\boldsymbol{\theta}}$ are known, and the vector of fungible parameter values is obtained by perturbing ML estimates $\hat{\boldsymbol{\theta}}$ such that these perturbations yield $\hat{F}^*$.

In summary, likelihood-based confidence regions may be constructed by inverting the LRT G^2. From Equation 4, the size of these confidence regions is determined by the selected error rate α, the number of parameters involved, and some assumed distribution. In contrast, fungible parameter contours are constructed from a chosen level of suboptimal model fit $\hat{F}^*$. Hence, the size of fungible parameter contours is directly determined by the magnitude of perturbation introduced.

1.3 Computing Confidence Regions and Fungible Contours

1.3.1 Existing Algorithms for Likelihood-Based Confidence Regions

Several algorithms have been proposed to obtain likelihood-based confidence intervals for a single parameter where $k = 1$. Venzon and Moolgavkar (1988) developed a modified Newton-Raphson algorithm based on analytical derivatives to solve for the limits of Equation 4. Developing this work further, Neale and Miller (1997) introduced a more flexible algorithm which is instead based on numerical derivatives. These approaches are computationally more efficient compared to a systematic search over the parameter space, but do not provide exact solutions to Equation 4. In some cases, biased estimates to confidence intervals have been reported (Neale & Miller, 1997). Additionally, these algorithms have not been generalized to compute confidence bounds for $k > 1$.

Computing exact likelihood-based confidence intervals typically involves a grid search (Stryhn & Christensen, 2003). For simplicity, consider constructing a confidence interval for a single parameter θ where $k = 1$. To obtain the lower bound of a confidence interval θ_L, a reasonable lower bound θ_l is first selected; for example, -5 times the standard error of $\hat{\theta}$. This is followed by constructing a grid of values ranging from θ_l to $\hat{\theta}$. A G^2 test statistic value is obtained for each grid value θ_t and the estimated lower bound $\hat{\theta}_L$ is the smallest grid value θ_t for which Equation 4 holds. The upper bound $\hat{\theta}_U$ may be obtained in a similar manner by starting with a reasonable upper bound θ_u.

For $k = 2$ parameters, the search for a joint confidence bound occurs over a two-dimensional grid. First, reasonable lower and upper bounds for the two parameters θ_{1l}, θ_{2l}, θ_{1u} and θ_{2u} are selected. Then, a two-dimensional grid of values ranging from θ_{1l} to θ_{1u} on the first dimension and from θ_{2l} to θ_{2u} on the second dimension is constructed. Similar to the one-dimensional case, a G^2 test statistic value is obtained for

every point θ_t on the two-dimensional grid. The estimated confidence bound will be an elliptical figure surrounding the parameter estimates $\hat{\boldsymbol{\theta}} = (\hat{\theta}_1, \hat{\theta}_2)'$, which will take on certain values of grid points. In particular, the grid points that make up the confidence bound are the ones located furthest away from the parameter estimates $\hat{\boldsymbol{\theta}}$ and satisfying Equation 4.

In theory, this grid search may be generalized to k-parameters. In place of a one- or two-dimensional grid, a k-dimensional grid is constructed for the search. At the end of the search, a k-dimensional confidence bound is obtained. In practice, computing a k-dimensional confidence bound from the large number of grid points is computationally burdensome. As an alternative to a crude search based on a grid as outlined above, a systematic search procedure may be used to obtain exact likelihood-based confidence regions. However, such an algorithm has not yet been implemented in popular SEM software.

1.3.2 Estimating Fungible Contours

The root finding algorithm (Brent, 1973) was applied by MacCallum, Browne and Lee (2009) to obtain fungible parameter values in SEM. Recall that fungible values are computed by perturbing the ML estimates $\hat{\boldsymbol{\theta}}$ such that the perturbations yield a user-specified sample discrepancy function value $\hat{F}^*$ that is slightly suboptimal as defined in Equation 9. This perturbation of $\hat{\boldsymbol{\theta}}$ is achieved by adding a term

$$\hat{\boldsymbol{\theta}}_t^* = \hat{\boldsymbol{\theta}} + \boldsymbol{\kappa}_t \mathbf{d}_t \tag{9}$$

where $\mathbf{d}_t$ is one of T unit length vectors and $\boldsymbol{\kappa}_t$ is one of T scaling constants to be determined. With $k = 1$, $\mathbf{d}_t$ spans a line and only $T = 2$ direction vectors are required. Suppose that with $k = 2$, $\mathbf{d}_t$ adequately spans a two-dimensional plane with T directional vectors. For $k = 3$, T^2 directional vectors are required to adequately

span the three-dimensional space with equal coverage as the two-dimensional plane. It follows that for k parameters, $\mathbf{d}_t$ spans a k-dimensional space with T^{k-1} directional vectors. Vectors of fungible parameter values $\hat{\boldsymbol{\theta}}_t^*$ are obtained by solving for $\boldsymbol{\kappa}_t$ in the following expression

$$F(\boldsymbol{\Sigma}(\hat{\boldsymbol{\theta}} + \boldsymbol{\kappa}_t \mathbf{d}_t), \mathbf{S}) - \hat{F}^* = 0. \tag{10}$$

Note that $\boldsymbol{\kappa}_t$ is iteratively solved via the Brent (1973) algorithm and the computational burden of obtaining fungible parameter contours increases exponentially with the k number of parameters involved.

1.3.3   Obtaining Confidence Regions via the Brent (1973) Algorithm

The computational procedure applied by MacCallum, Browne and Lee (2009) to compute fungible parameter contours may be generalized to compute exact likelihood-based confidence bounds. First, G^2 in Equation 4 may be re-expressed in terms of discrepancy function values

$$G^2 = (N - 1)[F(\boldsymbol{\Sigma}(\boldsymbol{\theta}_0), \mathbf{S}) - \hat{F}] \tag{11}$$

where N is the sample size, $\boldsymbol{\Sigma}(\boldsymbol{\theta}_0)$ is the population covariance matrix under the null hypothesis and $\hat{F}$ is the sample discrepancy function value. From Equation 4, population values of $\boldsymbol{\theta}_0$ falling within the $(100 - \alpha)\%$ confidence region are obtained by perturbing ML estimates $\hat{\boldsymbol{\theta}}$ such that these perturbations satisfy the equation

$$(N - 1)[F(\boldsymbol{\Sigma}(\boldsymbol{\theta}_0), \mathbf{S}) - \hat{F}] = \chi^2_{1-\alpha,k}$$

or equivalently,

$$(N - 1)[F(\boldsymbol{\Sigma}(\boldsymbol{\theta}_0), \mathbf{S}) - \hat{F}] - \chi^2_{1-\alpha,k} = 0. \tag{12}$$

Similar to obtaining fungible parameter values, values of $\boldsymbol{\theta}_0$ in Equation 12 could be obtained by perturbing the ML estimates $\hat{\boldsymbol{\theta}}$ by Equation 9. Here, T confidence boundary points are obtained in the search. By combining Equations 9 and 12, values of $\boldsymbol{\theta}_0$ are obtained by solving for $\boldsymbol{\kappa}_t$ in the following expression

$$(N-1)[F(\boldsymbol{\Sigma}(\hat{\boldsymbol{\theta}}+\boldsymbol{\kappa}_t\mathbf{d}_t),\mathbf{S})-\hat{F}]-\chi^2_{1-\alpha,k}=0$$

or equivalently,

$$F(\boldsymbol{\Sigma}(\hat{\boldsymbol{\theta}}+\boldsymbol{\kappa}_t\mathbf{d}_t),\mathbf{S})-[\hat{F}+\chi^2_{1-\alpha,k}/(N-1)]=0. \tag{13}$$

1.4   Analytical Relations between Confidence Regions and Fungible Contours

Given that computations of confidence regions and fungible parameter values are based on the likelihood function, we shall now consider the issue of when these two kinds of parameter uncertainty are numerically equivalent. By comparing Equations 10 and 13 of the general perturbation framework, it can be seen that confidence bounds and fungible parameter contours are numerically equivalent if and only if

$$\hat{F}^* = \hat{F} + \chi^2_{1-\alpha,k}/(N-1).$$

or equivalently

$$\hat{F}+F_p = \hat{F}+\chi^2_{1-\alpha,k}/(N-1) \tag{14}$$

where F_p is the perturbation to $\hat{F}$ or $(\hat{F}^*-\hat{F})$. As discussed earlier, F_p may be a perturbation in the scale of RMSEA ($\tilde{\epsilon}$ from Equation 7) or a predetermined percentage of $\hat{F}$. From Equation 14, it can be seen that $(N-1)F_p = \chi^2_{1-\alpha,k}$.

When the magnitude of perturbation in model fit F_p is equivalent to the distance from the ML estimates used to construct confidence bounds $\chi^2_{1-\alpha,k}/(N-1)$, fungible parameter contours and confidence bounds are numerically equivalent. Sup-

14

pose we have a sample of size $N = 150$ and fit a common factor model with correlated factors and simple structure to data collected on six MVs such that three MVs load onto the first factor and the remaining three MVs load onto the second factor. In this model, $k = 13$ and $df = 8$. Suppose further that we are interested in obtaining a confidence region and a fungible parameter contour for the three factor loadings associated with the first factor such that $k_f = 3$.

Let $\hat{F} = 0.082$ with RMSEA $\hat{\epsilon} = 0.059$. To construct a 95% confidence interval for $k_f = 3$, $\chi^2_{.95,3}/(150 - 1) = 0.052$. From Equation 14, this 95% confidence bound would be numerically equivalent to the fungible parameter contour from a perturbation to model fit of $\hat{F}^* = 0.082 + 0.052 = 0.134$. From Equations 6 and 7, this perturbation in the discrepancy function value scale may be translated to a perturbation of the RMSEA of $\tilde{\epsilon} = 0.041$, resulting in a perturbed RMSEA of $\epsilon^* = 0.059 + 0.041 = 0.100$. Likewise, this perturbation may be translated to a percentage of $\hat{F}$ or $\%\hat{F} = 0.052/0.082 \times 100 = 63.4\%$. Alternatively, from a sensitivity analysis using a chosen $\tilde{\epsilon} = 0.005$, the perturbed RMSEA $\epsilon^* = 0.059 + 0.005 = 0.064$ or $\hat{F}^* = 0.086$. This RMSEA perturbation translates to a perturbation of $\%\hat{F} = 4.9\%$. Given the value of $\hat{F}^*$, $F_p = 0.086 - 0.082 = 0.004$. From Equation 14, $\chi^2_{1-\alpha,3}/(150 - 1) = 0.004$ which translates to an error rate of $\alpha = 0.111$ or a 88.89% confidence region. Instead of applying an RMSEA perturbation $\tilde{\epsilon}$, perturbations based on a percentage of $\hat{F}$ or $\%\hat{F}$ may alternatively used.

Although numerical equivalence of fungible parameter contours and confidence bounds is established analytically in Equation 14, these two kinds of uncertainty are *not* substantively equivalent. Fungible parameter contours communicate uncertainty of estimates in terms of their robustness/sensitivity to minor perturbations to model fit. In the given example, a 95% confidence bound translates to a relatively large perturbation of $\tilde{\epsilon} = 0.041$ or $\%\hat{F} = 63.4\%$ in model fit. This magnitude of perturbation in model fit is quite different from the optimal ML solution, and does not translate to

a meaningful sensitivity analysis. Alternatively, the small perturbation of $\tilde{\epsilon} = 0.005$ or $\%\hat{F} = 4.9\%$ in the given example obtains meaningful fungible parameter contours and translates to a confidence bound of 88.89% which may be associated with less than optimal coverage values.

In summary, likelihood-based confidence regions and fungible parameter contours have several different properties that contribute to their theoretical distinction even though they share the commonality of being based on the likelihood function. Confidence regions are a device of statistical inference which allows for statements to be made regarding the population parameter. Specifically, confidence regions communicate the precision of point estimates and the extent of their cross-validity. Confidence bounds are intended to contain the population parameters based on some pre-specified α level. Therefore, confidence bounds are limits to a range of estimates which are plausible population parameter values, and the region within these bounds are meaningful. For instance, a 95% confidence interval provides a range of plausible population parameter values 95% of the time over repeated sampling. Tight confidence regions are optimal in that they convey better precision of the estimates and limited sampling variability. Proper coverage of likelihood-based confidence bounds requires the assumption that the population implied model is correctly specified. Hence, strictly speaking, confidence bounds are applicable only to a correctly specified maximum likelihood. Likelihood-based confidence regions are also constructed from assuming that the LRT in Equation 4 follows a known distribution. For Equation 4 to follow an asymptotic χ^2 distribution with k degrees of freedom, the k estimates for $\boldsymbol{\theta}$ may be ML estimates. In this context, likelihood-based confidence bounds are tied to the ML discrepancy function defined in Equation 1. From Equation 13, the k-dimensional confidence region depends on sample size N and a specified coverage probability α. Hence, these two factors have a direct effect on the size of the confidence bounds.

In contrast, fungible parameter contours are computed as part of a sensitivity

analysis to assess the sensitivity/ robustness of parameter estimates under a practically insignificant perturbation to model fit. Fungible contours are alternative explanations of the data (with equivalent minimally suboptimal model fit) that are practically the same as the optimal solution. Unlike confidence regions, where the area located within the bounds is meaningful, only points on the fungible parameter contour are of interest in that they are associated with the user-specified perturbation to model fit; fungible parameter values lying within the fungible contour are associated with a smaller than specified perturbation to model fit. Tight fungible contours are desirable as they imply limited or tolerable parameter variation in describing the data under a practically equivalent model fit. Conversely, large fungible contours imply unstable model descriptions of the data. In the context of obtaining fungible parameter values, the optimal solution need not necessarily be ML estimates. Indeed, fungible values may be obtained from any discrepancy function such as ordinary least squares (OLS), two-stage least squares (2SLS), generalized least squares (GLS) and ADF (Browne, 1984) approaches. Hence, another main distinction between these two kinds of parameter uncertainty is that distributional assumptions are required in the construction of confidence regions but not fungible parameter contours. From Equation 10, the k-dimensional fungible hyper-contour depends on a specified perturbation of the sample discrepancy function value $\hat{F}^*$ whereas the k-dimensional confidence region in Equation 13 depends on the $\chi^2_{1-\alpha}(k)$ distribution based on ML estimation.

The construction of confidence regions and fungible parameter contours in Equations 13 and 10 respectively suggest that different factors might have an effect on the size of each kind of parameter uncertainty. The determination of $\hat{\boldsymbol{\theta}}^*$ in Equation 10 to obtain fungible parameter values does not explicitly involve sample size N. However, the determination of $\boldsymbol{\theta}_0$ in Equation 13 to obtain confidence bounds involves sample size N. In particular, given smaller sample size, the kernel $F(\hat{\boldsymbol{\Sigma}}(\hat{\boldsymbol{\theta}} + \boldsymbol{\kappa}_t \mathbf{d}_t), \mathbf{S}) - \hat{F}$ in Equation 13 requires larger numbers for the equation to hold and therefore re-

sults in larger ranges of $\boldsymbol{\theta}_0$. Stated differently, decreasing sample size is associated with larger likelihood-based confidence regions. Clearly, confidence regions incorporate information about sampling variability whereas fungible values mainly portray characteristics of the postulated model (cf. Green, 1977).

1.5 Accounting for Nuisance Parameters

When the number of model parameters k is not small, the general perturbation framework to obtaining confidence regions and fungible parameter contours using the method of root finding (Brent, 1973) outlined above is not computationally feasible. With increasing numbers of parameters, locating the desired contour from the k-dimensional likelihood function of a multi-parameter SEM becomes computationally burdensome. In the context of $k = 2$ parameters, suppose that T directional vectors are required to adequately sample the two-dimensional parameter space. With $k = 3$ parameters, T^2 directional vectors are required to sample the three-dimensional parameter space with equal coverage as the two-dimensional scenario. In general, with k-dimensions, T^{k-1} directional vectors are required to sample the hypercube while maintaining the same coverage as the lower-dimensional scenarios.

Computations thus rapidly become intractable with increasing parameter dimensionality. Additionally, multi-dimensional parameter confidence regions and fungible contours are difficult to describe and communicate. In a $k = 2$ dimensional parameter space, confidence regions and fungible contours may be easily visualized as elliptical shapes. In a $k = 3$ dimensional parameter space, wire frame plots may be employed to visually depict the regions and contours as ellipsoidal forms. However, visualizing a multidimensional space beyond $k = 3$ is less than optimal as it typically requires dimensional reduction of the space, and then plotting elliptical or ellipsoidal figures.

It may often be the case in practice that only a few key or focal parameters in

the multi-parameter model are of interest. Recall that the parameter vector $\boldsymbol{\theta}$ may be partitioned into focal and nuisance parameters $\boldsymbol{\theta} = (\boldsymbol{\theta}_f, \boldsymbol{\theta}_n)'$. When focal parameters are of interest, the dimensionality of the likelihood may then be reduced to the dimension of $\boldsymbol{\theta}_f$ by various methods of dealing with nuisance parameters to be reviewed. Once a reduced likelihood is obtained, the computational algorithms described in the above sections may be implemented to obtain confidence regions and fungible parameter contours. We will focus on implementing the Brent (1973) algorithm to obtain estimates of confidence regions and fungible parameter contours from the reduced likelihood.

1.5.1 Profile Likelihood Method

The profile likelihood offers a simple approach to obtaining the reduced likelihood of focal parameters; nuisance parameters are eliminated by substituting the latter with their ML estimates. The joint multivariate normal likelihood in terms of focal and nuisance parameters may be expressed as $L(\boldsymbol{\theta}) = L(\boldsymbol{\theta}_f, \boldsymbol{\theta}_n)$. The profile likelihood of $\boldsymbol{\theta}_f$ is then

$$L(\theta_f) = \max_{\boldsymbol{\theta}_n} L(\boldsymbol{\theta}_f, \boldsymbol{\theta}_n) \tag{15}$$

where the estimation of $\boldsymbol{\theta}_n$ is performed at fixed values of $\boldsymbol{\theta}_f$. Let the ML estimates of $\boldsymbol{\theta}_n$ in Equation 15 be denoted as $\tilde{\boldsymbol{\theta}}_n$. Note that these ML estimates of the nuisance parameters $\boldsymbol{\theta}_n$ are distinct from the ML estimates obtained for the vector of model parameters $\hat{\boldsymbol{\theta}} = (\hat{\boldsymbol{\theta}}_f, \hat{\boldsymbol{\theta}}_n)'$. In Equation 15, $\tilde{\boldsymbol{\theta}}_n$ is estimated while holding $\boldsymbol{\theta}_f$ fixed whereas $\hat{\boldsymbol{\theta}}_n$ is estimated jointly with $\hat{\boldsymbol{\theta}}_f$.

Only the Newton-Raphson based computation algorithms (Venzon & Moolgavkar, 1988; Neale & Miller, 1997) seem to have been implemented in the context of a single-parameter profile likelihood to obtain confidence intervals. While these algorithms are computationally efficient, they obtain only approximate estimates. Additionally, these algorithms have not been extended to compute confidence regions for

$k > 1$ parameters. Neither the grid search nor root finding method (Brent, 1973) have been implemented to obtain estimates from the profile likelihood in Equation 15. Given the better precision of estimates obtained from the Brent (1973) algorithm due to its exact computational nature, this algorithm will be extended to obtain exact estimates of confidence regions and fungible parameter contours for $k \geq 1$ parameters.

1.5.1.1 Profile Likelihood-Based Confidence Bounds

Using the method of root finding, profile likelihood-based confidence bounds for $\boldsymbol{\theta}_f$ are obtained by solving for values of $\boldsymbol{\kappa}_t$ by modifying the expression in Equation 13 to account for the partitioning of focal parameters from nuisance parameters as follows:

$$F(\boldsymbol{\Sigma}(\tilde{\boldsymbol{\theta}}_n, \hat{\boldsymbol{\theta}}_f + \boldsymbol{\kappa}_t \mathbf{d}_t), \mathbf{S}) - [\hat{F} + \chi^2_{1-\alpha}(k)/(N-1)] = 0 \tag{16}$$

where $\hat{\boldsymbol{\theta}}_f$ contains the ML estimates obtained jointly with $\hat{\boldsymbol{\theta}}_n$. Similar to Equation 15, the ML estimates of the nuisance parameters $\hat{\boldsymbol{\theta}}_n$, obtained jointly with the ML estimates of the focal parameters $\hat{\boldsymbol{\theta}}_f$, are distinct from $\tilde{\boldsymbol{\theta}}_n$ or the ML estimates obtained while holding $\hat{\boldsymbol{\theta}}_f + \boldsymbol{\kappa}_t \mathbf{d}_t$ fixed.

In terms of implementation, for each of the $t = 1, \cdots, T$ unit length direction vectors $\mathbf{d}_t$, boundary points of the confidence region are located via the Brent(1973) algorithm by solving for the scaling constants $\boldsymbol{\kappa}_t$. For every candidate scaling constant $\dot{\boldsymbol{\kappa}}_t$, assessed by the root funding algorithm, the nuisance parameters $\boldsymbol{\theta}_n$ are re-estimated by optimizing the ML discrepancy function in Equation 1 while holding the values of the focal parameters fixed at $\hat{\boldsymbol{\theta}}_f + \dot{\boldsymbol{\kappa}}_t \mathbf{d}_t$. Therefore, for every $\dot{\boldsymbol{\kappa}}_t$ a new set of $\tilde{\boldsymbol{\theta}}_n$ are estimated. Once Equation 16 is satisfied, $\dot{\boldsymbol{\kappa}}_t$ is taken to be $\boldsymbol{\kappa}_t$ and boundary points to the confidence region are calculated as $\hat{\boldsymbol{\theta}}_f + \boldsymbol{\kappa}_t \mathbf{d}_t$.

1.5.1.2 Profile Likelihood-Based Fungible Parameter Contours

Similar to profile likelihood-based confidence bounds, fungible parameter contours for $\boldsymbol{\theta}_f$ may be obtained by re-expressing Equation 10 to account for the partitioning of focal from nuisance parameters as follows:

$$F(\boldsymbol{\Sigma}(\tilde{\boldsymbol{\theta}}_n, \hat{\boldsymbol{\theta}}_f + \boldsymbol{\kappa}_t\mathbf{d}_t), \mathbf{S}) - \hat{F}^* = 0. \tag{17}$$

Again, $\hat{\boldsymbol{\theta}}_f$ is the vector of ML estimates obtained jointly with the vector of nuisance parameters $\hat{\boldsymbol{\theta}}_n$, and $\tilde{\boldsymbol{\theta}}_n$ contains the ML estimates of the nuisance parameters computed while holding $\hat{\boldsymbol{\theta}}_f + \boldsymbol{\kappa}_t\mathbf{d}_t$ fixed.

1.5.2 Marginal and Conditional Likelihood Methods

In addition to the profile likelihood method, there are two major alternative theoretical approaches to eliminating nuisance parameters. The first obtains a marginal likelihood from the joint multivariate normal likelihood $L(\boldsymbol{\theta}_f, \boldsymbol{\theta}_n)$. The second approach is to obtain a conditional likelihood. The method of marginalizing is appropriate when the joint likelihood of focal and nuisance parameters can be re-expressed as

$$L(\boldsymbol{\theta}_f, \boldsymbol{\theta}_n) = p_{\boldsymbol{\theta}_f, \boldsymbol{\theta}_n}(\mathbf{y}_f, \mathbf{y}_n) = p_{\boldsymbol{\theta}_f}(\mathbf{y}_f)p_{\boldsymbol{\theta}_n, \boldsymbol{\theta}_f}(\mathbf{y}_n|\mathbf{y}_f)$$
$$= L_m(\boldsymbol{\theta}_f)L_c(\boldsymbol{\theta}_n) \tag{18}$$

where $p(.)$ denotes some probability distribution function and $\mathbf{y}$ is the vector of MVs associated with the parameters in $\boldsymbol{\theta}$. The marginal likelihood of $\boldsymbol{\theta}_f$ is then $L_m(\boldsymbol{\theta}_f) = p_{\boldsymbol{\theta}_f}(\mathbf{y}_f)$, where this expression does not contain the nuisance parameters $\boldsymbol{\theta}_n$.

Alternatively, the method of conditioning may be employed when the joint like-

lihood may be re-expressed as

$$L(\boldsymbol{\theta}_f, \boldsymbol{\theta}_n) = p_{\boldsymbol{\theta}_f, \boldsymbol{\theta}_n}(\mathbf{y}_f|\mathbf{y}_n)p_{\boldsymbol{\theta}_n}(\mathbf{y}_n)$$

$$= L_c(\boldsymbol{\theta}_f)L_m(\boldsymbol{\theta}_n) \tag{19}$$

where the conditional likelihood for $\boldsymbol{\theta}_f$ is $L_c(\boldsymbol{\theta}_f) = p_{\boldsymbol{\theta}_f}(\mathbf{y}_f|\mathbf{y}_n)$. Note that this conditional likelihood does not include the vector of nuisance parameters $\boldsymbol{\theta}_n$.

Unfortunately, the likelihood for SEMs cannot be easily re-expressed into Equations 18 or 19 as the model implied likelihood is expressed in terms of the covariance matrix $\boldsymbol{\Sigma}(\boldsymbol{\theta})$, which is a function of simultaneous equations of the parameters. Only for special cases involving limited types of models have conditional likelihoods been worked out (for example, see duToit & Cudeck, 2009). Hence, we will focus on profile likelihood-based approaches in computing confidence bounds and fungible parameter values.

1.6 Likelihood-Based Estimation in Practice

The implementation of the Brent (1973) algorithm by MacCallum, Browne, and Lee (2009) to obtain fungible parameter values is distinct from the profile likelihood approach outlined in Equation 17. Instead, these authors computed fungible parameter values from the estimated or pseudo likelihood. This estimated likelihood is a simplified version of the profile likelihood where $\tilde{\boldsymbol{\theta}}_n$ is replaced by $\hat{\boldsymbol{\theta}}_n$ such that the nuisance parameters are not re-estimated with every $\hat{\boldsymbol{\theta}}_f + \boldsymbol{\kappa}_t\mathbf{d}_t$ from Equation 9. In place of Equation 17, fungible parameter values were computed from the following expression:

$$F(\boldsymbol{\Sigma}(\hat{\boldsymbol{\theta}}_n, \hat{\boldsymbol{\theta}}_f + \boldsymbol{\kappa}_t\mathbf{d}_t), \mathbf{S}) - \hat{F}^* = 0 \tag{20}$$

where $\hat{\boldsymbol{\theta}}_n$ is the vector of ML estimates for the nuisance parameters obtained jointly with the focal parameters $\hat{\boldsymbol{\theta}}_f$. While T sets of ML estimates $\tilde{\boldsymbol{\theta}}_n$ are computed in

Equation 17, only a single set of ML estimates $\hat{\boldsymbol{\theta}} = (\hat{\boldsymbol{\theta}}_f, \hat{\boldsymbol{\theta}}_n)'$ is employed in the computations for Equation 20. Compared to obtaining estimates from the profile likelihood in Equation 17, estimates obtained from the estimated likelihood in Equation 20 are computationally more efficient as the latter requires only a single optimization to obtain estimates for the nuisance parameters $\boldsymbol{\theta}_n$.

Confidence bounds may be similarly computed from the estimated likelihood. Here, instead of optimizing Equation 16, confidence regions are computed from

$$F(\boldsymbol{\Sigma}(\hat{\boldsymbol{\theta}}_n, \hat{\boldsymbol{\theta}}_f + \boldsymbol{\kappa}_t \mathbf{d}_t), \mathbf{S}) - [\hat{F} + \chi^2_{1-\alpha}(k)/(N-1)] = 0 \tag{21}$$

where $\tilde{\boldsymbol{\theta}}_n$ is replaced by $\hat{\boldsymbol{\theta}}_n$ in the same fashion as fungible parameter contours.

Although obtaining confidence regions and fungible parameter contours from the estimated likelihood has the advantage of computational efficiency over the profile likelihood, the estimated bounds and contours come with the price of potential bias and overly optimistic precision (Pawitan, 2001). By substituting $\hat{\boldsymbol{\theta}}_n$ for $\tilde{\boldsymbol{\theta}}_n$, the estimated likelihood does not take into account the uncertainty inherent in the nuisance parameters, nor the correlations among the nuisance and focal parameters. Hence, computed confidence regions and fungible parameter contours based on the estimated likelihood will be smaller in magnitude compared to those computed from the proper profile likelihood. In the following section, an empirical demonstration using published data will be used to illustrate the computation of confidence regions and fungible bounds. We have implemented the method of Brent (1973) to obtaining confidence bounds and fungible parameter contours from the profile likelihood, and the following computations are based on the profile likelihood via the root finding algorithm of Brent (1973).

23

1.7 An Empirical Demonstration

As an illustration, confidence bounds and fungible parameter contours are obtained from a published example in social psychology (Schmitt, Branscombe, Kobrynowicz & Owen, 2002). The authors fit a latent variable (LV) mediation model to data obtained from a group of women ($N = 220$) where the effect of perceived discrimination against one's in-group on psychological well-being was hypothesized to be mediated by in-group identification. Perceived discrimination was indicated by four measured variables (MVs) - in-group disadvantage (y_1), out-group privilege (y_2), prejudice across contexts (y_3) and past experience with discrimination (y_4). In-group identification was indicated by four MVs quantifying the extent of emotional attachment to one's group - liking one's group (y_5), valuing one's group (y_6), having pride in one's group (y_7) and having positive experiences due to being a member of one's group (y_8). Finally, psychological well-being was indicated by five MVs - life satisfaction (y_9), self-esteem (y_{10}), positive affect (y_{11}), anxiety (y_{12}) and depression (y_{13}). To identify the model, all LVs were scaled according to their first indicators by fixing respective factor loadings to 1.0. Figure 1 is a path diagram of the model with standardized ML estimates.

For simplicity, profile likelihood-based confidence intervals and fungible parameter values are computed for a single parameter first. Of interest, is the direct effect of perceived discrimination on well-being. To illustrate that the profile likelihood-based computational method may be extended to multi-parameter contexts, confidence bounds and fungible parameter contours are computed for two parameters next. Here, the mediation effect of in-group identification between perceived discrimination and psychological well-being will be examined. In this published example, the sample discrepancy function value is $\hat{F} = 0.576$, the number of estimated parameters is $k = 29$, $df = 62$ and the estimated RMSEA is $\hat{\epsilon} = 0.0687$.

Figure 1: Path Diagram for Schmitt et al. (2002) Mediation Model
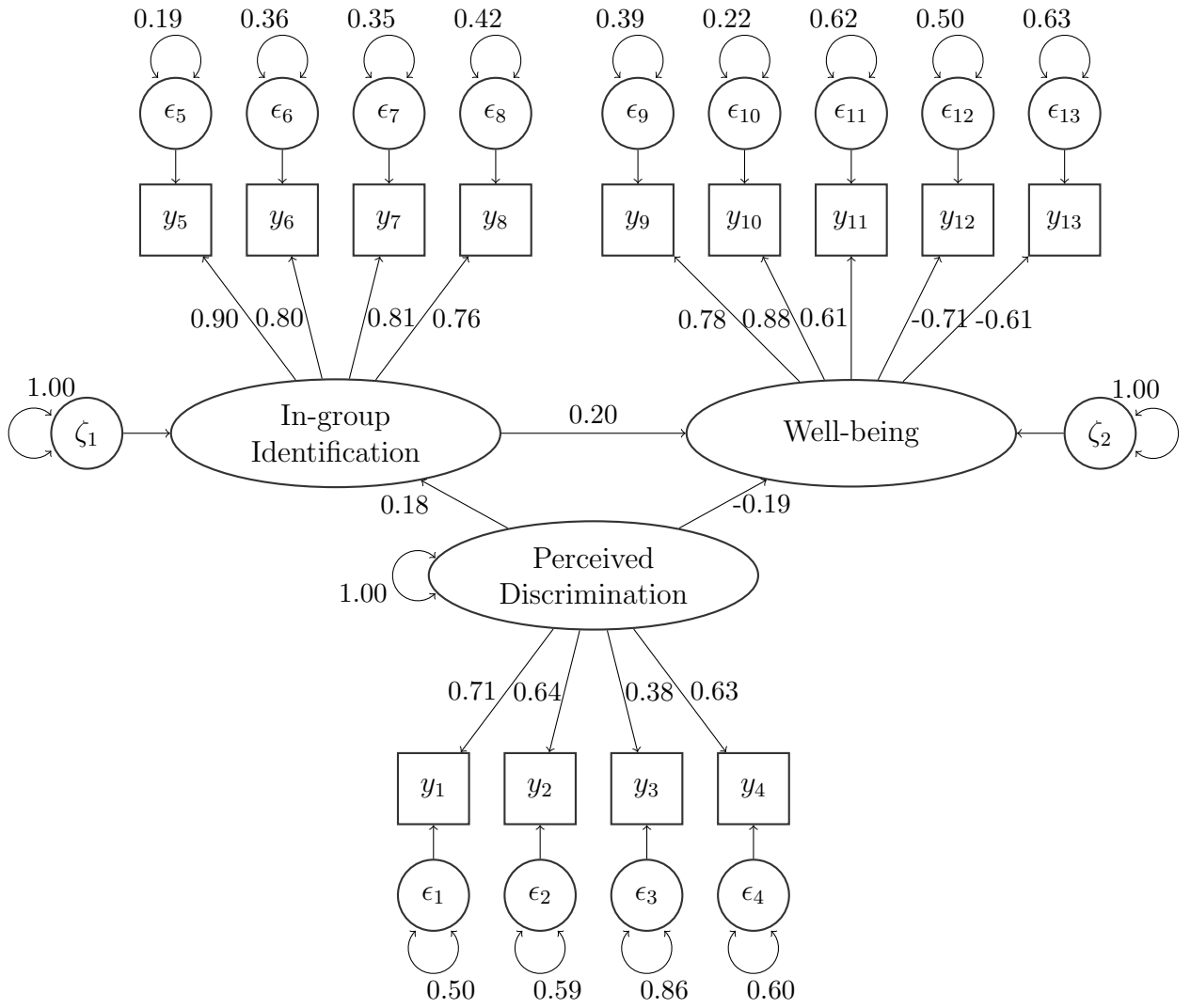
1.7.1 Direct Effect ($k = 1$)

The ML estimate for the direct effect of perceived discrimination on well-being is $\hat{\theta}_f = -0.19$. In order to compute a 95% confidence interval for this focal parameter, the perturbation applied to $\hat{F}$ as defined in Equation 13 is $\chi^2_{0.95}(1)/(220-1) = 0.0175$, and the profile likelihood-based confidence interval for this direct effect is $(-0.389, -0.010)$. As the confidence interval does not capture the value of $\theta_f = 0$, the direct effect of perceived discrimination on well-being is statistically significant at $p < .05$. Such a conclusion is consistent with Schmitt, et al. (2002) who would have obtained a standard error of 0.092, and a Wald-type confidence interval of $(-0.368, -0.008)$. Note that the Wald-type confidence interval is different from the estimated likelihood-based confidence interval due to the former using a quadratic approximation of the likelihood function.

To compute fungible parameter values, the RMSEA perturbation of $\tilde{\epsilon} = 0.005$ to model fit is specified, such that from Equations 6 and 7, $\hat{F}^* = 0.620$ and $F_p = 0.044$. In this example, the two fungible parameter values are $(-0.533, 0.097)$. Since these two values are of different signs, the direct effect of perceived discrimination on well-being is not consistently negative under the minor perturbation introduced to model fit. These results suggest that the effect of perceived discrimination on well-being is sensitive to a perturbation of model fit. Hence, the robustness of this significant direct effect is somewhat questionable, and the direct effect is said to be sensitive to a perturbation resulting in practically the same model fit as the ML solution. Note that these fungible parameter values are larger in magnitude compared to the confidence bounds as the perturbation applied to the ML estimate for the former ($F_p = 0.044$) is larger than the latter ($F_p = 0.0175$).

Recall that the two kinds of uncertainty are analytically related as shown in Equation 14. From this equation, the confidence interval translates to an $F^* = 0.576 + 0.0175 = 0.593$, or a perturbed RMSEA of $\epsilon^* = \sqrt{\max(0.593/62 - 1/(220-1))} =$

0.071. This is equivalent to perturbing the RMSEA by $\tilde{\epsilon} = 0.071 - 0.0687 = 0.002$, a value smaller than the specified perturbation of $\tilde{\epsilon} = 0.005$, which was used to compute the two fungible parameter values above. Alternatively, the perturbation associated with the fungible values translates to $\chi^2_{1-\alpha}(1) = (220 - 1)(0.578 - 0.576) = 9.672$, which is associated with a 99.81% confidence interval along with $\alpha = 0.002$.

The above calculations show that confidence bounds may be translated to fungible parameter values and vice versa. However, the conversion of one measure of uncertainty to the other may not necessarily be meaningful. First, the fungible parameter values are numerically equivalent to constructing a 99.81% confidence interval. However, the associated small error rate of $\alpha = 0.002$ is not practically useful in making statistical inferences. Second, the 95% confidence interval is equivalent to a model perturbation of $\tilde{\epsilon} = 0.002$. While this perturbation is smaller than the specified perturbation used to compute fungible parameter values, $\tilde{\epsilon} = 0.002$ is practically no different from $\tilde{\epsilon} = 0.005$ in terms of model fit. The small difference of 0.003 between these two perturbations of RMSEA was associated with fungible parameter values with different conclusions regarding $\theta_f = 0$, implying that the direct effect is sensitive to the magnitude of perturbation applied to model fit.

1.7.2 Indirect Effect ($k = 2$)

The effect of perceived discrimination on psychological well-being was hypothesized to be mediated by in-group identification, and the ML estimates for the effect of perceived discrimination on in-group identification and the effect of in-group identification on well-being are $\hat{\theta}_f = (0.18, 0.20)'$. To compute the 95% confidence bound for the focal parameters, we apply a perturbation of $\chi^2_{0.95}(2)/(220 - 1) = 0.0273$ as defined in Equation 13. Recall that a perturbation of $\tilde{\epsilon} = 0.005$ or $F_p = 0.044$ is used to compute fungible parameter values. Similar to the one-parameter illustration, the perturbation applied to the ML estimate to compute the confidence region is smaller than that of

the fungible parameter contour. Hence, it is expected that the latter has larger values than the former. Figure 2 depicts the simultaneous 95% confidence region (as blue colored crosses) and the fungible parameter contour (as red colored circles) based on the profile likelihood.

Figure 2: Profile Likelihood-Based Confidence Bounds and Fungible Contours for the Indirect Effect of Perceived Discrimination on Well-being.
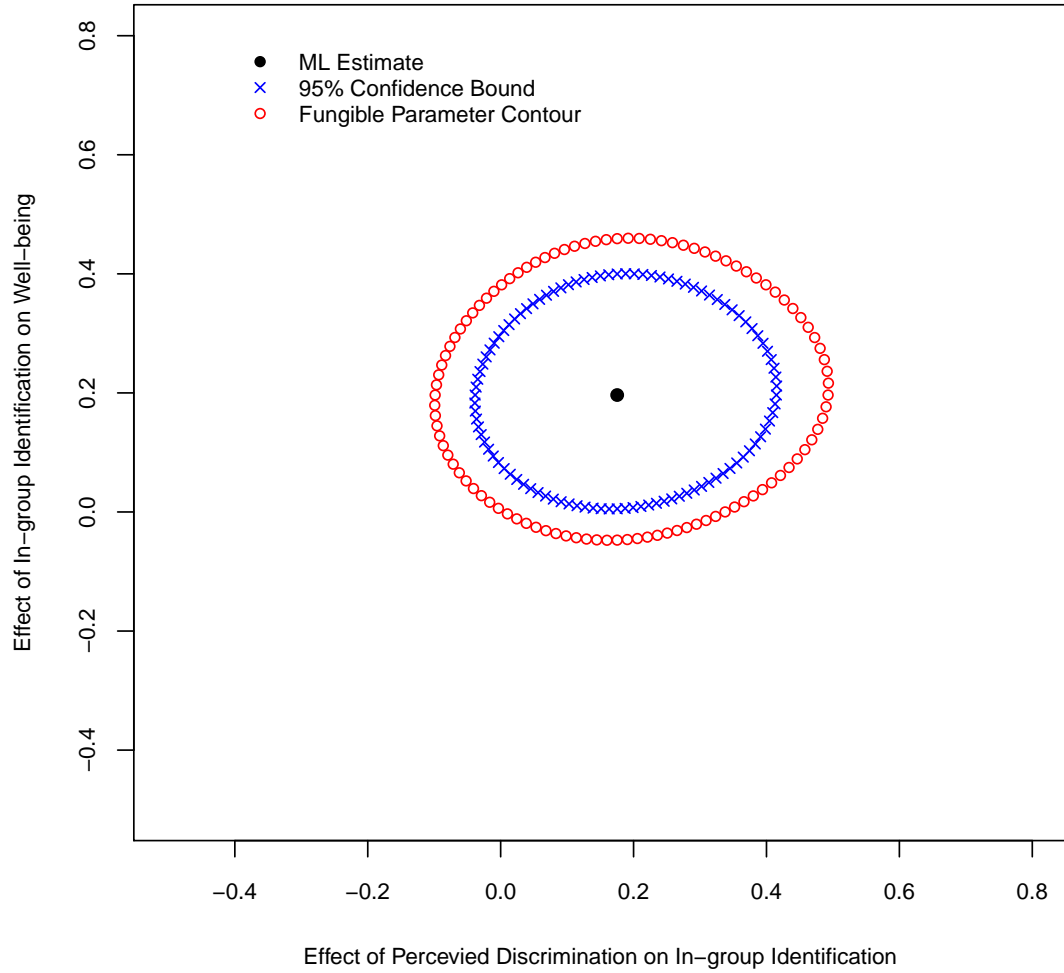
In Figure 2, the dot in the center of the elliptical forms depicts the ML estimates from the optimal solution. Here, $T = 100$ points are computed for the confidence bound and fungible parameter contour as can be seen from the 100 crosses and 100 open circles. From Figure 2, the confidence bound contains the zero-point or

$\theta_f = (0,0)'$, implying that the estimated effects are not simultaneously significant at $p < .05$. Additionally, the fungible parameter values take on all possible combinations of positive and negative values for each of the effects, suggesting that the results are sensitive to a perturbation to model fit. Hence, the distinct information on parameter uncertainty, as depicted in the elliptical forms of Figure 2, implies that the mediation effect may not be interpreted vigorously.

It is noted that Schmitt et al. (2002) drew the opposite conclusion that the two effects are significant at $p < .05$. However, there are at least two explanations for this inconsistency. First, Schmitt, et al. (2002) conducted their hypothesis tests using the Wald test. Although the two effects were statistically significant at $p < .05$, the Wald-type confidence intervals were close to $\theta_f = (0,0)'$; the intervals are $(0.004, 0.346)$ and $(0.042, 0.352)$ for the effect of perceived discrimination on in-group identification and the effect of in-group identification on psychological well-being respectively. Additionally, the profile likelihood-based confidence regions reported here are, however, based on an LRT. While the Wald test and LRT are asymptotically equivalent, a sample of $N = 220$ may not be large enough for these two test results to converge. It is noteworthy to mention here that the LRT is usually more reliable than the Wald test for small to mid-sized samples (Agresti, 2002).

Second, the Wald tests conducted by Schmitt, et al. (2002) are non-simultaneous; the effect of perceived discrimination on in-group identification is tested independently of the effect of in-group identification on well-being despite these effects being slightly positively correlated. Stated differently, the Wald tests carried out by Schmitt, et al. (2002) do not take into account the correlation between these two focal effects. This positive correlation is graphically evident in Figure 2 as the confidence region does not fall onto a perfect circle. In contrast to the independent Wald tests, the profile likelihood-based confidence region is associated with a joint LRT where both effects are tested simultaneously. In such joint tests, the correlation between the focal param-

eter estimates is accounted for. Therefore, the non-simultaneous Wald tests reported in Schmitt, et al. (2002) tended to be overpowered compared to a joint test associated with the confidence region in Figure 2.

As the fungible parameter values in Figure 2 take on all combinations of positive and negative values, the sign of both effects may be reversed given a practically similar model fit to the optimal ML solution. Observe that the range of the fungible values for the effect of perceived discrimination on in-group identification is wider than the effect of in-group identification on well being; this suggests that the latter effect is relatively less sensitive to the former effect under a small perturbation to model fit. The two measures of uncertainty, computed from the estimated likelihood, suggest that the indirect effect of perceived discrimination on well-being should not be interpreted rigorously.

Numerical association between the simultaneous confidence region and fungible parameter contour may also be established in this two-parameter illustration. From Equation 14, the confidence region translates to an $\hat{F}^* = 0.576 + 0.0273 = 0.603$ or a perturbed RMSEA of $\epsilon^* = \sqrt{\max(0.603/62 - 1/(220 - 1), 0)} = 0.0718$ that results in an RMSEA perturbation of $\tilde{\epsilon} = .0718 - 0.0687 = 0.003$. As with the one-parameter example, this perturbation is substantively no different from the specified perturbation of $\tilde{\epsilon} = 0.005$ used to compute the fungible parameter contour. Hence, these results are sensitive to model fit perturbations. Conversely, the fungible parameter contour translates to $\chi^2_{1-\alpha}(2) = (220 - 1)(0.603 - 0.576) = 9.673$, such that it is equivalent to an extremely large 99.2% confidence region with $\alpha = 0.008$. Similar to the single parameter example, although the numerical equivalence of the confidence region and parameter contour in this two-parameter illustration may be determined, the conversion of one measure of uncertainty to the other may not be substantively meaningful.

1.7.3 Summary and Extensions

Confidence regions may be translated to fungible parameter contours and vice-versa as demonstrated in the empirical illustration. However, the example showed that the resulting information gained from translating confidence regions into fungible parameter contours may be of limited value. In particular, the equivalence of these estimates was achieved at the expense of their interpretability, especially for confidence regions. However, it may not always be the case that the equivalence between confidence regions and fungible parameter values occur under unrealistic or substantively less meaningful conditions. In situations where these two kinds of parameter uncertainty are meaningful numerical translations of each other, they provide unique and useful information to the analyst.

The different information provided by these two distinct kinds of parameter uncertainty informs analysts of the extent to which results may be interpreted rigorously. Confidence bounds allow researchers to make inferential statements about effects in terms of estimate precision, sampling variability and predictive validity. Fungible contours convey the robustness of parameter estimates under a small perturbation to model fit. Hence, these contours communicate how stable parameter estimates remain in describing the data under a practically indifferent model fit. Another important distinction to note is that confidence regions span a range of plausible population values whereas fungible parameter contours are point values that are associated with a specific perturbation to model fit. Therefore, confidence bounds are limits to a range of estimates whereas fungible parameter contours are not. Stated differently, the region located within a confidence bound is meaningful in that any point within the region is a plausible set of population parameter values for some specified α level. With regards to fungible parameter values, however, only points lying on the contour are of interest in that they are exchangeable parameter values associated with the user-specified perturbation to model fit; parameter values lying within the fungible parameter contour

are associated with a smaller perturbation to model fit than what the user specified.

The limitations of the current empirical demonstration call for several extensions. Primarily, little is known about the behavior of confidence regions and fungible parameter contours under different modelling conditions. Thus, a simulation study was conducted to assess how certain factors influence these two kinds of parameter uncertainty. As the empirical demonstration made use of only one perturbation scheme to compute fungible parameters, it was a secondary goal to examine fungible parameter contours using more than one perturbation scheme. Additionally, computations for the empirical example were based on the profile likelihood outlined in Equations 16 and 17 although previous work on fungible parameter contours (MacCallum, Browne & Lee, 2009) were based on the empirical likelihood. Therefore, a third aim in the simulation study was to compare results obtained from the empirical likelihood versus the profile likelihood.

Chapter 2

METHODS

There were three objectives of the project. The first two aims of establishing the analytical relationship between confidence regions and fungible parameter contours, and implementing computations to be based on the profile likelihood have been accomplished. The remaining objective is to assesses how certain factors affect confidence regions and fungible parameter contours. These factors involve certain modelling conditions, the perturbation schemes used to construct fungible parameter contours, as well as whether computations are based on the empirical or profile likelihood. The following sections describe how each of these factors are examined in the simulation study.

2.1 Modelling Factors that May Impact Parameter Uncertainty

To better understand the nature of the two kinds of parameter uncertainty - confidence bounds and fungible parameter values - it is proposed that certain modelling factors which may influence them are examined. The three factors explored are sample size, overall model fit, and the magnitude of correlations among MVs. As this aspect of the project is exploratory, the following suggested hypotheses on how the three factors may affect the two kinds of parameter uncertainty differently are only working hypotheses based on informed speculation.

First, sample size is expected to affect the size of confidence regions but not fungible parameter contours. From Equation 13, the computation of likelihood-based confidence regions directly involves sample size N whereas the computation of fungible parameter contours in Equation 10 does not. Therefore, it is expected that increas-

ing sample size would lead to tighter confidence regions, reflecting higher precision and lower sampling variability of the estimates. It is also expected that changes in sample size will not affect the size of fungible parameter contours. Stated differently, fungible parameter contours are expected to be independent of sample size. Yet with different sample sizes, fungible parameter values should not remain constant; instead these contours are expected to shift slightly from sample to sample, reflecting sampling variability. Note that the sampling variability expected to be reflected in fungible parameter values does not result from the effect of sample size, but the variation in the correlations among MVs across the different samples.

Second, from limited exploratory computations of fungible parameter values on published examples, an apparent tendency for the size of fungible parameter contours to be related to model fit has been observed. In particular, larger fungible parameter contours were found to be associated with less well-fitting models. Alternatively, smaller fungible parameter contours were found to be observed when the fit of the model was good. It is plausible that the likelihood surface would be less peaked when model fit is not extremely good (Michael Browne, personal communication March 2011). A basis for conjecture regarding this phenomenon is that when model fit is not very good, the sample discrepancy function values based on ML and GLS estimation can differ substantially (Browne, MacCallum & Kim, 2002), possibly implying a flatter likelihood surface. Alternatively, when the sample discrepancy function values based on ML and GLS estimation coincide in the context of good model fit, the likelihood function may tend to be more peaked. With a more peaked likelihood surface, fungible parameter contours as well as confidence regions are anticipated to be tighter compared to a flatter likelihood surface.

The third factor examined concerns the correlations among MVs. In general, larger correlations compared to smaller correlations are associated with smaller variances which lead to more power to reject false models (Neale & Miller, 1997). In other

words, fewer models can fit well to data structures with large correlations among MVs compared to data structures with small correlations among MVs. This limited number of models in data structures with larger correlations translates to more peaked likelihood surfaces which are expected to be associated with tighter confidence bounds and fungible parameter contours. Stated differently, higher correlations are expected to be associated with fungible parameter values that provide data descriptions that are tolerably different from the ML solution. Likewise, holding sample size constant, larger correlations are expected to be associated with more precise confidence regions.

The following section describes the exploratory simulation study used to assess the effect of sample size, model fit and the magnitude of correlations among MVs on the size of confidence regions and fungible parameter contours. Additionally, the assertion that parameter sensitivity (or parameter fungibility) is a property of the model (Green, 1977) and not the sample is empirically examined.

2.1.1 Population Generating Models

The empirical illustration based on Schmitt, et al. (2002) will serve as the blueprint to generating data for the proposed exploratory simulation study. Recall that there were 13 MVs and 3 LVs involved in this model of LV mediation (see Figure 1). The general SEM model in covariance structure form is expressed as

$$\boldsymbol{\Sigma} = \boldsymbol{\Lambda}(\mathbf{I} - \mathbf{B})\boldsymbol{\Phi}(\mathbf{I} - \mathbf{B})'\boldsymbol{\Lambda}' + \boldsymbol{\Psi} \tag{22}$$

where $\boldsymbol{\Lambda}$ is a 13×3 matrix of factor loadings , $\mathbf{I}$ is a 3×3 identity matrix and $\mathbf{B}$ is the 3×3 matrix of structural paths; $\boldsymbol{\Phi}$ is a 3×3 matrix which contains the variance and covariances of the exogenous LV as well as the variances and covariances of the endogenous LV residuals, and $\boldsymbol{\Psi}$ is a 13×13 matrix of unique variances of the MVs.

In particular, the population generating model has the following specified matrices:

$$
\mathbf{\Lambda} = \begin{pmatrix}
0.8073 & 0 & 0 \\
0.8102 & 0 & 0 \\
0.8047 & 0 & 0 \\
0.8059 & 0 & 0 \\
0 & 0.8086 & 0 \\
0 & 0.8072 & 0 \\
0 & 0.8038 & 0 \\
0 & 0.8017 & 0 \\
0 & 0 & 0.8007 \\
0 & 0 & 0.8043 \\
0 & 0 & 0.8004 \\
0 & 0 & 0.8081 \\
0 & 0 & 0.8055
\end{pmatrix}
\quad \text{and } \mathbf{\Phi} = \begin{pmatrix}
1.0 & & \\
0 & 1.0 & \\
0 & 0 & 1.0
\end{pmatrix}.
$$

The values for $\mathbf{\Psi}$ and $\mathbf{B}$ will be introduced in the following section where different magnitudes of correlations between the MVs are specified. Note that these population values for $\mathbf{\Lambda}$ and $\mathbf{\Psi}$ are based on the estimated values reported in Schmitt et al. (2002).

2.1.1.1 Magnitude of Correlations

Two different approaches are adopted to control the magnitude of correlations between the MVs. Based on the work of Browne, MacCallum and Kim (2002), the first approach alters the size of unique variances in $\mathbf{\Psi}$ to manipulate the magnitude of correlations. The second approach specifies different effect sizes of the three structural paths of the LV mediation in $\mathbf{B}$. These two different approaches were considered as some substantive research is solely focused on measurement models while others place

more weight on structural paths. The study will fully cross these two methods for manipulating the correlations among MVs.

The size of unique variances indirectly affects correlations between MVs. The variance of each MV is attributable to three sources of variation - common variance, specific variance, and error variance. The common variance is attributable to the common factor or LV, the specific variance represents systematic factors affecting a given MV and the error variance represents random error of measurement or unreliability. Hence, reliable variance in any given MV is made up of common and specific variances. Unique variance is made up of the sum of specific and error variances. Small unique variances indirectly translate to larger correlations between MVs as they reflect accuracy of measurement associated with increased power to reject false models. Additionally, when MVs have smaller unique variances, effect sizes tend to be larger and power of the LRT will be high (Browne, MacCallum & Kim, 2002), implying tighter confidence regions due to a more peaked likelihood surface. As fungible parameter contours are also based on the peakedness of the likelihood surface, they are expected to be tighter when unique variances of MVs are small. Large measurement errors take on values close to $\mathbf{\Psi}_{p,p} = 0.50$ where $p = 1, \cdots, 13$. These unique variances are not exactly 0.50, but randomly vary very slightly from one another to avoid equivalent population parameter values. In addition, these values were chosen to follow the unique variances observed in Schmitt, et al. (2002) where $0.19 \leq \mathbf{\Psi}_{p,p} \leq 0.86$. Small measurement errors similarly take on values close to $\mathbf{\Psi}_{p,p} = 0.10$.

Effect sizes of the structural pathways among the LVs directly affect the magnitude of correlations among the MVs through $\mathbf{B}$ as can be seen from Equation 22. In general, the larger the effect size, the larger the correlations between the MVs. Small

effect sizes are specified using

$$\mathbf{B} = \begin{pmatrix} 0 & 0 & 0 \\ 0.2076 & 0 & 0 \\ -0.1989 & 0.2015 & 0 \end{pmatrix},$$

which reflects the values observed by Schmitt, et al. (2002) where $\beta_{2,1} = 0.17$, $\beta_{3,1} = -0.18$ and $\beta_{3,2} = 0.19$. In contrast, large effect sizes are specified using

$$\mathbf{B} = \begin{pmatrix} 0 & 0 & 0 \\ 0.6076 & 0 & 0 \\ -0.5989 & 0.6015 & 0 \end{pmatrix}.$$

With the two different specifications of $\mathbf{\Psi}$ and the two different specifications of $\mathbf{B}$, there are four possible population covariance matrices. Let the subscripts $\mathbf{\Psi}_L$ and $\mathbf{\Psi}_H$ denote low and high correlations among MVs due to controlling the size of unique variances. Similarly, let the subscripts $\mathbf{B}_L$ and $\mathbf{B}_H$ denote low and high correlations resulting from manipulating the size of the structural effects respectively. It is emphasized that L and H refer to low and high correlations among MVs due to manipulating $\mathbf{\Psi}$ and $\mathbf{B}$, and not the values within these two matrices themselves. Hence, $\mathbf{\Sigma}_{\mathbf{\Psi}_L \mathbf{B}_L}$ refers to the population covariance matrix based on large unique variances and small structural effect sizes. It follows that $\mathbf{\Sigma}_{\mathbf{\Psi}_H \mathbf{B}_L}$ refers to the population covariance matrix defined by small unique variances and small structural effect sizes, $\mathbf{\Sigma}_{\mathbf{\Psi}_L \mathbf{B}_H}$ is the population covariance matrix due to large unique variances and large effect sizes and $\mathbf{\Sigma}_{\mathbf{\Psi}_H \mathbf{B}_H}$ is the population covariance matrix derived from small unique variances and large structural effects. Let $\mathbf{P}_{\mathbf{\Psi}_L \mathbf{B}_L}$, $\mathbf{P}_{\mathbf{\Psi}_H \mathbf{B}_L}$, $\mathbf{P}_{\mathbf{\Psi}_L \mathbf{B}_H}$ and $\mathbf{P}_{\mathbf{\Psi}_H \mathbf{B}_H}$ denote their commensurate population correlation matrices.

To illustrate, by using the specified values for the matrices in the SEM Equation 22, the population covariance and correlation matrix associated with large unique

variances and small effect sizes is

$\boldsymbol{\Sigma}_{\boldsymbol{\Psi}_L \mathbf{B}_L}$ and $\mathbf{P}_{\boldsymbol{\Psi}_L \mathbf{B}_L} =$

$$
\begin{pmatrix}
\mathbf{1.15} & \mathit{0.57} & \mathit{0.56} & \mathit{0.56} & \mathit{0.12} & \mathit{0.12} & \mathit{0.12} & \mathit{0.12} & \mathit{0.13} & \mathit{0.13} & \mathit{0.13} & \mathit{0.13} & \mathit{0.13} \\
0.65 & \mathbf{1.16} & \mathit{0.56} & \mathit{0.56} & \mathit{0.12} & \mathit{0.12} & \mathit{0.12} & \mathit{0.12} & \mathit{0.13} & \mathit{0.13} & \mathit{0.13} & \mathit{0.13} & \mathit{0.13} \\
0.65 & 0.65 & \mathbf{1.16} & \mathit{0.56} & \mathit{0.12} & \mathit{0.12} & \mathit{0.11} & \mathit{0.11} & \mathit{0.13} & \mathit{0.13} & \mathit{0.13} & \mathit{0.13} & \mathit{0.13} \\
0.65 & 0.65 & 0.65 & \mathbf{1.16} & \mathit{0.12} & \mathit{0.12} & \mathit{0.11} & \mathit{0.11} & \mathit{0.13} & \mathit{0.13} & \mathit{0.13} & \mathit{0.13} & \mathit{0.13} \\
0.14 & 0.14 & 0.14 & 0.14 & \mathbf{1.18} & \mathit{0.57} & \mathit{0.57} & \mathit{0.57} & \mathit{0.14} & \mathit{0.14} & \mathit{0.14} & \mathit{0.14} & \mathit{0.14} \\
0.14 & 0.14 & 0.13 & 0.14 & 0.68 & \mathbf{1.18} & \mathit{0.57} & \mathit{0.57} & \mathit{0.14} & \mathit{0.14} & \mathit{0.14} & \mathit{0.14} & \mathit{0.14} \\
0.13 & 0.14 & 0.13 & 0.13 & 0.68 & 0.68 & \mathbf{1.18} & \mathit{0.57} & \mathit{0.14} & \mathit{0.14} & \mathit{0.14} & \mathit{0.14} & \mathit{0.14} \\
0.13 & 0.13 & 0.13 & 0.13 & 0.68 & 0.68 & 0.67 & \mathbf{1.18} & \mathit{0.14} & \mathit{0.14} & \mathit{0.14} & \mathit{0.14} & \mathit{0.14} \\
0.16 & 0.16 & 0.16 & 0.16 & 0.16 & 0.16 & 0.16 & 0.16 & \mathbf{1.21} & \mathit{0.58} & \mathit{0.58} & \mathit{0.59} & \mathit{0.59} \\
0.16 & 0.16 & 0.16 & 0.16 & 0.16 & 0.16 & 0.16 & 0.16 & 0.71 & \mathbf{1.22} & \mathit{0.58} & \mathit{0.58} & \mathit{0.59} \\
0.16 & 0.16 & 0.16 & 0.16 & 0.16 & 0.16 & 0.16 & 0.16 & 0.70 & 0.71 & \mathbf{1.21} & \mathit{0.58} & \mathit{0.58} \\
0.16 & 0.16 & 0.16 & 0.16 & 0.16 & 0.16 & 0.16 & 0.16 & 0.71 & 0.71 & 0.71 & \mathbf{1.22} & \mathit{0.59} \\
0.16 & 0.16 & 0.16 & 0.16 & 0.16 & 0.16 & 0.16 & 0.16 & 0.71 & 0.71 & 0.71 & 0.72 & \mathbf{1.21}
\end{pmatrix}
$$

where the covariances among the MVs are presented in the lower triangular matrix, the variances are bold in the diagonal of the matrix, and the correlations are italicized in the upper triangular matrix. Note that $\boldsymbol{\Sigma}_{\boldsymbol{\Psi}_L \mathbf{B}_L}$ and $\mathbf{P}_{\boldsymbol{\Psi}_L \mathbf{B}_L}$ have values based on Schmitt et al.'s (2002) empirical study. The remaining three population covariance matrices ($\boldsymbol{\Sigma}_{\boldsymbol{\Psi}_H \mathbf{B}_L}$, $\boldsymbol{\Sigma}_{\boldsymbol{\Psi}_L \mathbf{B}_H}$, and $\boldsymbol{\Sigma}_{\boldsymbol{\Psi}_H \mathbf{B}_H}$) as well as correlation matrices ($\mathbf{P}_{\boldsymbol{\Psi}_H \mathbf{B}_L}$, $\mathbf{P}_{\boldsymbol{\Psi}_L \mathbf{B}_H}$, and $\mathbf{P}_{\boldsymbol{\Psi}_H \mathbf{B}_H}$) are presented in Appendix A.

2.1.1.2   Model Fit

Overall model fit was controlled by using the Cudeck and Browne (1992) method to constructing a covariance matrix that yields a specified minimum discrepancy function value F. This method adds realism to the data generation process as actual data

do not appear to follow models which hold exactly in the samples (Tucker, Koopman & Linn, 1969). Introducing noise to the regularity of the population generating model reflects any variety of unsystematic or unknown aspects of the process which gave rise to the observed data. Two levels of model fit - good and poor - are predetermined. For good model fit, a population RMSEA value of $\epsilon = 0.03$ is used. Alternatively, for poor model fit, a population RMSEA value of $\epsilon = 0.09$ is specified.

To illustrate, the population covariance and correlation matrix associated with large unique variances and small effect sizes for good model fit is

$\mathbf{\Sigma}_{\mathbf{\Psi}_L \mathbf{B}_L G}$ and $\mathbf{P}_{\mathbf{\Psi}_L \mathbf{B}_L G} =$

$$
\begin{pmatrix}
\mathbf{1.15} & \mathit{0.58} & \mathit{0.55} & \mathit{0.56} & \mathit{0.12} & \mathit{0.11} & \mathit{0.14} & \mathit{0.12} & \mathit{0.13} & \mathit{0.13} & \mathit{0.15} & \mathit{0.14} & \mathit{0.15} \\
0.67 & \mathbf{1.16} & \mathit{0.56} & \mathit{0.55} & \mathit{0.13} & \mathit{0.13} & \mathit{0.11} & \mathit{0.10} & \mathit{0.12} & \mathit{0.13} & \mathit{0.14} & \mathit{0.12} & \mathit{0.14} \\
0.63 & 0.65 & \mathbf{1.16} & \mathit{0.58} & \mathit{0.11} & \mathit{0.11} & \mathit{0.08} & \mathit{0.10} & \mathit{0.11} & \mathit{0.12} & \mathit{0.14} & \mathit{0.10} & \mathit{0.11} \\
0.64 & 0.64 & 0.67 & \mathbf{1.16} & \mathit{0.13} & \mathit{0.10} & \mathit{0.11} & \mathit{0.15} & \mathit{0.14} & \mathit{0.15} & \mathit{0.16} & \mathit{0.13} & \mathit{0.14} \\
0.14 & 0.15 & 0.13 & 0.16 & \mathbf{1.18} & \mathit{0.59} & \mathit{0.58} & \mathit{0.56} & \mathit{0.12} & \mathit{0.17} & \mathit{0.18} & \mathit{0.12} & \mathit{0.14} \\
0.13 & 0.15 & 0.13 & 0.11 & 0.69 & \mathbf{1.18} & \mathit{0.56} & \mathit{0.57} & \mathit{0.11} & \mathit{0.13} & \mathit{0.14} & \mathit{0.12} & \mathit{0.13} \\
0.16 & 0.13 & 0.10 & 0.13 & 0.68 & 0.66 & \mathbf{1.18} & \mathit{0.58} & \mathit{0.13} & \mathit{0.13} & \mathit{0.12} & \mathit{0.11} & \mathit{0.11} \\
0.14 & 0.12 & 0.12 & 0.17 & 0.66 & 0.68 & 0.69 & \mathbf{1.18} & \mathit{0.14} & \mathit{0.15} & \mathit{0.16} & \mathit{0.13} & \mathit{0.18} \\
0.15 & 0.14 & 0.13 & 0.17 & 0.14 & 0.13 & 0.16 & 0.16 & \mathbf{1.21} & \mathit{0.57} & \mathit{0.59} & \mathit{0.60} & \mathit{0.57} \\
0.16 & 0.15 & 0.15 & 0.18 & 0.20 & 0.16 & 0.15 & 0.18 & 0.70 & \mathbf{1.22} & \mathit{0.59} & \mathit{0.57} & \mathit{0.60} \\
0.17 & 0.16 & 0.17 & 0.19 & 0.21 & 0.17 & 0.14 & 0.19 & 0.71 & 0.71 & \mathbf{1.21} & \mathit{0.58} & \mathit{0.57} \\
0.16 & 0.15 & 0.12 & 0.16 & 0.15 & 0.15 & 0.13 & 0.15 & 0.73 & 0.70 & 0.70 & \mathbf{1.22} & \mathit{0.59} \\
0.18 & 0.16 & 0.13 & 0.17 & 0.17 & 0.16 & 0.14 & 0.21 & 0.70 & 0.73 & 0.70 & 0.72 & \mathbf{1.21}
\end{pmatrix}
$$

where covariances are presented in the lower triangular matrix, the variances are bold in the diagonal, and the correlations are italicized in the upper triangular matrix. As will be elaborated later, the subscript G denotes good model fit. The remaining population covariances and variances with model lack of fit are presented in Appendix B.

2.1.1.3 Sample Size

Two sample sizes were chosen to cover the range of designs that are used in applied psychological research. The moderate sample size is $N = 200$ and the large sample size is $N = 1000$. The large difference in these values is meant to cover a broad range of sample sizes in addition to amplifying the effect of sample size on confidence bounds and fungible parameter values.

2.1.2 Study Conditions

From the model specifications laid out, there are four derived population covariances constructed with (a) large unique variances and small structural effects $\boldsymbol{\Sigma}_{\boldsymbol{\Psi}_L \mathbf{B}_L}$, (b) small unique variances and small structural effects $\boldsymbol{\Sigma}_{\boldsymbol{\Psi}_H \mathbf{B}_L}$, (c) large unique variances and large structural effects $\boldsymbol{\Sigma}_{\boldsymbol{\Psi}_L \mathbf{B}_H}$ and (d) small unique variances and large structural effects $\boldsymbol{\Sigma}_{\boldsymbol{\Psi}_H \mathbf{B}_H}$. To be explicit, let the subscript 0 denote covariance matrices which hold exactly in the population. For example, $\boldsymbol{\Sigma}_{\boldsymbol{\Psi}_L \mathbf{B}_L 0}$ is the population covariance matrix based on large unique variances and small structural effects which holds exactly in the population.

Noise may then be added to these four population covariance matrices, which hold exactly, via the Cudeck and Browne (1992) method. Let the subscripts G and P denote good and poor model fit respectively. Therefore, $\boldsymbol{\Sigma}_{\boldsymbol{\Psi}_L \mathbf{B}_L G}$ is the population covariance matrix based on large unique variances, small structural effects and good model fit, $\boldsymbol{\Sigma}_{\boldsymbol{\Psi}_L \mathbf{B}_L P}$ is the population covariance matrix based on large unique variances, small structural effects and poor model fit, and so on. By adding two levels of model error to the four population covariances, there are a total of $4 \times 3 = 12$ population covariance matrices (see Appendices A and B).

Finally, a single random sample for moderate ($N = 200$) and large ($N = 1000$) sizes is drawn from each of the 12 population covariance matrices defined above, resulting in 24 sample covariances. Only a single sample for each condition is examined

as computing profile likelihood-based confidence regions and fungible parameter contours is computationally intensive. Additionally, we are not focused on the repeated sampling properties of likelihood-based confidence intervals and fungible parameter contours. Let the subscripts N_{200} and N_{1000} denote the moderate and large sample sizes. Following the established notation, let $\mathbf{S}_{\Psi_L \mathbf{B}_L G N_{200}}$ denote the sample covariance matrix constructed with large unique variances, small structural effects, good model fit and moderate sample size; likewise, $\mathbf{S}_{\Psi_L \mathbf{B}_L G N_{1000}}$ is the sample covariance matrix based on large unique variances, small structural effects, good model fit and large sample size, and so forth.

In summary, there are a total of 12 proposed population conditions where only fungible parameter values can be obtained. Additionally, we will compute both likelihood-based confidence bounds and fungible parameter contours for the 24 sample conditions. Of interest, is the indirect effect of the LV mediation concerning the focal parameters of $\boldsymbol{\theta}_f = (\beta_{2,1}, \beta_{3,2})'$. Hence, the study has a total of $24 + 12 = 36$ conditions. Table 1 summarizes the 36 cells associated with the proposed design. Estimation will be carried out using R (R Development Core Team, 2010).

Beyond the factors of sample size, model fit and the magnitude of correlations among MVs, the effect of two different perturbation schemes on fungible parameter contours are also explored. The next section provides more detail on the perturbations used to compute both confidence regions and fungible parameter contours.

Table 1: Proposed Simulation Study Conditions

Model Fit	$\boldsymbol{\Psi}_L\boldsymbol{B}_L$			$\boldsymbol{\Psi}_H\boldsymbol{B}_L$		
	$\epsilon = 0$	$\epsilon = 0.03$	$\epsilon = 0.09$	$\epsilon = 0$	$\epsilon = 0.03$	$\epsilon = 0.09$
Population	$\Sigma_{\boldsymbol{\Psi}_L\mathbf{B}_L0}$	$\Sigma_{\boldsymbol{\Psi}_L\mathbf{B}_LG}$	$\Sigma_{\boldsymbol{\Psi}_L\mathbf{B}_LP}$	$\Sigma_{\boldsymbol{\Psi}_H\mathbf{B}_L0}$	$\Sigma_{\boldsymbol{\Psi}_H\mathbf{B}_LG}$	$\Sigma_{\boldsymbol{\Psi}_H\mathbf{B}_LP}$
$N = 1000$	$\mathbf{S}_{\boldsymbol{\Psi}_L\mathbf{B}_L0N_{1000}}$	$\mathbf{S}_{\boldsymbol{\Psi}_L\mathbf{B}_LGN_{1000}}$	$\mathbf{S}_{\boldsymbol{\Psi}_L\mathbf{B}_LPN_{1000}}$	$\mathbf{S}_{\boldsymbol{\Psi}_H\mathbf{B}_L0N_{1000}}$	$\mathbf{S}_{\boldsymbol{\Psi}_H\mathbf{B}_LGN_{1000}}$	$\mathbf{S}_{\boldsymbol{\Psi}_H\mathbf{B}_LPN_{1000}}$
$N = 200$	$\mathbf{S}_{\boldsymbol{\Psi}_L\mathbf{B}_L0N_{200}}$	$\mathbf{S}_{\boldsymbol{\Psi}_L\mathbf{B}_LGN_{200}}$	$\mathbf{S}_{\boldsymbol{\Psi}_L\mathbf{B}_LPN_{200}}$	$\mathbf{S}_{\boldsymbol{\Psi}_H\mathbf{B}_L0N_{200}}$	$\mathbf{S}_{\boldsymbol{\Psi}_H\mathbf{B}_LGN_{200}}$	$\mathbf{S}_{\boldsymbol{\Psi}_H\mathbf{B}_LPN_{200}}$

Model Fit	$\boldsymbol{\Psi}_L\boldsymbol{B}_H$			$\boldsymbol{\Psi}_H\boldsymbol{B}_H$		
	$\epsilon = 0$	$\epsilon = 0.03$	$\epsilon = 0.09$	$\epsilon = 0$	$\epsilon = 0.03$	$\epsilon = 0.09$
Population	$\Sigma_{\boldsymbol{\Psi}_L\mathbf{B}_H0}$	$\Sigma_{\boldsymbol{\Psi}_L\mathbf{B}_HG}$	$\Sigma_{\boldsymbol{\Psi}_L\mathbf{B}_HP}$	$\Sigma_{\boldsymbol{\Psi}_H\mathbf{B}_H0}$	$\Sigma_{\boldsymbol{\Psi}_H\mathbf{B}_HG}$	$\Sigma_{\boldsymbol{\Psi}_H\mathbf{B}_HP}$
$N = 1000$	$\mathbf{S}_{\boldsymbol{\Psi}_L\mathbf{B}_H0N_{1000}}$	$\mathbf{S}_{\boldsymbol{\Psi}_L\mathbf{B}_HGN_{1000}}$	$\mathbf{S}_{\boldsymbol{\Psi}_L\mathbf{B}_HPN_{1000}}$	$\mathbf{S}_{\boldsymbol{\Psi}_H\mathbf{B}_H0N_{1000}}$	$\mathbf{S}_{\boldsymbol{\Psi}_H\mathbf{B}_HGN_{1000}}$	$\mathbf{S}_{\boldsymbol{\Psi}_H\mathbf{B}_HPN_{1000}}$
$N = 200$	$\mathbf{S}_{\boldsymbol{\Psi}_L\mathbf{B}_H0N_{200}}$	$\mathbf{S}_{\boldsymbol{\Psi}_L\mathbf{B}_HGN_{200}}$	$\mathbf{S}_{\boldsymbol{\Psi}_L\mathbf{B}_HPN_{200}}$	$\mathbf{S}_{\boldsymbol{\Psi}_H\mathbf{B}_H0N_{200}}$	$\mathbf{S}_{\boldsymbol{\Psi}_H\mathbf{B}_HGN_{200}}$	$\mathbf{S}_{\boldsymbol{\Psi}_H\mathbf{B}_HPN_{200}}$

Note. $\boldsymbol{\Psi}_L$ = large unique variances, $\boldsymbol{\Psi}_H$ = small unique variances, $\mathbf{B}_L$ = small structural effects, $\mathbf{B}_H$ = large structural effects, $\epsilon = RMS$ and N = sample size.

2.2   Perturbation Schemes

Confidence regions and fungible parameter contours may be constructed from the general perturbation framework as laid out in Equations 10 and 13. The "perturbation" applied to obtain confidence regions is derived directly from the LRT, and is an objective function of sample size and the quantiles of the χ^2 distribution (see Equation 13). Following convention, we will construct 95% confidence regions where $\alpha = 0.05$.

In contrast to confidence regions, the choice of perturbations to be used to compute fungible parameter contours is a subjective one. As a general principle, perturbations should be very small such that the change in model fit is practically no different from the fit of the optimal solution; the constructed fungible parameter contour will therefore contain alternative exchangeable parameter values that describe the data almost as well as the optimal solution in terms of model fit. As suggested by MacCallum, Browne and Lee (2009), and consistent with the perturbation scheme used in our empirical demonstration, we continue to use the perturbation based on RMSEA for all study cells. Specifically, the RMSEA perturbation is chosen to be $\tilde{\epsilon} = 0.005$, corresponding to a practically insignificant difference in model fit.

Additionally we implemented a perturbation directly to the sample discrepancy function value $\hat{F}$ to compute fungible parameter contours. In particular, a small percentage of $\hat{F}$ was used as the alternative perturbation scheme. For a subset of the study cells, a perturbation of $\%\hat{F} = 5\%$ or $\hat{F}^* = 1.05\hat{F}$ will be used to compute fungible parameter contours. These two perturbation schemes were applied to the conditions of large unique variances and small structural effects ($\boldsymbol{\Psi}_L\boldsymbol{B}_L$) as well as small unique variances and large structural effects ($\boldsymbol{\Psi}_H\boldsymbol{B}_H$) to obtain two distinct sets of fungible parameter contours. These conditions were chosen as their respective fungible parameter contours were expected to be the most distinct among the study conditions.

2.3 Profile and Empirical Likelihood-Based Computation

Estimates based on the empirical likelihood, as implemented by MacCallum, Browne and Lee (2009), have the advantage of computational efficiency over estimates based on the profile likelihood. In a multi-parameter context, where interest is in a selected set of focal parameters $\boldsymbol{\theta}_f$, the estimated likelihood makes use of a single ML solution to take account of the nuisance parameters $\boldsymbol{\theta}_n$. Here, the nuisance parameters take on values of $\hat{\boldsymbol{\theta}}_n$ which are the estimates of the nuisance parameters obtained jointly with the focal parameters, $\hat{\boldsymbol{\theta}}_f$. In other words, the estimated likelihood does not re-compute $\boldsymbol{\theta}_n$ or $\tilde{\boldsymbol{\theta}}_n$ in the search for fungible parameter values or confidence bounds (see Equations 20 and 21). However, confidence bounds and fungible parameter contours based on the empirical likelihood may be biased downward. Stated differently, confidence bounds computed from the estimated likelihood, compared to the profile likelihood, may communicate overly optimistic precision (Pawitan, 2001). Likewise, fungible parameter contours obtained from the estimated likelihood may be tighter than contours obtained from the profile likelihood. By substituting $\hat{\boldsymbol{\theta}}_n$ for $\tilde{\boldsymbol{\theta}}_n$, the estimated likelihood does not take account of the uncertainty of the nuisance parameters and the correlations among the nuisance and focal parameters, causing potential bias in estimates.

The advantage of obtaining less biased estimates from the profile likelihood outweighs the computational burden of having to re-compute $\tilde{\boldsymbol{\theta}}_n$ for every point on the confidence bound or fungible parameter contour (see Equations 16 and 17). From the empirical demonstration, obtaining confidence regions and fungible parameter contours from the profile likelihood is computationally tractable. To evaluate the extent of bias present in the estimates obtained from the empirical likelihood, empirical likelihood-based confidence regions and fungible parameter contours will be computed from a subset of the study cells. Note that profile likelihood-based confidence regions and fun-

gible parameter contours will be computed for every study cell.

2.4 Hypothesized Results

Comparisons between the different study conditions will be made to assess the effect of the three factors - sample size, magnitude of MV correlations and model fit - on the size of likelihood-based confidence regions and fungible parameter contours. A matrix of plots for each study cell will be employed to summarize the findings and aid in making visual comparisons. Confidence regions and fungible parameter contours for different conditions may also be overlaid in a single plot to aid in visual comparisons.

Besides a graphical approach, we will compute and report the length of the major axis and minor axis of the confidence bound and fungible parameter contour. Note that the major axis cuts the center of the elliptical figure, and has antipodal points which are of maximum distance. Conversely, the minor axis cuts the center of the elliptical shape, but has antipodal points which are of minimum distance. Given that the likelihood surface has a single maximum value - the ML solution - it is expected that confidence regions and fungible parameter bounds based on the same covariance matrix do not cross each other. As many of the comparisons involve multiple cells, these numerical values can be summarized using descriptive statistics such as means and standard deviations.

2.4.1 Sample Size

Sample size effects may be observed from comparisons made between confidence regions and fungible parameter contours obtained from sample covariances based on $N = 200$ versus sample covariances based on $N = 1000$. For example, estimates from $\mathbf{S}_{\boldsymbol{\Psi}_L \mathbf{B}_L 0 N_{200}}$ versus $\mathbf{S}_{\boldsymbol{\Psi}_L \mathbf{B}_L 0 N_{1000}}$, $\mathbf{S}_{\boldsymbol{\Psi}_L \mathbf{B}_L G N_{200}}$ versus $\mathbf{S}_{\boldsymbol{\Psi}_L \mathbf{B}_L G N_{1000}}$, $\mathbf{S}_{\boldsymbol{\Psi}_L \mathbf{B}_L P N_{200}}$ versus $\mathbf{S}_{\boldsymbol{\Psi}_L \mathbf{B}_L P N_{1000}}$, and so forth are compared against each other. There are a total of 12 such comparisons. Holding the magnitude of MV correlations and model fit con-

stant, it is hypothesized that confidence regions will be smaller in the large sample size compared to the moderate sample size due to the effect of N on the perturbation applied to obtain confidence regions as shown in Equation 13. It is also expected that sample size will not affect fungible parameter contours, but the different fungible contours will exhibit sampling variability, by small shifts in the contours, due to them being computed from different samples.

2.4.2 Model Fit

The effect of model fit on the size of confidence regions and fungible parameter contours may be examined by comparing estimates from sample covariances with subscripts 0, G and P, holding all other factors constant. For instance, with three levels of model fit, estimates from the three sample covariances, $\mathbf{S}_{\mathbf{\Psi}_H \mathbf{B}_H 0 N_{200}}$, $\mathbf{S}_{\mathbf{\Psi}_H \mathbf{B}_H G N_{200}}$ and $\mathbf{S}_{\mathbf{\Psi}_H \mathbf{B}_H P N_{200}}$ may be compared against one another to assess the effect of increasing model error. There are a total of 8 sets of such comparisons. Holding all other factors constant, it is hypothesized that both confidence bounds and fungible parameter contours will increase in size as model fit changes from exact to good and then to poor.

2.4.3 Magnitude of Correlations

Recall that there are two approaches to manipulating the size of correlations among the MVs. First, the effect of the size of MV correlations on the two kinds of parameter uncertainty, due to manipulating unique variances, may be assessed by comparing estimates obtained from sample covariances with subscripts $\mathbf{\Psi}_L$ and $\mathbf{\Psi}_H$ while holding sample size, model fit and structural effects constant. For example, confidence bounds and fungible contours from $\mathbf{S}_{\mathbf{\Psi}_L \mathbf{B}_H G N_{200}}$ are compared against those from $\mathbf{S}_{\mathbf{\Psi}_H \mathbf{B}_H G N_{200}}$. A total of 12 such comparisons may be made. It is hypothesized that confidence regions and fungible parameter contours from lower sample correlations among MVs, due to larger unique variances, will be larger than those obtained from higher MV correla-

tions, resulting from smaller unique variances.

Second, the magnitude of correlations among the MVs is also controlled by altering the size of the structural effects in $\mathbf{B}$. The effect of such a manipulation may be investigated by comparing estimates obtained from sample covariances with subscripts $\mathbf{B}_L$ against subscripts $\mathbf{B}_H$, holding all other factors constant. There are a total of 12 such comparisons. Similar to the effect of altering unique variances to manipulate the size of MV correlations, it is expected that confidence regions and fungible parameter contours from higher MV correlations due to larger effect sizes are tighter than those computed from lower MV correlations because of smaller effect sizes.

Additionally, comparisons between estimates obtained from sample covariances with subscripts $\mathbf{B}_L$ versus subscripts $\mathbf{B}_H$ may be used to empirically check that manipulating focal parameters - the structural effects - shifts the center of the confidence bounds and fungible parameter contours. Note that the center of these bounds and contours is the ML solution. In particular, it is expected that the center of the confidence bounds and fungible parameter contours be further away from $\boldsymbol{\theta}_f = \mathbf{0}$ given larger structural effects compared to smaller structural effects. Therefore, these comparisons also serve to confirm that larger effect sizes are associated with estimates which may be interpreted with more rigor as it is less likely for confidence bounds and fungible parameter contours to capture $\boldsymbol{\theta}_f = \mathbf{0}$ when the center of their ellipses are further away from the zero point.

Finally, the joint effect of the two approaches of manipulating the size of MV correlations may be assessed by comparing estimates obtained from sample covariances with subscripts $\boldsymbol{\Psi}_L \mathbf{B}_L$ against estimates obtained from covariances with subscripts $\boldsymbol{\Psi}_H \mathbf{B}_H$, holding all other factors constant. These two conditions were chosen as they correspond to the smallest and largest correlations among the MVs respectively. For instance, confidence bounds and fungible parameter contours from $\mathbf{S}_{\boldsymbol{\Psi}_L \mathbf{B}_L 0 N_{1000}}$ are compared against those computed from $\mathbf{S}_{\boldsymbol{\Psi}_H \mathbf{B}_H 0 N_{1000}}$. For all of these 6 comparisons, it

is expected that confidence regions and fungible contours estimated from lower sample correlations among MVs will be larger than those estimated from higher sample MV correlations. Note that there are no specific expectations regarding comparisons made between sample covariances with subscripts $\boldsymbol{\Psi}_L$ versus $\mathbf{B}_L$ or $\boldsymbol{\Psi}_H$ versus $\mathbf{B}_H$. This is because the effect of manipulating unique variances on MV correlations does not share a common scale with the effect of manipulating structural effect sizes on MV correlations. For the same reason, there are no specific hypotheses for comparisons between sample covariances with subscripts $\boldsymbol{\Psi}_L$ versus $\mathbf{B}_H$ and $\boldsymbol{\Psi}_H$ versus $\mathbf{B}_L$.

2.4.4 Population Covariances

Unlike confidence regions, fungible parameter contours may be computed at the level of the population. This is because sample size N is required for computing likelihood-based confidence bounds as shown in Equation 13. Stated differently, confidence regions cannot be computed for the population as sampling error does not exist. To examine whether parameter fungibility is free of sampling variability, we will compare fungible values obtained from sample covariances and their population counterparts. For example, we compare fungible parameter contours computed from $\boldsymbol{\Sigma}_{\boldsymbol{\Psi}_H \mathbf{B}_H G}$ versus $\mathbf{S}_{\boldsymbol{\Psi}_H \mathbf{B}_H G N_{1000}}$ as well as $\boldsymbol{\Sigma}_{\boldsymbol{\Psi}_H \mathbf{B}_H G}$ versus $\mathbf{S}_{\boldsymbol{\Psi}_H \mathbf{B}_H G N_{200}}$. From the 36 conditions, there are a total of 24 such comparisons. If parameter fungibility is indeed a property of the model (Green, 1977), it is expected that fungible parameter contours are no different when obtained at the level of the population versus the sample; these estimates will only show variability in the form of contours shifting slightly from condition to condition.

2.4.5 Profile and Empirical Likelihood-Based Computation

The extent of bias present in solutions based on the empirical likelihood may be evaluated against solutions based on the profile likelihood. Holding sample size,

model fit and the magnitude of correlations among MVs constant, it is expected that the profile likelihood solutions will communicate more parameter uncertainty compared to the estimated likelihood solutions. Stated differently, confidence regions and fungible parameter contours based on the empirical likelihood are anticipated to be tighter than those based on the profile likelihood.

Chapter 3

RESULTS

Results from the simulation study are organized into preliminary and primary analysis. To validate the generated data, we conducted manipulation checks in our preliminary analysis. Following these preliminaries, our primary analysis focuses on testing the hypotheses of the simulation study.

3.1 Preliminary Analysis Evaluating Generated Data

Prior to examining how certain factors affect confidence regions and fungible parameter contours, preliminary analysis were conducted. First, we describe the magnitude of variances, covariances and correlations of the measured variables (MVs) due to controlling unique variances and structural effects. Second, population standardized covariance residuals are used to describe and quantify good and poor levels of model fit, specified as population RMSEA values of $\epsilon = 0.03$ and $\epsilon = 0.09$ respectively. Third, we report model fit information for all the study conditions.

3.1.1 Correlations among Measured Variables

Recall that the magnitude of correlations among MVs was manipulated in two ways, either by controlling the size of unique variances in $\boldsymbol{\Psi}$ or by controlling the size of the structural effects in $\mathbf{B}$. To quantify the effect of these manipulations on the magnitude of correlations among MVs, Table 2 reports descriptive statistics of the various types of elements in each of the four different population generating covariance and correlation matrices. Note that the matrices examined are free of model and sampling

error. Within each matrix, there are 13 variances and 78 covariances or correlations among the 13 MVs.

From Table 2, manipulating the size of unique variances in $\boldsymbol{\Psi}$ altered only the variances of the MVs and not their covariances; large unique variances are associated with larger variances and small unique variances vice-versa. As anticipated, the magnitude of correlations was affected in that smaller unique variances ($\boldsymbol{\Psi}_H$) were associated with larger correlations whereas larger unique variances ($\boldsymbol{\Psi}_L$) were associated with smaller correlations. Manipulating the size of structural effects in $\boldsymbol{B}$, however, affected both population variances and covariances among the MVs in that larger structural effects are associated with larger variances and covariances whereas smaller structural effects are associated with smaller variances and covariances. As expected, large structural effects ($\boldsymbol{B}_H$) were associated with larger correlations and small structural effects ($\boldsymbol{B}_L$) were associated with smaller correlations.

Table 2: Descriptive Statistics of Elements within Population Matrices

Population Matrix	Variances		Covariances		Correlations	
	Mean	SD	Mean	SD	Mean	SD
$\Sigma_{\boldsymbol{\Psi}_L \boldsymbol{B}_L 0}$	1.187	0.026	0.303	0.242	0.255	0.202
$\Sigma_{\boldsymbol{\Psi}_H \boldsymbol{B}_L 0}$	0.787	0.026	0.303	0.242	0.384	0.304
$\Sigma_{\boldsymbol{\Psi}_L \boldsymbol{B}_H 0}$	1.550	0.375	0.748	0.320	0.476	0.137
$\Sigma_{\boldsymbol{\Psi}_H \boldsymbol{B}_H 0}$	1.150	0.375	0.748	0.320	0.652	0.168

Note. SD = standard deviation, $\boldsymbol{\Psi}_L$ = large unique variances, $\boldsymbol{\Psi}_H$ = small unique variances, $\mathbf{B}_L$ = small structural effects and $\mathbf{B}_H$ = large structural effects.

There was a clear rank order of population generating conditions in terms of the average size of correlations among the 13 MVs. In particular, the condition with large unique variances and small structural effects ($\boldsymbol{\Psi}_L \boldsymbol{B}_L$) had the smallest mean correlations followed by the condition with small unique variances and small structural

effects ($\mathbf{\Psi}_H\mathbf{B}_L$). As anticipated, the condition with small unique variances and large structural effects ($\mathbf{\Psi}_H\mathbf{B}_H$) had the largest mean correlations followed by the condition with large unique variances and large structural effects ($\mathbf{\Psi}_L\mathbf{B}_H$). These observations validate the two approaches to controlling the size of correlations among MVs, and confirm that the population generating matrices had the desired properties.

3.1.2 Model Fit in Terms of Covariance Residuals

As an alternative calibration of model error associated with population RMSEA values of $\epsilon = 0.03$ and $\epsilon = 0.09$, which reflect good and poor model fit respectively, Table 3 presents the range of the standardized population residuals for the four population covariance matrices. Recall that these covariance residuals were generated via the Cudeck and Browne (1992) method.

Table 3: Range of Standardized Population Residuals

Condition	$\epsilon = 0.03$			$\epsilon = 0.09$		
	Minimum	Maximum	Range	Minimum	Maximum	Range
$\mathbf{\Psi}_L\mathbf{B}_L$	-0.031	0.042	0.073	-0.091	0.122	0.213
$\mathbf{\Psi}_H\mathbf{B}_L$	-0.015	0.028	0.043	-0.045	0.082	0.126
$\mathbf{\Psi}_L\mathbf{B}_H$	-0.027	0.029	0.056	-0.080	0.084	0.164
$\mathbf{\Psi}_H\mathbf{B}_H$	-0.011	0.024	0.036	-0.033	0.072	0.105
Mean	-0.021	0.031	0.052	-0.062	0.090	0.152

Note. ϵ = population RMSEA, $\mathbf{\Psi}_L$ = large unique variances, $\mathbf{\Psi}_H$ = small unique variances, $\mathbf{B}_L$ = small structural effects and $\mathbf{B}_H$ = large structural effects..

From Table 3, across the four different population covariance or correlation matrices, the range of these residuals is much smaller when $\epsilon = 0.03$ compared to when $\epsilon = 0.09$. On average, the range of standardized population residuals for $\epsilon = 0.09$ is about three times larger than those for $\epsilon = 0.03$. Note that the mean and median of

the population residuals for each of the four generating models is zero. The pattern of standardized population residuals in Table 3 validates our manipulation of model error, and confirm that our population generating matrices reflected substantively different levels of model fit.

3.1.3 Maximum Likelihood Estimates of Model Fit

The population generating models were fit to their respective generated data structures to obtain ML estimates. Table 4 summarizes model fit information for the 36 study conditions. Although the columns containing fit information in Table 3 are ordered from left to right according to increasing correlations between the MVs, the magnitude of MV correlations did not largely affect estimated model fit. Within each level of population model fit (exact $\epsilon = 0$, good $\epsilon = 0.03$ and poor $\epsilon = 0.09$), the effect of sampling error on the estimates may be observed with decreasing sample size.

In general, the sample RMSEA $\hat{\epsilon} = 0$ when the model fit the data exactly. For population covariances (represented by $N = \infty$ in Table 4), the sample RMSEA values are equivalent to the population RMSEA values or $\hat{\epsilon} = \epsilon$. Within the good model fit condition ($\epsilon = 0.03$), increasing sampling error is associated with more bias in the direction of better model fit. Stated differently, the sample RMSEA $\hat{\epsilon}$ for $N = 1000$ and $N = 200$ are smaller than the population RMSEA value $\epsilon = 0.03$ with the latter estimate being smaller than the former estimate. It may also be observed from Table 4 that there is little effect of sampling variability on estimated model fit in the poor model fit condition or $\epsilon = 0.09$; the $\hat{\epsilon}$ values were very close to ϵ.

In sum, the data generated for the simulation study displayed the properties required to assess the effect of sample size, model fit and the magnitude of correlations on the size of fungible parameter contours and confidence regions. Before examining how these factors influence parameter uncertainty, the next section describes how the different kinds of perturbations, used in the study to compute fungible parameter con-

Table 4: Model Fit Information for Study Conditions

ϵ	N	$\boldsymbol{\Psi}_L\boldsymbol{B}_L$		$\boldsymbol{\Psi}_H\boldsymbol{B}_L$		$\boldsymbol{\Psi}_L\boldsymbol{B}_H$		$\boldsymbol{\Psi}_H\boldsymbol{B}_H$	
		$\hat{F}$	$\hat{\epsilon}$	$\hat{F}$	$\hat{\epsilon}$	$\hat{F}$	$\hat{\epsilon}$	$\hat{F}$	$\hat{\epsilon}$
0	∞	0	0	0	0	0	0	0	0
0	1000	0.059	0	0.056	0	0.056	0	0.054	0
0	200	0.277	0	0.280	0	0.289	0	0.283	0
0.03	∞	0.056	0.030	0.056	0.030	0.056	0.030	0.056	0.030
0.03	1000	0.106	0.027	0.110	0.028	0.102	0.025	0.104	0.026
0.03	200	0.338	0.021	0.338	0.021	0.343	0.022	0.337	0.020
0.09	∞	0.502	0.090	0.502	0.090	0.502	0.090	0.502	0.090
0.09	1000	0.530	0.087	0.544	0.088	0.526	0.086	0.534	0.087
0.09	200	0.793	0.088	0.784	0.087	0.781	0.087	0.774	0.086

Note. ϵ = population RMSEA, N = sample size, $\hat{F}$ = sample discrepancy function value, $\hat{\epsilon}$ = sample RMSEA, $\boldsymbol{\Psi}_L$ = large unique variances, $\boldsymbol{\Psi}_H$ = small unique variances, $\boldsymbol{B}_L$ = small structural effects and $\boldsymbol{B}_H$ = large structural effects.

tours and confidence regions, are related to one another.

3.2 Relationship among Different Kinds of Perturbations

Under the perturbation framework, the first step in the process of computing estimates for the two kinds of parameter uncertainty is to perturb the sample discrepancy function value $\hat{F}$ (see Equations 8 and 13). As described earlier, we used two perturbation schemes in the computation of fungible parameter contours; one based on a fixed value in the scale of RMSEA or $\tilde{\epsilon}$ and another based on a fixed percentage of $\hat{F}$ or $\%\hat{F}$. These two perturbation schemes are explicitly tied to some estimate of model fit. Stated differently, the size of the perturbations are in some scale of model fit. In contrast, although confidence regions may be computed from a perturbation

Table 5: Perturbation Values in Different Scales

	ϵ	N	95% Confidence Region			$\tilde{\epsilon} = 0.005$ Fungible Contour			$5\%\hat{F}$ Fungible Contour		
			F_p	$\tilde{\epsilon}$	$\%\hat{F}$	F_p	χ^2 Quantile	$\%\hat{F}$	F_p	χ^2 Quantile	$\tilde{\epsilon}$
	0	1000	0.006	0.007	9.19	0.004	0.88	7.30	0.003	0.88	0.002
	0	200	0.030	0.000	9.82	0.037	0.97	13.21	0.014	0.97	0
$\mathbf{\Psi}_L \boldsymbol{B}_L$	0.03	1000	0.006	0.002	5.35	0.018	1.00	17.03	0.005	1.00	0.002
	0.03	200	0.030	0.010	8.18	0.014	0.76	4.24	0.017	0.76	0.006
	0.09	1000	0.006	0.001	1.12	0.055	1.00	10.46	0.026	1.00	0.002
	0.09	200	0.030	0.003	3.66	0.056	1.00	7.08	0.040	1.00	0.004
	0	1000	0.006	0	9.93	0.009	0.99	16.89	0.003	0.99	0
	0	200	0.030	0.006	9.61	0.030	0.95	10.51	0.014	0.95	0
$\mathbf{\Psi}_H \boldsymbol{B}_H$	0.03	1000	0.006	0.002	5.44	0.018	1.00	17.00	0.005	1.00	0.002
	0.03	200	0.030	0.010	8.21	0.014	0.75	4.17	0.017	0.75	0.006
	0.09	1000	0.006	0.001	1.11	0.056	1.00	10.42	0.027	1.00	0.002
	0.09	200	0.030	0.003	3.75	0.055	1.00	7.12	0.039	1.00	0.004

Note. ϵ = population RMSEA, N = sample size, F_p = perturbation in the $\hat{F}$ scale, $\tilde{\epsilon}$ = perturbation in RMSEA scale, $\%\hat{F}$ = perturbation as percentage of $\hat{F}$, $\mathbf{\Psi}_L$ = large unique variances, $\mathbf{\Psi}_H$ = small unique variances, $\boldsymbol{B}_L$ = small structural effects and $\boldsymbol{B}_H$ = large structural effects.

framework, such a "perturbation" is tied to sample size and quantiles of the χ^2 distribution (see Equation 13). Hence, the construction of confidence regions is not explicitly tied to model fit in contrast to the construction of fungible parameter contours.

Table 5 presents these three different perturbations in four different scales - minimum discrepancy function value (F_p), RMSEA ($\tilde{\epsilon}$), percentage of the sample discrepancy function value ($\%\hat{F}$) and χ^2 quantiles. Recall that $F_p = (\hat{F}^* - \hat{F})$. Note that of these scales, the first three are measures of model fit. We only report perturbation values for study conditions where all three perturbation schemes were applied. As confidence regions cannot be constructed at the level of the population, perturbations applied to population covariance matrices were not reported. Hence, Table 5 reports perturbation values for the conditions involving large unique variances and small structural effects or $\boldsymbol{\Psi}_L \boldsymbol{B}_L$ as well as small unique variances and large structural effects or $\boldsymbol{\Psi}_H \boldsymbol{B}_H$, which allow for comparisons between generating models with the largest versus the smallest correlations among MVs.

From Table 5, the perturbations applied to obtain 95% confidence regions in the scale of F, as shown in the F_p column, are constant regardless of model fit or magnitude of correlations among MVs. These perturbations are translations from the 0.95 χ^2 quantile into the scale of F, and are affected only by sample size. Specifically, for $N = 1000$ and $N = 200$, regardless of model fit and the generating model, the perturbations used to obtain 95% confidence regions in the scale of F are 0.006 and 0.030 respectively. Therefore, controlling for sample size, if a perturbation of a fixed value in F or F_p is used to compute fungible parameter values across different levels of model fit, such an approach is no different from constructing boundary points of a confidence region.

The first perturbation scheme used to compute fungible parameter contours was based on a specified RMSEA value. In particular an RMSEA perturbation of $\tilde{\epsilon} = 0.005$ was applied as this value may be interpreted as a practically insignificant change

in model fit (MacCallum, Browne & Lee, 2009). Recall that the choice of the magnitude of $\tilde{\epsilon}$ remains subjective, but rests on the principle that perturbations applied to obtain fungible parameter contours should be small to the extent that the perturbed model fit is practically no different from the fit obtained in the optimal solution. As RMSEA takes into account sample size and model error (see Equation 6), much variability was observed across the different levels of model fit, sample size and the magnitude of correlations among MVs when $\tilde{\epsilon} = 0.005$ was translated into the F scale, χ^2 quantiles and some percentage of $\hat{F}$. From Table 5, under the $\tilde{\epsilon} = 0.005$ Fungible Contour column, it may be observed that the values for F_p, χ^2 quantile and $\%\hat{F}$ do not follow a regular pattern with decreasing sample size or increasing model error. In general, when model fit is either good or poor, $\tilde{\epsilon} = 0.005$ translates into larger percentages of $\hat{F}$ and larger χ^2 quantiles for $N = 1000$ compared to $N = 200$.

The second perturbation scheme applied in the computation of fungible parameter contours was based on $\hat{F}$ directly. This perturbation was arbitrarily chosen to be 5% of $\hat{F}$. Similar to the perturbation scheme based on RMSEA, taking a percentage of $\hat{F}$ as a perturbation takes into account both model and sampling error because both types of error are incorporated in the estimates of $\hat{F}$. The translation of the perturbation value of 5% of $\hat{F}$ into the scale of F was identical across the two different levels of correlations among MVs, after controlling for model fit and sample size. For instance, in Table 5, $F_p = 0.017$ when $\epsilon = 0.03$ and $N = 200$ across the conditions of $\boldsymbol{\Psi}_L \boldsymbol{B}_L$ and $\boldsymbol{\Psi}_H \boldsymbol{B}_H$.

In sum, the perturbations used to construct confidence regions are independent of model fit and magnitude of correlations among MVs. As shown in Equation 12, these perturbations are a function of sample size, the number of focal parameters, the error rate α and the χ^2 distribution. Conversely, in order to construct meaningful fungible parameter contours, the perturbation scheme incorporates model fit information. An RMSEA perturbation $\tilde{\epsilon}$ of some fixed value is in a meaningful scale of model fit,

but this perturbation scheme does not translate to a consistent value in the scale of F or a percentage of $\hat{F}$ across the different conditions examined. Hence, fungible parameter contours constructed using $\tilde{\epsilon}$ are not comparable in the scale of F or $\%\hat{F}$. Note that RMSEA corrects for the bias in $\hat{F}$ due to sampling variability (see Equation 6). Alternatively, at the cost of interpretability in terms of model fit, a perturbation as a percentage of $\hat{F}$ allows for relative comparisons between fungible parameter contours in a scale based on the sample discrepancy function value. However, unlike RMSEA, $\hat{F}$ in itself does not correct for bias due to sampling variability. Additionally, the perturbation of $\tilde{\epsilon}$ was shown to be more sensitive to the size of correlations among MVs compared to $\%\hat{F}$. Given the advantages of using $\tilde{\epsilon}$ to construct fungible parameter contours over $\%\hat{F}$, the results to follow will mainly focus on the former approach to computing fungible parameter contours.

3.3 Factors that Impact Parameter Uncertainty

Three factors were examined for their effects on the size of confidence regions and fungible parameter contours. They are sample size, model fit, and magnitude of correlations among MVs. The following four figures (Figures 3 to 6) are visual representations of the confidence regions and fungible parameter contours obtained from the profile likelihood. Each figure corresponds to one of the four different magnitudes of correlations among MVs such that Figure 3 presents results for the large unique variances and small structural effects ($\boldsymbol{\Psi}_L\boldsymbol{B}_L$), Figure 4 corresponds to small unique variances and small structural effects ($\boldsymbol{\Psi}_H\boldsymbol{B}_L$), Figure 5 presents results for the large unique variances and large structural effects ($\boldsymbol{\Psi}_L\boldsymbol{B}_H$) and Figure 6 corresponds to small unique variances and large structural effects ($\boldsymbol{\Psi}_H\boldsymbol{B}_H$). Note that the ordering of these Figures are in terms of increasing correlations among MVs as described in Table 2. Hence, the effect of the magnitude of correlations on the size of confidence bounds and fungible parameter contours may be assessed by making visual comparisons among

these four figures.

Within each figure, the ML estimates of the focal parameters $\hat{\boldsymbol{\theta}}_f = (\hat{\beta}_{2,1}, \hat{\beta}_{3,2})'$ are represented by a black dot, located within the confidence bounds and fungible parameter contours. Confidence bounds are represented by blue colored crosses and fungible parameter contours are represented by red colored circles. For the conditions of $\boldsymbol{\Psi}_L \boldsymbol{B}_L$ and $\boldsymbol{\Psi}_H \boldsymbol{B}_H$, two sets of fungible parameter contours are represented; fungible parameter values represented by medium red colored circles are based on the $\tilde{\epsilon} = 0.005$ perturbation whereas fungible parameter values represented by dark red colored circles are based on a 5% perturbation to $\hat{F}$ (see Figures 3 and 6).

The panels within each figure are arranged such that sampling variability increases as one moves from the top panels to the bottom panels. Additionally, within each figure, the panels are arranged such that model error increases as one moves from the left panels to the right panels. Therefore, controlling for the magnitude of correlations among MVs, the effect of sample size on the two kinds of parameter uncertainty may be gleaned from making visual comparisons between the top to middle, top to bottom and middle to bottom panels within each figure. In a similar fashion, controlling for the magnitude of correlations among MVs, the effect of model fit on the size of the two kinds of parameter uncertainty may be visually assessed by comparing the left to middle, left to right and middle to right panels within each figure. It follows that the joint effect of increasing sampling variability and increasing model error, controlling for the magnitude among the MVs, may be observed from visually comparing panels along the diagonals within each figure. For example, the top left panel is compared to the middle panel and finally to the bottom right panel.

In the following subsections, the effect of each of the three factors on the size of confidence bounds and fungible parameter contours is examined. First, the effect of sample size on the two kinds of parameter uncertainty is investigated, followed by the effect of model error and finally the effect of the magnitude of MV correlations.

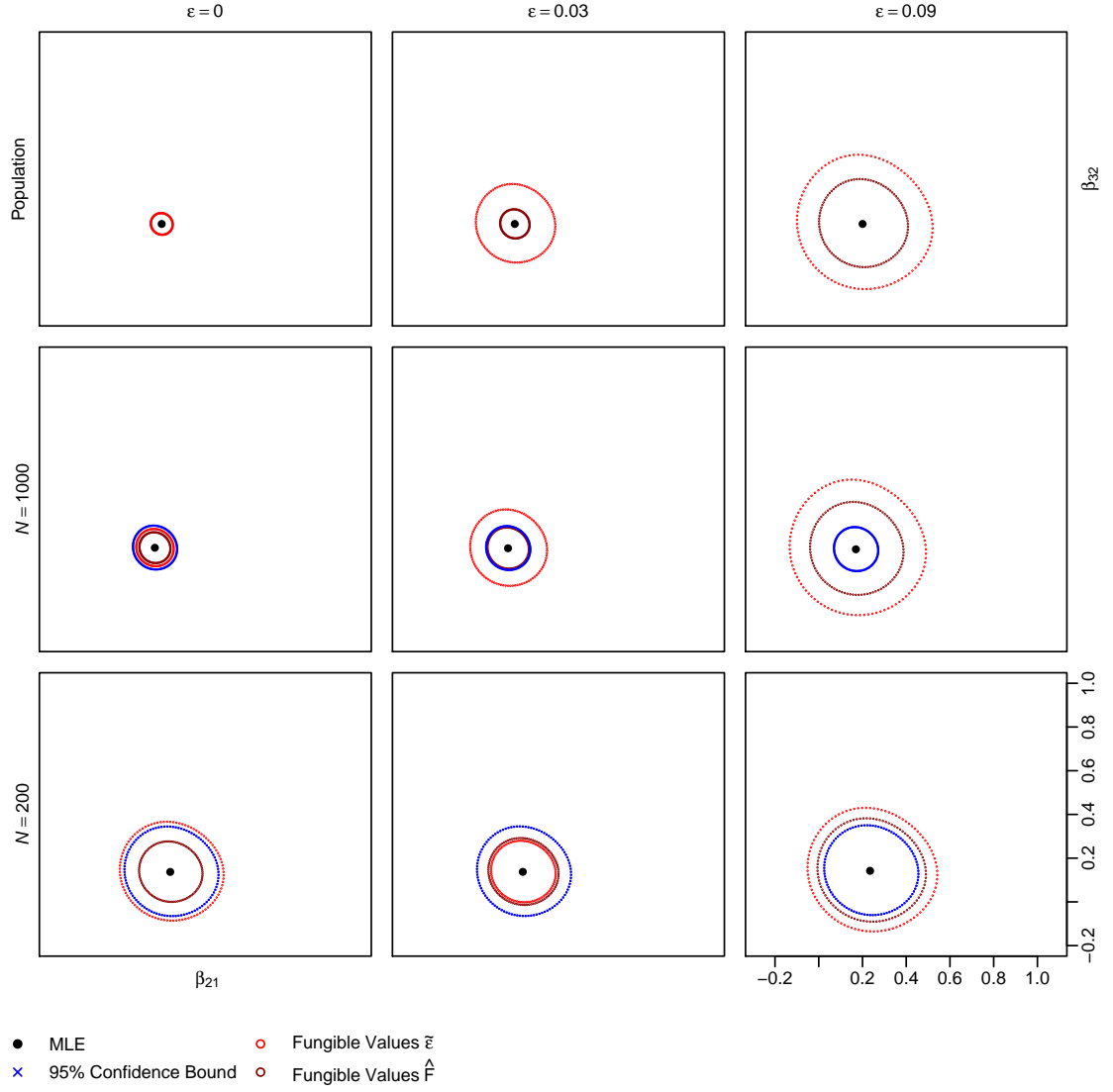Figure 3: Profile Likelihood-Based Confidence Bounds and Fungible Contours of $\beta_{2,1}$ and $\beta_{3,2}$ for $\boldsymbol{\Psi}_L \boldsymbol{B}_L$.

Figure 4: Profile Likelihood-Based Confidence Bounds and Fungible Contours of $\beta_{2,1}$ and $\beta_{3,2}$ for $\boldsymbol{\Psi}_H \boldsymbol{B}_L$.

Figure 5: Profile Likelihood-Based Confidence Bounds and Fungible Contours of $\beta_{2,1}$ and $\beta_{3,2}$ for $\boldsymbol{\Psi}_L \boldsymbol{B}_H$.
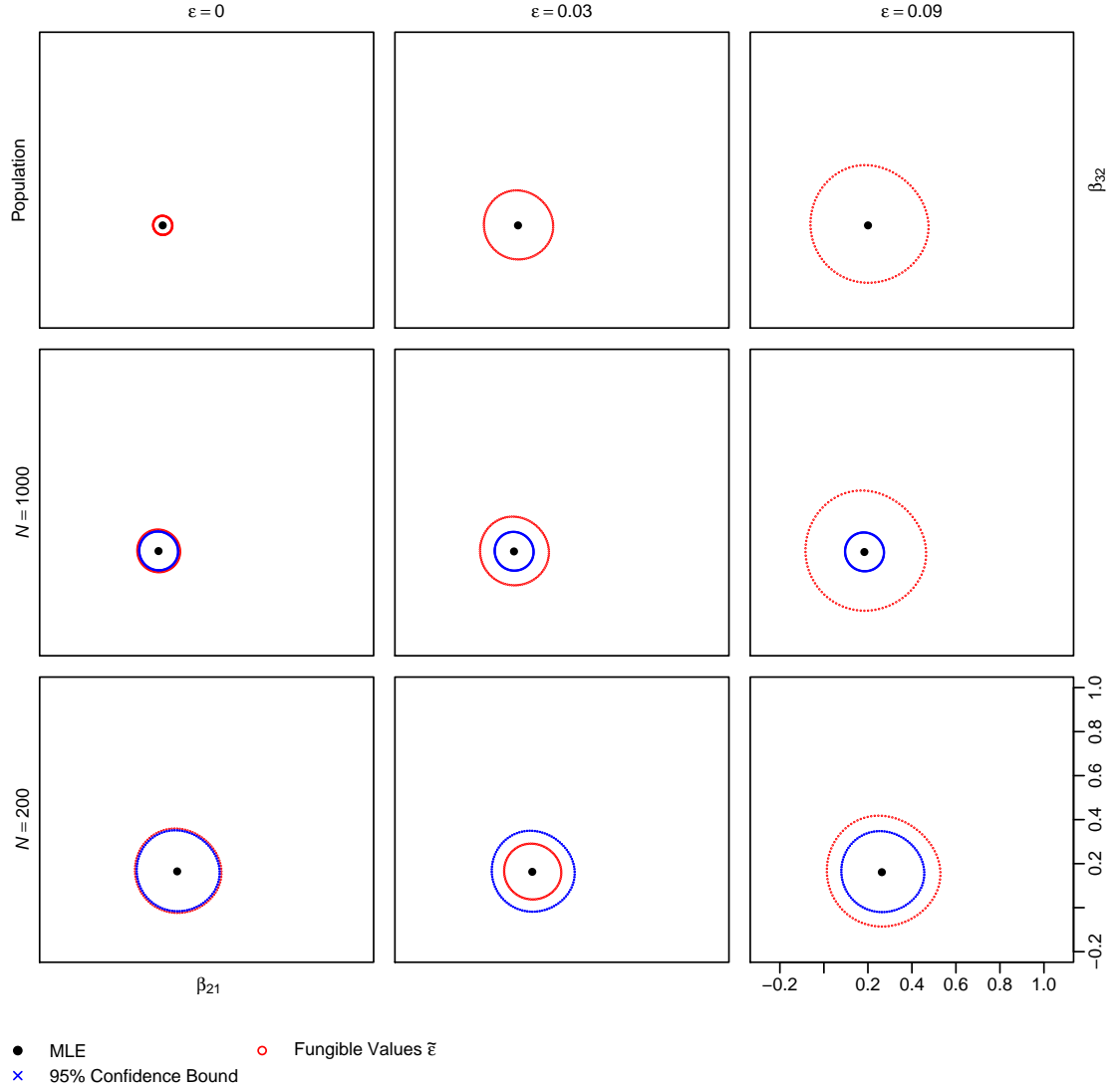
Figure 6: Profile Likelihood-Based Confidence Bounds and Fungible Contours of $\beta_{2,1}$ and $\beta_{3,2}$ for $\boldsymbol{\Psi}_H \boldsymbol{B}_H$.
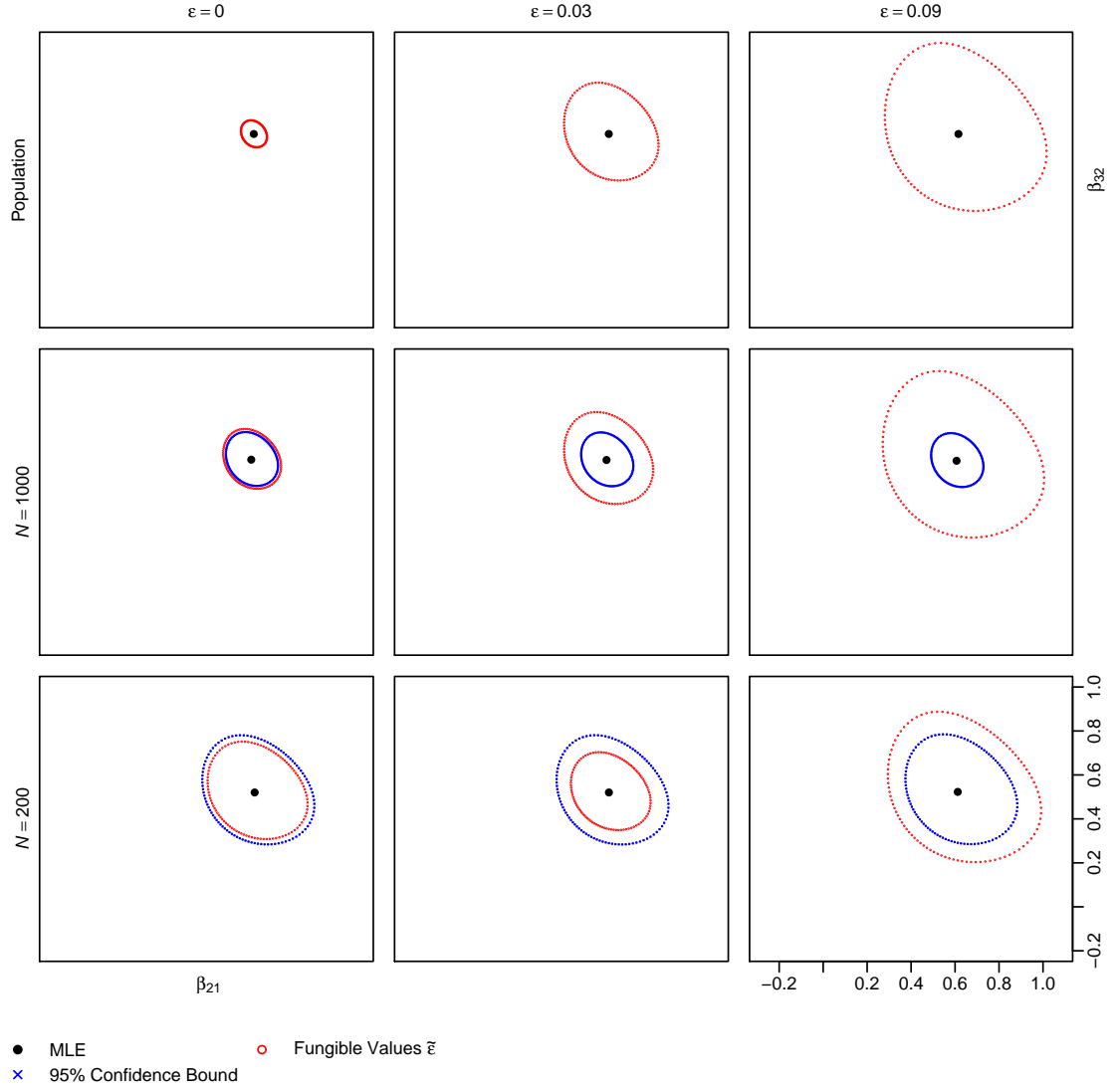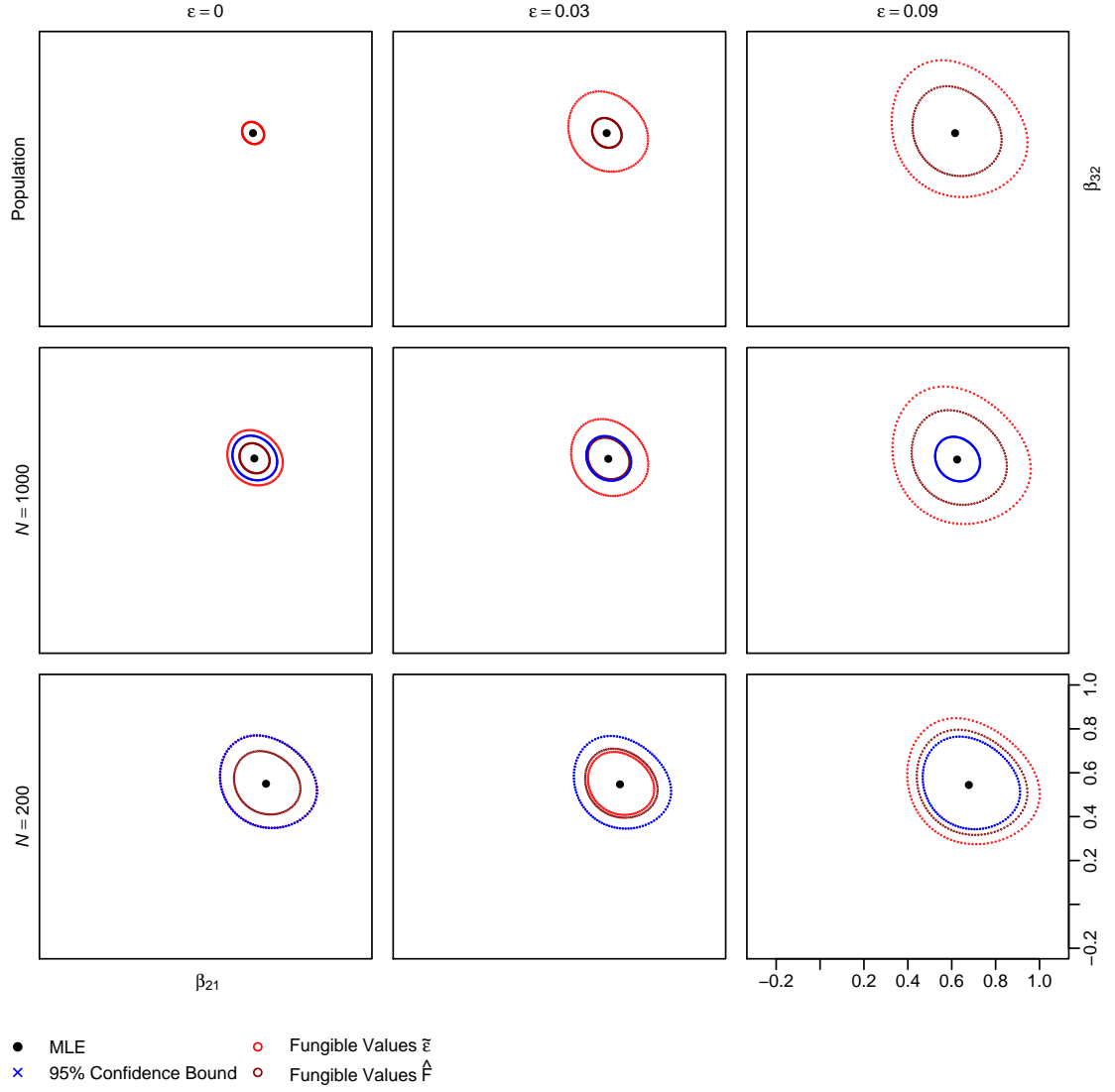
3.3.1 Sample Size

In general, sample size effects on confidence regions and fungible parameter contours can be observed by comparing the second and third rows of the plots within Figures 3 to 6. These plots suggest that with decreasing sample size, confidence regions increase in size while fungible parameter values remain somewhat constant. A more formal visual comparison may be made by overlaying plots across the levels of model fit as shown in Figure 7. In Figure 7, there are six different conditions (two levels of sample size and three levels of model fit) presented within a panel. The top panels of Figure 7 present confidence bounds and the bottom panels present fungible parameter contours. Additionally, the magnitude of correlations between the MVs increases as one moves from the left panel to the right panel.

Figure 7: Profile Likelihood-Based Confidence Bounds and Fungible Contours of $\beta_{2,1}$ and $\beta_{3,2}$ by Magnitude of Correlations among Measured Variables.
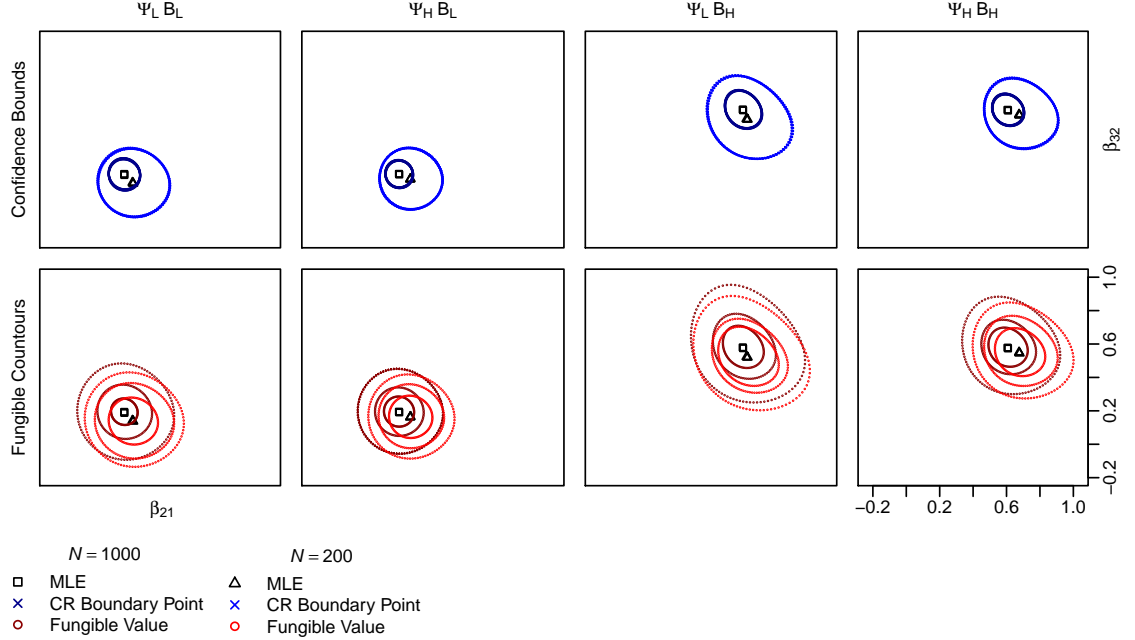

The size of confidence regions is clearly determined by sample size as shown in the top panels of Figure 7. Although there are six different elliptical forms within each

panel, it is striking that only two elliptical shapes may be observed, implying that the confidence regions for different levels of model fit within a given sample size are almost identical. Regardless of model fit, confidence bounds for the $N = 1000$ conditions as represented by dark blue colored crosses are smaller than those of the $N = 200$ conditions as represented by medium blue colored crosses. This observation is confirmed by Table 6, which presents descriptive statistics of the major and minor axes of the elliptical plots.

Table 6: Major and Minor Axis across Model Fit

		Confidence Region				Fungible Contour			
		Major Axis		Minor Axis		Major Axis		Minor Axis	
	N	Mean	SD	Mean	SD	Mean	SD	Mean	SD
$\boldsymbol{\Psi}_L\boldsymbol{B}_L$	1000	0.192	0	0.182	0	0.361	0.213	0.343	0.203
	200	0.435	0.001	0.403	0	0.459	0.151	0.425	0.139
$\boldsymbol{\Psi}_H\boldsymbol{B}_L$	1000	0.166	0	0.162	0	0.330	0.168	0.321	0.163
	200	0.379	0	0.364	0	0.391	0.128	0.376	0.123
$\boldsymbol{\Psi}_L\boldsymbol{B}_H$	1000	0.247	0	0.198	0	0.482	0.244	0.388	0.199
	200	0.555	0.001	0.435	0	0.550	0.186	0.431	0.145
$\boldsymbol{\Psi}_H\boldsymbol{B}_H$	1000	0.203	0	0.174	0	0.407	0.191	0.350	0.165
	200	0.464	0	0.393	0	0.469	0.156	0.398	0.133

Note. Fungible contours are constructed with the $\tilde{\epsilon}$ perturbation. N = sample size, $\boldsymbol{\Psi}_L$ = large unique variances, $\boldsymbol{\Psi}_H$ = small unique variances, $\mathbf{B}_L$ = small structural effects and $\mathbf{B}_H$ = large structural effects.

Across model fit and controlling for the magnitude of correlations among MVs, the major and minor axes for the confidence regions are consistently smaller for the larger sample. Additionally, the confidence regions for each sample size, across model fit, are essentially identical as evidenced by the zero and near zero standard deviations in Table 6. The non-zero standard deviations may be due to sampling variability in

that within a given sample size, the data used for the different levels of model fit are from different samples. Additionally, recall from Table 5 that the "perturbations" applied to obtain these confidence regions are identical across study conditions save for sample size. Hence, taken together, the results suggest that the size of confidence regions are not determined by model fit but by sample size and the magnitude of correlations among MVs.

Unlike confidence regions, six distinct fungible parameter contours can be observed within each of the lower panels of Figure 7. The dark red colored circles represent conditions where $N = 1000$ and the medium red colored circles represent conditions were $N = 200$. Within each panel representing fungible parameter contours, the different levels of sample size are represented by three elliptical figures, implying that the size of these fungible parameter contours are not strongly determined by sample size. There is, however, a small main effect of sample size on the size of fungible parameter contours as shown in Table 6; larger sample sizes are consistently associated with slightly smaller major and minor axes across the levels of model fit.

Sample size does not monotonically affect the size of fungible parameter contours when a perturbation based on RMSEA or $\tilde{\epsilon}$ is applied. Instead, sample size may effect the size of fungible contours in two ways. First, the $\tilde{\epsilon}$ perturbation itself is a nonlinear function of sample size, as the sample RMSEA is a nonlinear function of N (see Equation 6). Second, the minimum sample discrepancy function value $\hat{F}$, which RMSEA is a function of, incorporates sampling error in that smaller samples are associated with larger $\hat{F}$ (see Table 4). In contrast, the $\%\hat{F}$ perturbation scheme is monotonically influenced by sample size due to the sampling variability inherent in $\hat{F}$. From Table 5, the relationship between sample size and the two perturbation schemes used to compute fungible parameter contours may be observed from the F_p columns. For the $\tilde{\epsilon}$ perturbation, the size of the perturbation in the scale of F does not have a monotonic relationship with sample size, unlike the $\%\hat{F}$ perturbation. For the latter

perturbation scheme, larger sample sizes are consistently associated with smaller perturbations (in the scale of F) which results in smaller fungible parameter contours.

In sum, sample size directly affects the size of confidence regions due to its influence on the "perturbation" applied to construct them (see Equation 16). Although the size of fungible parameter contours are somewhat influenced by sample size, the effect of sample size is relatively small compared to that of model fit. In the next section, we explore how model fit affects confidence regions and fungible parameter contours.

3.3.2 Model Fit

As suggested in the previous section on sample size effects, confidence regions are independent of model fit. Visual comparisons moving from the left to the right panels within Figures 3 to 6 suggest that confidence regions remain essentially constant across the three levels of model fit. Alternatively, it may be observed from Figure 7 and Table 6 that there is little to no variability in the size of confidence regions across the three levels of model fit examined. This finding is clearly a result of the fact that confidence regions do not incorporate information on model fit in their construction.

In contrast, fungible parameter contours are strongly influenced by model fit as the perturbations applied to construct them are determined by some function of how well the estimated model fits to the data. The $\%\hat{F}$ perturbation directly incorporates model error as it is a function of $\hat{F}$ which quantifies the discrepancy between the model and data. Although the RMSEA perturbation $\tilde{\epsilon}$ is a fixed value, this fixed perturbation translates to very different values in the scale of F or F_p as demonstrated in Table 5 (cf. Chen, Curran, Bollen, Kirby & Paxton, 2008). Stated differently, the $\tilde{\epsilon} = 0.005$ perturbation translates into different values of F_p depending on sample size and model error.

From Figures 3 to 6, at the level of the population and at $N = 1000$, model

lack of fit shows a monotonic increasing relationship with the size of fungible parame-
ter contours constructed using $\tilde{\epsilon}$ and $\%\hat{F}$. As one makes visual comparisons moving
from the left to right panels within these four figures, the size of the fungible contours
increases with increasing model error. At $N = 200$, the size of fungible parameter con-
tours based on the $\%\hat{F}$ perturbation shows the same monotonic relationship in that
increasing model error is associated with larger contours (see Figures 3 and 6). How-
ever, the size of fungible parameter contours based on $\tilde{\epsilon}$ at $N = 200$ do not display
this monotonic increasing relationship with model fit (see third row of plots within Fig-
ures 3 to 6). Hence, when $\tilde{\epsilon}$ is applied to construct fungible parameter contours, sam-
ple size and model fit interact to influence the size of these contours.

These observations concerning the size of fungible parameter contours are cor-
roborated in Table 7 which presents descriptive statistics of the major and minor axes
of the concerned elliptical plots for $\boldsymbol{\Psi}_L\boldsymbol{B}_L$ and $\boldsymbol{\Psi}_H\boldsymbol{B}_H$. Note that the pattern of re-
sults for $\boldsymbol{\Psi}_H\boldsymbol{B}_L$ and $\boldsymbol{\Psi}_L\boldsymbol{B}_H$ is similar for the $\tilde{\epsilon}$ perturbation scheme and is thus not
presented. From Table 7, under the $\tilde{\epsilon}$ perturbation scheme, the minor and major axis
of the elliptical figures increase with increasing model error for the population ($N =$
∞) and $N = 1000$. However, for $N = 200$, the major and minor axis of the elliptical
figures are smallest for $\epsilon = 0.03$ followed by $\epsilon = 0$ and then $\epsilon = 0.09$. In comparison,
the major and minor axes of the fungible parameter contours, obtained from the alter-
native $\%\hat{F}$ perturbation scheme, displayed a monotonic increasing relationship with
model error.

The size of fungible parameter contours is mirrored by the magnitude of their
respective perturbations in the scale of F. We shall first focus on the interaction effect
between model fit and sample size on the size of fungible parameter contours based on
the RMSEA perturbation $\tilde{\epsilon}$. From Table 5, the value of F_p for $N = 200$ and $\boldsymbol{\Psi}_L\boldsymbol{B}_L$
is 0.037, 0.014 and 0.056 for perfect, good and poor levels of model fit, respectively; a
similar pattern may also be observed for $\boldsymbol{\Psi}_H\boldsymbol{B}_H$. For $N = 1000$, however, a mono-

Table 7: Major and Minor Axis for Two Sets of Fungible Parameter Contours

	ϵ	N	$\tilde{\epsilon}$ Fungible Contour		$\%\hat{F}$ Fungible Contour	
			Major Axis	Minor Axis	Major Axis	Minor Axis
	0	∞	0.095	0.090		
	0.03	∞	0.343	0.325	0.132	0.125
	0.09	∞	0.580	0.549	0.398	0.378
	0	1000	0.158	0.150	0.135	0.128
$\mathbf{\Psi}_L\mathbf{B}_L$	0.03	1000	0.323	0.307	0.180	0.171
	0.09	1000	0.566	0.538	0.404	0.384
	0	200	0.457	0.425	0.293	0.272
	0.03	200	0.285	0.266	0.324	0.301
	0.09	200	0.567	0.527	0.501	0.463
	0	∞	0.104	0.089		
	0.03	∞	0.376	0.322	0.140	0.119
	0.09	∞	0.635	0.545	0.420	0.359
	0	1000	0.252	0.216	0.137	0.117
$\mathbf{\Psi}_H\mathbf{B}_H$	0.03	1000	0.349	0.300	0.189	0.162
	0.09	1000	0.620	0.534	0.429	0.369
	0	200	0.462	0.391	0.318	0.269
	0.03	200	0.317	0.268	0.347	0.294
	0.09	200	0.628	0.534	0.526	0.446

Note. ϵ = population RMSEA, N = sample size, $\tilde{\epsilon}$ = perturbation in the RMSEA scale, $\%\hat{F}$ = perturbation as a percentage of $\hat{F}$, $\mathbf{\Psi}_L$ = large unique variances, $\mathbf{\Psi}_H$ = small unique variances, $\mathbf{B}_L$ = small structural effects and $\mathbf{B}_H$ = large structural effects.

tonic increasing relationship between F_p and model fit is observed for the RMSEA perturbation $\tilde{\epsilon}$. Hence, the complex relationship between model fit and sample size is manifested in the sizes of the fungible parameter contours as a function of the mag-

nitude of $\tilde{\epsilon}$ in the scale of F or F_p. Similarly, the size of fungible parameter contours constructed using the alternative $\%\hat{F}$ perturbation reflects the magnitude of the perturbation applied in F_p. Large fungible contours are associated with large F_p whereas small fungible contours are associated with small F_p.

In summary, confidence regions are not influenced by model fit. In contrast, the size of fungible parameter contours are strongly affected by model fit. Depending on the perturbation scheme, the effect of model fit may interact with sample size to affect the size of fungible parameter contours. Beyond sample size and model fit, the magnitude of correlations among MVs was also examined for its effect on the sizes of the two kinds of parameter uncertainty.

3.3.3   Magnitude of Correlations

Recall that there were four different levels of the magnitude of correlations among MVs (see Table 2). These four population covariances or correlations were derived from two approaches of controlling the size of correlations among MVs $-$ by manipulating either the size of unique variances in $\boldsymbol{\Psi}$ or the size of structural effects in $\boldsymbol{B}$. By comparing panels of the same location across Figures 3 to 6, the effect of the size of correlations among MVs may be observed. However, to aid in visual comparisons, Figure 8 presents the confidence regions and fungible parameter contours for the four different conditions within a single panel.

In Figure 8, the confidence regions are formed by blue colored crosses and the fungible parameter contours are formed by red colored circles. There are only two plots of confidence bounds for each level of sample size as confidence regions did not change across the different levels of model fit examined (see Tables 6 and 8). In contrast, because fungible parameter contours are influenced by model fit, there are six of these panels; moving from the left to right panels shows how increasing model error affects the size of the fungible parameter contours for the four different covariance structures.

Figure 8: Profile Likelihood-Based Confidence Bounds and Fungible Contours of $\beta_{2,1}$ and $\beta_{3,2}$ by Model Fit and Sample Size.
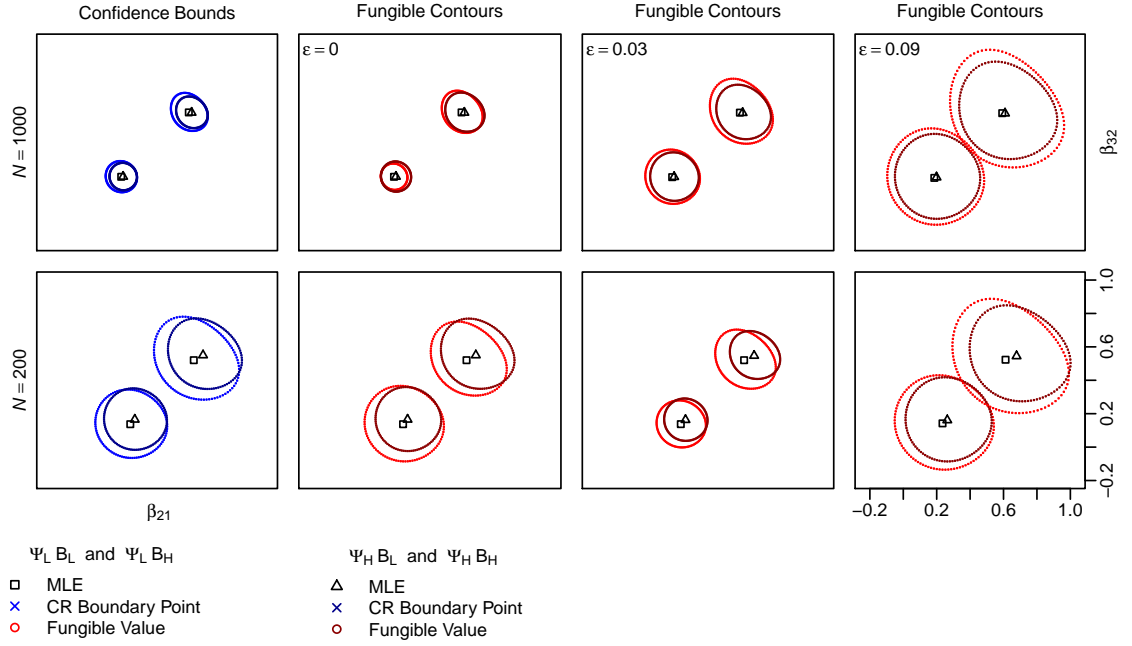
Additionally, the MLEs of the focal parameters $\hat{\boldsymbol{\theta}}_f = (\hat{\beta}_{2,1}, \hat{\beta}_{3,2})'$ are represented either as squares or triangles such that squares relate to estimates based on large unique variances $\boldsymbol{\Psi}_L$, and triangles relate to estimates based on small unique variances $\boldsymbol{\Psi}_H$. In a similar fashion, dark blue colored crosses and dark red colored circles, respectively, represent confidence regions and fungible parameter contours for solutions based on small unique variances $\boldsymbol{\Psi}_H$; medium colored blue crosses and medium colored red circles represent confidence bounds and fungible contours based on large unique variances $\boldsymbol{\Psi}_H$.

It may be observed from Figure 8 that confidence bounds and fungible parameter contours based on smaller unique variances $\boldsymbol{\Psi}_L$, holding structural effects constant, are smaller than those based on larger unique variances $\boldsymbol{\Psi}_H$. This pattern may be visually confirmed by comparing the dark blue and dark red colored figures with similar elliptical shapes against their medium blue and medium red colored counterparts. The darker colored figures are smaller than their lighter colored counterparts, save for the

fungible parameter contours where $N = 1000$, model fit is perfect and $\boldsymbol{B}_L$. This inconsistency may be attributed to the complex relationship between the magnitude of the perturbation $\tilde{\epsilon}$, in the scale of $\hat{F}$ with model error and sample size (see Table 5).

The effect of manipulating structural effects, holding unique variances constant, on the size of the two kinds of parameter uncertainty may be seen from comparing the same colored plots against each other within a panel of Figure 8. As anticipated, the focal parameter estimates $\hat{\boldsymbol{\theta}}_f$ associated with $\boldsymbol{B}_H$ are located further away from the zero point compared to those associated with $\boldsymbol{B}_L$; thus, the former estimates may be interpreted with more rigor as their confidence regions and fungible parameter contours are less likely to overlap $\boldsymbol{\theta}_f = \boldsymbol{0}$ compared to the latter estimates. Within each panel, the elliptical figures to the bottom left which have smaller structural effects are consistently smaller than the elliptical figures to the top right which have larger structural effects. In general, holding unique variances constant, smaller structural effects $\boldsymbol{B}_L$ are associated with smaller confidence regions and fungible parameter contours compared to larger structural effects $\boldsymbol{B}_H$. Additionally, the elliptical shapes associated with smaller structural effects are more circular in form compared to those associated with larger structural effects.

Although it was hypothesized that the sizes of confidence regions and fungible parameter contours for the large unique variances and small structural effects $\boldsymbol{\Psi}_L \boldsymbol{B}_L$ would be smaller than those for the small unique variances and large structural effects $\boldsymbol{\Psi}_H \boldsymbol{B}_H$, due to the latter having the largest correlations among MVs and the former having the smallest correlations among MVs (see Table 2), this hypothesis was not supported. From Figure 8, the lighter colored elliptical figures within each panel located to the bottom left were consistently smaller than the darker colored elliptical figures located to the top right. Therefore, contrary to expectations, the confidence regions and fungible parameter contours for $\boldsymbol{\Psi}_L \boldsymbol{B}_L$ were smaller than those for $\boldsymbol{\Psi}_H \boldsymbol{B}_H$. The sizes of confidence regions and fungible contours were smallest for $\boldsymbol{\Psi}_H \boldsymbol{B}_L$ and

largest for $\boldsymbol{\Psi}_L\boldsymbol{B}_H$. In Figure 8, within each of the eight panels, one may juxtapose the size of the darker colored elliptical figures located to the bottom left against the lighter colored elliptical figures located to the top right.

Table 8: Major and Minor Axis by Magnitude of Correlations among MVs

	Confidence Regions							
	\multicolumn{4}{c	}{N = 1000}			\multicolumn{4}{c}{N = 200}			
	Major Axis		Minor Axis		Major Axis		Minor Axis	
Condition	Mean	SD	Mean	SD	Mean	SD	Mean	SD
$\boldsymbol{\Psi}_L\boldsymbol{B}_L$	0.192	0	0.182	0	0.435	0.001	0.403	0
$\boldsymbol{\Psi}_H\boldsymbol{B}_L$	0.166	0	0.162	0	0.379	0	0.364	0
$\boldsymbol{\Psi}_L\boldsymbol{B}_H$	0.247	0	0.198	0	0.555	0.001	0.435	0
$\boldsymbol{\Psi}_H\boldsymbol{B}_H$	0.203	0	0.174	0	0.464	0	0.393	0

	Fungible Parameter Contours							
	\multicolumn{4}{c	}{N = 1000}			\multicolumn{4}{c}{N = 200}			
	Major Axis		Minor Axis		Major Axis		Minor Axis	
Condition	Mean	SD	Mean	SD	Mean	SD	Mean	SD
$\boldsymbol{\Psi}_L\boldsymbol{B}_L$	0.361	0.213	0.343	0.203	0.459	0.151	0.425	0.139
$\boldsymbol{\Psi}_H\boldsymbol{B}_L$	0.330	0.168	0.321	0.163	0.391	0.128	0.376	0.123
$\boldsymbol{\Psi}_L\boldsymbol{B}_H$	0.482	0.244	0.388	0.199	0.550	0.186	0.431	0.145
$\boldsymbol{\Psi}_H\boldsymbol{B}_H$	0.407	0.191	0.350	0.165	0.469	0.156	0.398	0.133

Note. N = sample size, $\boldsymbol{\Psi}_L$ = large unique variances, $\boldsymbol{\Psi}_H$ = small unique variances, $\mathbf{B}_L$ = small structural effects and $\mathbf{B}_H$ = large structural effects.

The observations drawn from Figure 8 are consistent with the size of the major and minor axes of these elliptical shapes in Table 8. The mean major and minor axes of the two kinds of parameter uncertainty are consistently larger for the $\boldsymbol{\Psi}_L$ con-

ditions compared to the $\boldsymbol{\Psi}_H$ conditions. For example, for fungible parameter contours at $N = 1000$ and large structural effects $\boldsymbol{B}_H$, the major and minor axes are larger for $\boldsymbol{\Psi}_L$ ($M = 0.482$, $SD = 0.244$ and $M = 0.388$, $SD = 0.199$) compared to $\boldsymbol{\Psi}_H$ ($M = 0.407$, $SD = 0.191$ and $M = 0.350$, $SD = 0.165$). In terms of structural effects, holding unique variances constant, the major and minor axes of the two kinds of parameter uncertainty are larger for $\boldsymbol{B}_H$ as opposed to $\boldsymbol{B}_L$. Additionally, contrary to our hypothesis, the major and minor axes of confidence regions and fungible parameter contours in Table 8 for $\boldsymbol{\Psi}_L\boldsymbol{B}_L$ are smaller than those of $\boldsymbol{\Psi}_H\boldsymbol{B}_H$. As observed in Figure 8, the major and minor axes of the two kinds of parameter uncertainty for $\boldsymbol{\Psi}_H\boldsymbol{B}_L$ are the smallest whereas they are largest for $\boldsymbol{\Psi}_L\boldsymbol{B}_H$.

These results suggest that it may not be the size of correlations among the MVs that directly affect the size of the confidence regions and fungible parameter contours, by changing the shape of the likelihood surface, but the magnitude of the variances and covariances of the MVs. A decrease in the MV variances from $\boldsymbol{\Psi}_L$ to $\boldsymbol{\Psi}_H$ (see Table 2) seems to be associated with a steeper likelihood surface as manifested by tighter confidence regions and fungible parameter contours as shown in Figure 8. In contrast, increasing the size of structural effects causes the shape of the likelihood surface (as manifested by confidence regions and fungible parameter contours) to become less steep and to depart from a circular form. Recall that an increase in the structural effects from $\boldsymbol{B}_L$ to $\boldsymbol{B}_H$ led to larger variances and covariances among the MVs as shown in Table 2. Hence, the increase in the size of the elliptical shapes from $\boldsymbol{B}_L$ to $\boldsymbol{B}_H$ may be due to the increase in the variances of the MVs. Additionally, the lengthening of the elliptical forms from $\boldsymbol{B}_L$ to $\boldsymbol{B}_H$ may be due to the focal parameters becoming more correlated in the latter condition; across all other factors, the covariance between the focal parameters for $\boldsymbol{B}_H$ was larger in magnitude ($M = -0.179$, $SD = 0.062$) compared to $\boldsymbol{B}_L$ ($M = -0.028$, $SD = 0.012$).

Taken together, these results suggest that manipulating the size of the corre-

lations among the MVs changes the likelihood surface, and that affects the size and shape of confidence regions and fungible parameter contours. However, it is not the magnitude of correlations among MVs that determine the degree of the two kinds of parameter uncertainty. Larger structural effects, resulting in larger correlations among MVs, were associated with larger confidence bounds and fungible parameter contours. Alternatively, smaller unique variances which resulted in larger correlations among MVs were associated with smaller confidence bounds and fungible contours. Instead, the effects of altering unique variances in $\boldsymbol{\Psi}$ and structural effects in $\boldsymbol{B}$ on the size of confidence regions and fungible parameter contours may be better understood by their effect on the variances and covariances of the MVs.

3.4   Population Covariances

Fungible parameter contours may be computed at the level of the population as shown in the first row of panels of Figures 3 to 6. Note that the perturbation $\tilde{\epsilon}$ which is added to the RMSEA in the population does not involve sample size (see Equation 5). We examine the extent to which fungible parameter contours are free of sampling variability by comparing contours computed at the population to their sample counterparts. Visual comparisons may be made within Figures 3 to 6 by comparing the top panels to the middle and bottom panels. To allow for better visual comparisons, Figure 9 presents fungible contours computed by the two perturbation schemes ($\tilde{\epsilon}$ and $\%\hat{F}$) by sample size and model fit for the conditions of $\boldsymbol{\Psi}_L\boldsymbol{B}_L$ and $\boldsymbol{\Psi}_H\boldsymbol{B}_H$. Fungible parameter contours, based on the RMSEA perturbation $\tilde{\epsilon}$, for the other conditions of $\boldsymbol{\Psi}_L\boldsymbol{B}_H$ and $\boldsymbol{\Psi}_H\boldsymbol{B}_L$ are similarly influenced by model fit and sample size and thus are not displayed for brevity.

In Figure 9, the first row of plots presents fungible parameter contours based on the RMSEA perturbation $\tilde{\epsilon}$. The second row of plots shows fungible parameter contours based on the $\%\hat{F}$ perturbation. The columns within Figure 9 display fungible

Figure 9: Profile Likelihood-Based Fungible Contours of $\beta_{2,1}$ and $\beta_{3,2}$ for $\mathbf{\Psi}_L \mathbf{B}_L$ and $\mathbf{\Psi}_H \mathbf{B}_H$ by Model Fit and Sample Size.
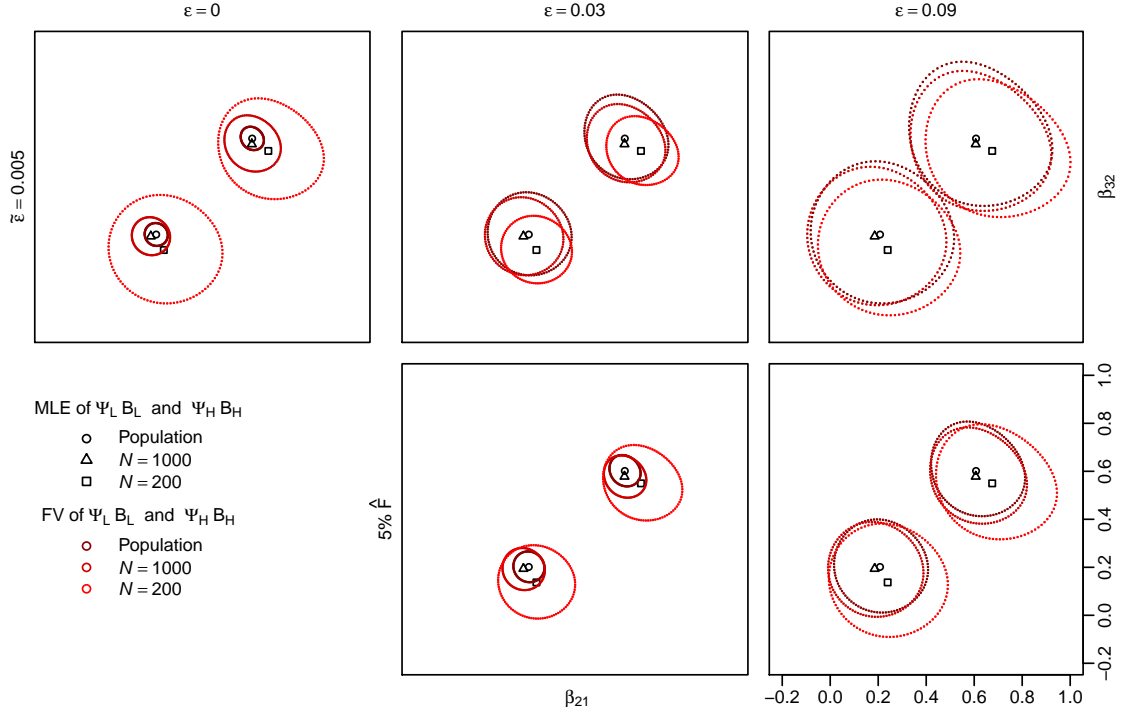
parameter values associated with different levels of model fit; moving from left to right within Figure 9 shows how these fungible contours change with increasing model error. Within each panel, the dark red colored circles represent population fungible values, the medium red colored circles represent fungible values when $N = 1000$ and the light red colored circles represent fungible values when $N = 200$. Note that fungible parameter contours based on the $\%\hat{F}$ perturbation cannot be computed when model fit is perfect in the population ($F = 0$) and thus were not plotted. Additionally, the elliptical forms to the bottom left of each panel in Figure 9 represent fungible parameter contours for $\mathbf{\Psi}_L \mathbf{B}_L$ and the elliptical forms to the top right of each panel are fungible parameter contours for $\mathbf{\Psi}_H \mathbf{B}_H$.

It may be observed from Figure 9 that fungible parameter contours computed from the $\%\hat{F}$ perturbation increase in size as sampling variability increases. Additionally, this pattern is also observed for fungible parameter contours computed from the

$\tilde{\epsilon}$ perturbation when model fit is perfect. For good model fit, the size of the fungible parameter contours based on the RMSEA perturbation $\tilde{\epsilon}$ seems to decrease with increasing sampling variability. Finally, for poor model fit, fungible parameter contours are largest in the population, followed by $N = 1000$ and then by $N = 200$; there is, however, little distinction between these contours for $N = 1000$ and $N = 200$.

Table 9: Descriptive Statistics of Major and Minor Axes for the Two Sets of Fungible Parameter Contours

| Model Fit | $\tilde{\epsilon} = 0.005$ | | $\%\hat{F} = 5\%$ | |
	Major Axis	Minor Axis	Major Axis	Minor Axis
Perfect ($\epsilon = 0$)	0.255 (0.168)	0.227 (0.148)	0.221 (0.099)	0.197 (0.086)
Good ($\epsilon = 0.03$)	0.332 (0.031)	0.298 (0.026)	0.219 (0.093)	0.195 (0.081)
Poor ($\epsilon = 0.09$)	0.599 (0.032)	0.538 (0.008)	0.447 (0.054)	0.400 (0.044)

Note. ϵ = population RMSEA. Descriptive statistics were obtained across two conditions of $\mathbf{\Psi}_L\mathbf{B}_L$ and $\mathbf{\Psi}_H\mathbf{B}_H$ and across the three levels of sampling variability. Standard deviations are presented in the parenthesis.

These observations are confirmed by the size of the major and minor axes presented in Table 7, and their respective descriptive statistics presented in Table 9 above. It is noted that the major and minor axes of the fungible parameter contours based on the $\tilde{\epsilon}$ perturbation scheme did not differ considerably between the three levels of sampling variability when model fit was good or poor as communicated by the relatively small standard deviations in Table 9. Recall that the size of these fungible parameter contours directly maps onto the magnitude of the perturbations, in the scale of F, applied to obtain them (see Table 5). Hence, the $\tilde{\epsilon}$ perturbation may be one approach that somewhat allows for comparisons between fungible parameter contours constructed from different levels of model fit and sample size.

In sum, contrary to expectation, fungible parameter contours are not based solely on model error, but incorporate information on sampling variability. Sampling

variability influences the magnitude of the perturbations used to compute fungible parameter contours as these perturbations are based on the sample minimum discrepancy function value $\hat{F}$. Controlling for model fit, the effect of sampling variability on the magnitude of $\%\hat{F}$ perturbations is monotonic and increasing (see second row of plots in Figure 9). When an RMSEA perturbation $\tilde{\epsilon}$ is used, however, sample size influences the size of these fungible parameter contours in a complex way as the sample RMSEA is a nonlinear function of sample size.

3.5 Profile and Empirical Likelihood-Based Computations

Confidence regions and fungible parameter contours may be computed from the empirical likelihood or the profile likelihood. The difference between these two likelihoods is in how nuisance parameters $\boldsymbol{\theta}_n$ are taken account of. In the empirical likelihood, the nuisance parameters $\boldsymbol{\theta}_n$ are not re-estimated with every boundary point of the confidence region or fungible parameter value; instead, nuisance parameters take on values of the ML estimates $\hat{\boldsymbol{\theta}}_n$ which were obtained jointly with the ML estimates of the focal parameters $\hat{\boldsymbol{\theta}}_f$ (see Equations 20 and 21). In contrast, nuisance parameters in the profile likelihood are re-computed (represented by $\tilde{\boldsymbol{\theta}}_n$) for every confidence bound estimate or fungible parameter value (see Equations 16 and 17). Note that the ML estimates of the nuisance parameters $\hat{\boldsymbol{\theta}}_n$, obtained jointly with the ML estimates of the focal parameters $\hat{\boldsymbol{\theta}}_f$, are distinct from $\tilde{\boldsymbol{\theta}}_n$ or the ML estimates obtained at a fixed confidence bound estimate or fungible parameter value.

Although we have presented results from the profile likelihood, we will examine how estimates of these two kinds of parameter uncertainty differ when they are computed from the profile likelihood versus the empirical likelihood. As the conditions of $\boldsymbol{\Psi}_H\boldsymbol{B}_L$ and $\boldsymbol{\Psi}_L\boldsymbol{B}_H$ are associated, respectively, with the smallest and largest confidence regions and fungible parameter contours in the profile likelihood, we will focus on these two study cells. Figure 10 presents plots of confidence regions and fungible

Figure 10: Estimated and Profile Likelihood-Based Confidence Regions and Fungible Contours of $\beta_{2,1}$ and $\beta_{3,2}$.
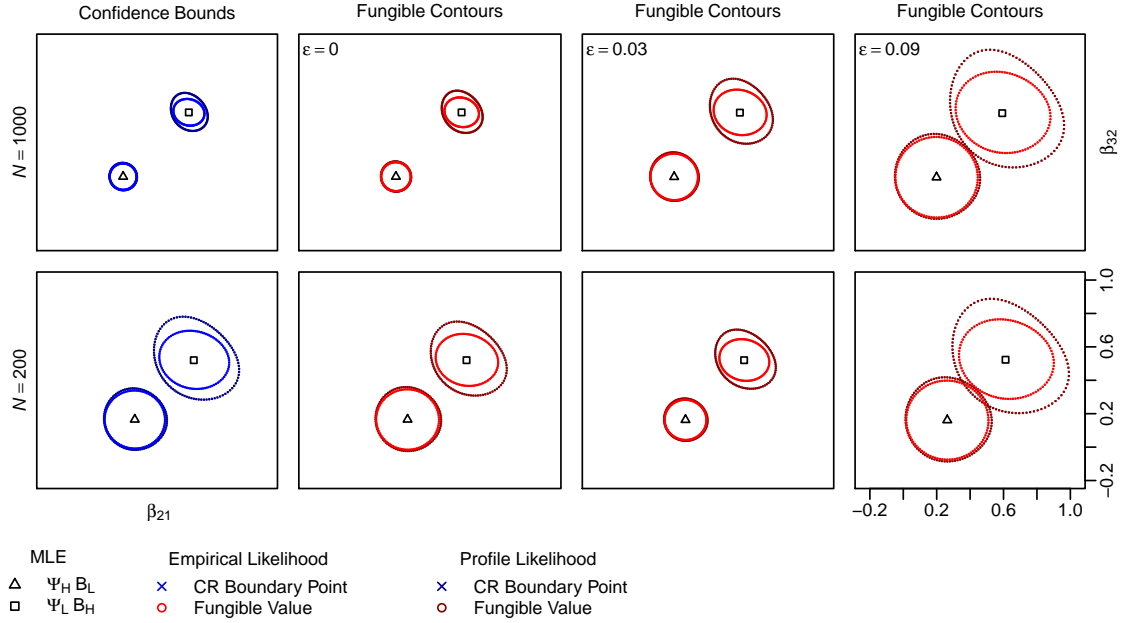
parameter contours where estimates from the empirical likelihood are overlaid with their commensurate estimates from the profile likelihood.

Confidence bounds are represented as blue colored crosses in Figure 10 and fungible parameter contours are represented as red colored circles. Note that the RMSEA perturbation $\tilde{\epsilon}$ was applied to construct these fungible parameter contours. As model fit did not influence the size of confidence regions (see Tables 6 and 8), these confidence regions are not shown for the varying levels of model fit as was done for fungible parameter contours. The panels representing fungible parameter contours are arranged such that moving from left to right is associated with increasing model error. Visual comparisons may be made between the top and bottom rows of panels within Figure 10 to assess the effect of sampling variability on the size of the confidence regions and fungible parameter contours computed from the empirical and profile likelihood. Within each panel of Figure 10, the elliptical forms situated at the bottom left are

based on small unique variances and small structural effects $\boldsymbol{\Psi}_H \boldsymbol{B}_L$ and the elliptical shapes located at the top right of each panel are based on large unique variances and large structural effects $\boldsymbol{\Psi}_L \boldsymbol{B}_H$. The two kinds of parameter uncertainty are represented in darker and lighter colors when they were computed from the profile and empirical likelihood respectively.

Table 10: Descriptive Statistics of Major and Minor Axes from the Empirical and Profile Likelihoods

Likelihood	Confidence Regions		Fungible Parameter Contours	
	Major Axis	Minor Axis	Major Axis	Minor Axis
Empirical	0.282 (0.113)	0.251 (0.098)	0.369 (0.136)	0.329 (0.123)
Profile	0.330 (0.140)	0.289 (0.114)	0.431 (0.167)	0.379 (0.140)

Note. Descriptive statistics were obtained across the four levels of magnitude of correlations between MVs, the two sample sizes and the three levels of model fit. Standard Deviations are presented in the parenthesis

It may be concluded from Figure 10 that both confidence regions and fungible parameter contours computed from the profile likelihood are consistently larger than their counterparts from the empirical likelihood. In Figure 10, the darker colored elliptical figures are larger in size compared to the lighter colored elliptical figures. Table 10 provides summary information on the major and minor axes of confidence regions and fungible parameter estimates based on the profile and estimated likelihoods, confirming these observations. Across all the study conditions involving samples, the major and minor axes of the confidence regions and fungible parameter contours are consistently larger when computations are based on the profile likelihood compared to the empirical likelihood.

In sum, when the confidence regions and fungible parameter contours are computed from the estimated likelihood, they have a tendency to communicate overly optimistic estimates of parameter uncertainty. Under the empirical likelihood, confidence

regions tend to convey optimistic precision; likewise, fungible parameter contours tend to suggest that the model description of the data under a small perturbation to model fit is more tolerable or robust. Such estimates from the profile likelihood take into account the uncertainty of the nuisance parameters $\boldsymbol{\theta}_n$, unlike the empirical likelihood. Interestingly, when the nuisance parameters are re-estimated in the profile likelihood, the shape of the likelihood surface of the focal parameters is less elliptical compared to that of the empirical likelihood in the context of large structural effects $\boldsymbol{B}_H$. Indeed, compared to the empirical likelihood, the larger and elongated profile likelihood surface for the focal parameters under the $\boldsymbol{B}_H$ condition not only takes account of the uncertainty inherent in the nuisance parameters $\boldsymbol{\theta}_n$, but also the correlations among $\boldsymbol{\theta}_n$.

Chapter 4

DISCUSSION

Confidence regions and fungible parameter values are similar in that they communicate parameter uncertainty and are both computed directly from the likelihood function. Due to these commonalities, we set out to clarify the relationship between confidence regions and fungible parameter contours by accomplishing three study objectives. First, we developed a general perturbation framework which served as a theoretical basis to lay out the analytical relationship between confidence regions and fungible parameter contours. Second, we carried out a simulation study to examine various factors that affect confidence regions and fungible parameter contours. Third, we successfully implemented a new computational procedure for obtaining confidence regions and fungible parameter contours that takes account of nuisance parameters by the profile likelihood method. In the following sections, we discuss findings for each of these objectives. We conclude with study contributions, directions for future research and end with a discussion of what applied researchers may gain from examining confidence regions and fungible parameter contours.

4.1   General Perturbation Framework

The general perturbation framework extends the theoretical framework outlined in MacCallum, Browne and Lee (2009), for constructing fungible parameter contours, to confidence regions. Hence, the two kinds of parameter uncertainty - confidence regions and fungible parameter contours - are unified under the same theoretical framework. It follows that this theoretical framework also serves as a basis for com-

puting confidence regions and fungible parameter contours from the same algorithm. Importantly, from the general perturbation framework, we show that confidence regions and fungible parameter contours are analytically related. One kind of parameter uncertainty may be numerically translated to the other, and vice versa. However, such translations may not be substantively meaningful. Even when confidence regions and fungible parameters are numerically identical, the distinction between these two kinds of parameter uncertainty continue to be important. Both kinds of parameter uncertainty contain unique information that enhance scientific conclusions.

In practice, confidence regions are a probabilistic device that convey the extent of statistical variation inherent in the parameter estimates; they provide a range of plausible population parameter values, and may be used for significance testing. Note that confidence bounds are limits to a range of parameter estimates in that any point located within the region is a set of plausible population parameter values. Furthermore, confidence regions communicate information regarding the precision of the parameter estimates, which in turn convey how well the parameter estimates generalize to the population. Additionally, confidence regions also quantify how well parameter estimates cross-validate in that with small sampling variability, parameter estimates obtained from a different sample of the same population will not differ considerably from the original parameter estimates. Hence, tight confidence regions promote strong scientific conclusions; parameter estimates with smaller confidence regions have a higher probability of being statistically significantly different from zero, have little uncertainty or more precision and tend to generalize and cross-validate better than parameter estimates with larger confidence regions. Therefore, by quantifying parameter uncertainty in relation to the population of interest, the information embodied by confidence regions allow analysts to make probabilistic inferences.

Fungible parameter contours, in contrast, convey information about how sensitive parameter estimates are to a perturbation to model fit. Unlike confidence re-

gions, fungible parameter contours do not contain information regarding the population which the sample is drawn from. Instead, they communicate parameter uncertainty of the solution in relation to model fit. Note that unlike confidence regions, only points lying on the fungible contour are of interest; these parameter values that make up the contour are exchangeable, alternative parameter values that are associated with the same model fit that is practically no different than the best model fit. Stated differently, fungible parameter values may be considered to be equally good descriptors of the data compared to the optimal solution. In this vein, fungible parameter contours carry diagnostic value. Small fungible contours imply that there is a limited range of parameter values that describe the sample data equally well in terms of model fit, giving assurance that the model description of the data is robust. Therefore, from a practical standpoint, tight fungible parameter contours promote strong scientific conclusions in that they show that parameter estimates are robust to a minute change in model fit.

Although fungible parameter values are alternative parameter values that describe the data practically as well as the ML estimates in terms of model fit, they are not strictly estimators for a set of population parameters. Therefore, fungible values do not have statistical properties such as unbiasedness, efficiency, sufficiency and consistency. Instead, fungible parameter contours are a diagnostic device used to assess the robustness of the solution to a small change in model fit. Alternatively, each fungible parameter value on the contour may be considered as potential ML estimates of competing models. In particular, these hypothetical competing models have the same user-specified model fit that is slightly poorer than the optimal solution. In this vein, if one considers fungible parameter values to be alternative ML solutions to hypothetical competing models with some user-specified lack of fit, these estimates would have statistical properties of unbiasedness, efficiency, sufficiency and consistency. However, this view is complicated by the fact that the full parametric specification of these hypothet-

ical alternative models is unknown and probably unknowable. For present purposes we find it most useful to consider fungible parameter values to simply represent alternative and optimal parameter values for a given model lacking any optimal statistical properties.

Associated with these interpretational differences, several modelling factors were found to affect confidence regions and fungible parameter contours differentially. We summarize how several modelling factors - sample size, model fit and the magnitude of correlations among measured variables (MVs) - affect these two kinds of parameter uncertainty.

4.2   Factors that Impact Parameter Uncertainty

Recall that confidence regions and fungible parameter contours are computed from the likelihood function, which combines information from the sample data and the specified model. In particular, the likelihood function represents the likelihood of the model parameters given the data. Under maximum likelihood (ML) estimation, the ML estimates of the parameters are estimates that make the observed data most likely. For a model with $k = 1$ parameter, the likelihood function spans a two-dimensional space; one dimension for the parameter, and the second dimension for its likelihood. For a model with $k = 2$ parameters, the likelihood function spans a three-dimensional space; one dimension for each parameter and the third dimension for their joint likelihood. It follows that for k parameters, the likelihood function spans a $k+1$-dimensional space. Note also that the ML parameter estimates are unique, and take on values where the likelihood is at its maximum. As the likelihood surface is convex, more than one set of parameter values is associated with likelihood values that are not the maximum.

Both confidence regions and fungible parameter contours consist of parameter values at some determined likelihood value that is not the ML. With $k = 1$ parame-

ter, two estimates make up the confidence interval, and there are two fungible parameter values. With $k = 2$ parameters, elliptical figures composed of parameter values make up the confidence bound and/or fungible parameter contours. More generally, with k parameters, the two kinds of parameter uncertainty would each be represented by k-dimensional hyper-elliptical forms. Regardless of the number of parameters, the k-dimensional confidence regions or fungible parameter contours may be regarded as slices of the likelihood function or surface. In general, given the same likelihood value, steeper likelihood surfaces are associated with tighter confidence regions and parameter contours whereas flatter likelihood surfaces are associated with more parameter uncertainty. Hence, confidence regions and fungible parameter contours are determined by the shape of the likelihood surface, as well as the likelihood value that defines their parameter values.

The modelling factors considered in our study affect confidence regions and fungible parameter contours in two main ways. First, they could influence the size of the perturbation applied to construct these two kinds of parameter uncertainty. Stated differently, these modelling factors could affect the likelihood value at which the parameter values are taken to form confidence regions and/or fungible parameter contours. Second, the modelling factors could change the shape of the likelihood surface thereby affecting confidence regions and fungible parameter contours. Below, we describe how sample size, model fit and the magnitude of correlations among MVs affected confidence regions and fungible parameter contours in these two ways.

4.2.1 Size of Perturbation

The "perturbation" applied as a first step to constructing confidence regions is determined by sample size, the error rate α and the χ^2 quantile. Larger sample sizes, larger error rates and smaller quantiles are associated with smaller "perturbations" and consequently tighter confidence regions. Conversely, smaller sample sizes, smaller er-

ror rates and larger quantiles are associated with larger "perturbations" that result in larger confidence regions. Additionally, the "perturbation" used to construct confidence regions is independent of model fit. In sum, as the "perturbation" applied to compute confidence regions is a function of sample size and not model fit, confidence regions carry information regarding sampling variability and not model error.

In comparison, the two different perturbation schemes used in our simulation study to compute fungible parameter contours are affected largely by model fit and, to a lesser extent, sample size. Recall that one perturbation was a fixed value of RMSEA or $\tilde{\epsilon}$ and the other was a specified percentage of the sample discrepancy function value or $\%\hat{F}$. Across these two perturbation schemes, larger perturbations (translated to the scale of the discrepancy function value F) are associated with larger fungible parameter contours and vice-versa. Unlike the "perturbation" applied to construct confidence regions, which is determined primarily by sample size, the perturbations used for computing fungible parameter contours primarily incorporate information on model fit and, to a much smaller extent, sample size.

Although the two perturbation schemes applied to compute fungible parameter contours displayed similar properties, there were several notable subtle differences. First, model fit and sample size interacted in a complex way to determine the size of the RMSEA perturbation or $\tilde{\epsilon}$ when it was transformed into the scale of F (see Table 5). In contrast, model error and sampling variability were strictly positively monotonically related to the size of the $\%\hat{F}$ perturbation. This distinction is due to the fact that the $\tilde{\epsilon}$ perturbation corrects for bias due to sampling variability whereas the $\%\hat{F}$ perturbation does not. Second, the $\tilde{\epsilon}$ perturbation takes on a fixed RMSEA value that is in a meaningful metric of model fit. The $\%\hat{F}$ perturbation, however, is relative and remains in the scale of F. By remaining in the scale of F, the $\%\hat{F}$ perturbation is difficult to interpret directly in terms of model fit. As a result, fungible parameter contours, across different data sets and models, that are constructed from a $\tilde{\epsilon}$ perturba-

tion may be compared against one another. In contrast, as the $\%\hat{F}$ perturbation is relative, fungible parameter contours based on this perturbation scheme may not be compared against similarly constructed fungible contours on some fixed level of model fit.

In sum, confidence regions and fungible parameter contours are distinct in that sample size and model fit differentially affect the size of the perturbations applied to construct these two kinds of parameter uncertainty. Specifically, the size of the perturbation used to compute confidence regions is affected by sample size. However, the size of perturbations applied to construct fungible parameter contours are affected primarily by model fit and, to a limited extent, sample size.

4.2.2 Likelihood Surface

As confidence regions and fungible parameter contours are both based on the likelihood surface, the factors that affect the likelihood surface would therefore affect both kinds of parameter uncertainty. Although it was hypothesized that changes in model fit and the magnitude of correlations among MVs would alter the shape of the likelihood surface, these hypotheses were disconfirmed. Instead, model fit was found to affect only the size of the perturbations used to compute fungible parameter contours. Additionally, it was the size of the MV variances that affected the steepness of the likelihood surface instead of the magnitude of the correlations among MVs. In general, the smaller the MV variances, the steeper the likelihood surface and vice-versa. With steeper likelihood surfaces, confidence regions and fungible parameter contours tend to be tighter. Conversely, shallower likelihood surfaces are associated with more parameter uncertainty.

The computational procedure used to take account of nuisance parameters also affects the observed steepness and shape of the likelihood surface of the focal parameters as manifested in the computed confidence regions and fungible parameter con-

tours. In the next section, we discuss uncertainty parameter computations based on the profile and empirical likelihood.

4.3 Computational Procedure

Confidence regions and fungible parameter contours, computed following the general perturbation framework, are based on the Brent (1973) method of root finding. These computations are exact, and are computationally more efficient compared to a basic grid search. Based on the work of MacCallum, Browne and Lee (2009), we have extended their computational procedure beyond obtaining fungible parameter contours to confidence regions. Additionally, these two kinds of parameter uncertainty may be obtained for more than two focal parameters. Note that computing these estimates of parameter uncertainty for some number of focal parameters is feasible only when there is a computationally tractable number of direction vectors required to adequately span the focal parameter space.

With increasing numbers of parameters, locating the desired confidence bound or fungible parameter contour becomes computationally burdensome. When $k = 1$ parameter, $T = 2$ direction vectors are required to span the one-dimensional parameter space. With $k = 2$ parameters, suppose that T directional vectors adequately sample the two-dimensional parameter space. When $k = 3$, T^2 directional vectors are required to sample the three-dimensional space with the same coverage as the two-dimensional case. In this vein, with k parameters, T^{k-1} directional vectors are required to sample the hypercube with the same coverage as the lower dimensional scenarios. Clearly, computations rapidly become intractable with increasing parameter dimensionality. In large models with many parameters, computing confidence regions or fungible parameter contours for the full set of parameters is not feasible. As a workaround, the dimensionality of the parameter space may be reduced to a few key or focal parameters $\boldsymbol{\theta}_f$. Here, the non-focal parameters or nuisance parameters $\boldsymbol{\theta}_n$ may

90

be taken account of by the empirical or profile likelihood methods.

When the computational procedure is applied to compute confidence regions and fungible parameter contours from the empirical likelihood, the ML estimates of the nuisance parameters $\hat{\boldsymbol{\theta}}_n$ obtained jointly with the focal parameters $\hat{\boldsymbol{\theta}}_f$ are substituted for every boundary point of the confidence region or fungible parameter value. Under the profile likelihood approach, however, the uncertainty of the nuisance parameters as well as their correlations with the focal parameters are taken account of. Here, the nuisance parameters $\boldsymbol{\theta}_n$ are re-estimated to obtain $\tilde{\boldsymbol{\theta}}_n$ for every focal parameter value of the confidence bound or fungible parameter contour.

This difference in the treatment of nuisance parameters between the empirical and profile likelihoods manifests in the computational time required to obtain estimates of parameter uncertainty. Suppose that T directional vectors are employed to adequately span the parameter space so as to construct confidence regions and fungible parameter contours. In general, computations based on the profile likelihood take at least T times as long as computations based on the empirical likelihood. The empirical likelihood approach requires only a single optimization to obtain parameter estimates for the nuisance parameters whereas at least T such optimizations are required by the profile likelihood method. Beyond this difference in computational efficiency, there are also important practical differences between estimates of parameter uncertainty based on the empirical versus the profile likelihood.

4.3.1 Empirical Likelihood

In general, the observed empirical likelihood surface seems to be consistently steeper and more elliptical compared to the observed profile likelihood, as manifest in the two kinds of parameter uncertainty. Therefore, as expected, computations of parameter uncertainty based on the empirical likelihood tend to communicate overly optimistic parameter uncertainty. Compared to profile likelihood-based estimates, es-

timated likelihood-based confidence regions tend to be tighter. Such tighter than optimal confidence regions would be associated with an overly liberal test or an inflated α error rate. Additionally, such confidence regions would erroneously convey overly optimistic precision, cross-validity and generalizability of the focal parameter estimates. Under the empirical likelihood, fungible parameter contours would similarly be smaller than optimal. Therefore, these fungible contours would falsely imply that the model description of the data is overly robust to a small perturbation to model fit. In sum, when the two kinds of parameter uncertainty are based on the empirical likelihood, they tend to convey less uncertainty than is actually present.

4.3.2 Profile Likelihood

Unlike empirical likelihood-based computations, the profile likelihood takes into account the uncertainty of the nuisance parameters as well as the correlations among the nuisance and focal parameters by re-estimating $\boldsymbol{\theta}_n$ for every confidence region boundary point or fungible value of the focal parameters. As such, compared to the empirical likelihood, computations based on the profile likelihood more completely communicate the two kinds of parameter uncertainty at the cost of computational time. For a small number of focal parameters and a large number of nuisance parameters, computing confidence regions and fungible parameter contours from the profile likelihood are computationally tractable. Therefore, we recommend obtaining confidence regions and fungible parameter contours from the profile likelihood over the empirical likelihood in general.

4.4 Study Contributions

The theoretical contribution of the study rests on the development of the general perturbation framework, which unifies confidence regions and fungible parameter contours under a single framework. With such a unification, we have shown how con-

fidence regions and fungible parameter contours are analytically related, even though they represent distinct aspects of parameter uncertainty. Additionally, the general perturbation framework allows for the computation of both kinds of parameter uncertainty from the same algorithm. Further, our simulation results confirmed the distinction between confidence regions and fungible parameter contours. Although both kinds of parameter uncertainty were affected by the magnitude of correlations among the MVs, confidence regions were primarily influenced by sample size whereas fungible parameter contours were influenced primarily by model fit and, to a lesser extent, sample size.

Based on the general perturbation framework, we have extended the computation of parameter uncertainty estimates to include confidence regions in addition to fungible parameter contours. Importantly, we have implemented a new algorithm based on the profile likelihood, which has the advantage over the existing empirical likelihood method (MacCallum, Browne & Lee, 2009) of taking account of the uncertainty inherent in the nuisance parameters. This new computational procedure therefore communicates parameter uncertainty more completely than the existing procedure. Additionally, confidence regions and fungible parameter contours, based on the profile likelihood, may be obtained for more than one focal parameter in the presence of many nuisance parameters.

Although we have clarified the distinction between confidence regions and fungible parameter contours, as well as provided an improved method of computing them, there remain several areas that merit further study.

4.5   Future Directions

To better understand the nature of confidence regions and fungible parameter contours, other factors that affect them beyond sample size, model fit, and the magnitude of correlations among MVs may be explored. These factors are the number of pa-

rameters in the model and the types of parameters in the model. Specifically, the two kinds of parameter uncertainty may be influenced by how many focal versus nuisance parameters are specified in the model. Additionally, whether focal and/or nuisance parameters are means, variances, intercepts or residuals may play a role in changing the size and shape of confidence regions and fungible parameter contours.

The "perturbation" applied as a first step to compute confidence regions is fixed. However, the perturbation used to obtain fungible parameter contours remains a subjective choice. Importantly, the perturbation associated with fungible parameter contours determines how these fungible contours are interpreted. Although we have used two different perturbation schemes, there exist many other types of perturbation schemes for the construction of fungible parameter contours. For future study, other types of perturbations to model fit may be explored. For example, perturbations based on the Tucker-Lewis Index (TLI; Tucker & Lewis, 1973), or information criteria such as the Akaike Information Criteria (AIC; Akaike, 1973) or the Bayes Information Criteria (BIC; Schwartz, 1978) may be considered.

In terms of computations, confidence regions and fungible parameter contours based on the profile likelihood are preferable over the empirical likelihood; the former incorporates more information about the nuisance parameters compared to the latter. However, the profile likelihood remains to be evaluated on how well it takes account of the set of nuisance parameters. In particular, confidence regions and fungible parameter contours based on the profile likelihood should be examined against confidence regions and fungible parameter contours computed for all model parameters jointly. Such an evaluation would clarify what limitations are inherent in the profile likelihood method to reducing the dimensionality of the parameter space to focal parameters.

4.6 Conclusion

Confidence regions and fungible parameter contours are distinct kinds of parameter uncertainty that provide useful and unique information to the analyst. Confidence regions are an inferential device and convey information that is strictly tied to sampling variability. As one type of parameter uncertainty, confidence regions inform analysts of the statistical significance of parameter estimates, the accuracy of these estimates, as well as how well these estimates generalize to the population and cross-validate to a similar sample. Beyond confidence regions, fungible parameter contours convey parameter uncertainty with respect to model fit. Hence, what is gained from computing fungible parameter contours is a quantification of how robust or sensitive the model description is of the data under a perturbation to model fit. Both kinds of parameter uncertainty therefore provide distinctive information that have the potential to buttress the case for strong scientific conclusions.

The population covariance matrices without model error ($\epsilon = 0$) are presented in the lower triangular matrix, the variances are bold in the matrix diagonal and the population correlation matrices are presented in the upper diagonal (in italics) for the conditions of (a) small unique variances and large structural effects ($\mathbf{\Psi}_H \mathbf{B}_L$), (b) large unique variances and large structural effects ($\mathbf{\Psi}_L \mathbf{B}_H$) and (c) small unique variances and large structural effects ($\mathbf{\Psi}_H \mathbf{B}_H$). Recall that the subscript 0 denotes exact model fit. The covariance and correlation matrix for small unique variances and small structural effects has been presented in the text.

The population covariance and correlation matrix associated with small unique variances and small effect sizes with perfect model fit is

$$\mathbf{\Sigma}_{\mathbf{\Psi}_H \mathbf{B}_L 0} \text{ and } \mathbf{P}_{\mathbf{\Psi}_H \mathbf{B}_L 0} =$$

$$
\begin{pmatrix}
\mathbf{0.75} & 0.87 & 0.86 & 0.86 & 0.18 & 0.18 & 0.18 & 0.18 & 0.20 & 0.20 & 0.20 & 0.20 & 0.20 \\
0.65 & \mathbf{0.76} & 0.86 & 0.86 & 0.18 & 0.18 & 0.18 & 0.18 & 0.20 & 0.20 & 0.20 & 0.20 & 0.20 \\
0.65 & 0.65 & \mathbf{0.76} & 0.86 & 0.18 & 0.18 & 0.17 & 0.17 & 0.20 & 0.20 & 0.20 & 0.20 & 0.20 \\
0.65 & 0.65 & 0.65 & \mathbf{0.76} & 0.18 & 0.17 & 0.17 & 0.17 & 0.20 & 0.20 & 0.20 & 0.20 & 0.20 \\
0.14 & 0.14 & 0.14 & 0.14 & \mathbf{0.78} & 0.87 & 0.87 & 0.86 & 0.20 & 0.20 & 0.20 & 0.20 & 0.21 \\
0.14 & 0.14 & 0.13 & 0.14 & 0.68 & \mathbf{0.78} & 0.87 & 0.86 & 0.20 & 0.20 & 0.20 & 0.20 & 0.20 \\
0.13 & 0.14 & 0.13 & 0.13 & 0.68 & 0.68 & \mathbf{0.78} & 0.86 & 0.20 & 0.20 & 0.20 & 0.20 & 0.20 \\
0.13 & 0.13 & 0.13 & 0.13 & 0.68 & 0.68 & 0.67 & \mathbf{0.78} & 0.20 & 0.20 & 0.20 & 0.20 & 0.20 \\
0.16 & 0.16 & 0.16 & 0.16 & 0.16 & 0.16 & 0.16 & 0.16 & \mathbf{0.81} & 0.87 & 0.87 & 0.87 & 0.87 \\
0.16 & 0.16 & 0.16 & 0.16 & 0.16 & 0.16 & 0.16 & 0.16 & 0.71 & \mathbf{0.82} & 0.87 & 0.87 & 0.87 \\
0.16 & 0.16 & 0.16 & 0.16 & 0.16 & 0.16 & 0.16 & 0.16 & 0.70 & 0.71 & \mathbf{0.81} & 0.87 & 0.87 \\
0.16 & 0.16 & 0.16 & 0.16 & 0.16 & 0.16 & 0.16 & 0.16 & 0.71 & 0.71 & 0.71 & \mathbf{0.82} & 0.87 \\
0.16 & 0.16 & 0.16 & 0.16 & 0.16 & 0.16 & 0.16 & 0.16 & 0.71 & 0.71 & 0.71 & 0.72 & \mathbf{0.81}
\end{pmatrix}
$$

The population covariance and correlation matrix associated with large unique variances and large effect sizes with perfect model fit is

$\Sigma_{\Psi_L \mathbf{B}_H 0}$ and $\mathbf{P}_{\Psi_L \mathbf{B}_H 0} =$

$$
\begin{pmatrix}
\mathbf{1.15} & 0.57 & 0.56 & 0.56 & 0.31 & 0.31 & 0.31 & 0.31 & 0.41 & 0.41 & 0.41 & 0.42 & 0.42 \\
0.65 & \mathbf{1.16} & 0.56 & 0.56 & 0.31 & 0.31 & 0.31 & 0.31 & 0.41 & 0.41 & 0.41 & 0.42 & 0.42 \\
0.65 & 0.65 & \mathbf{1.16} & 0.56 & 0.31 & 0.31 & 0.31 & 0.31 & 0.41 & 0.41 & 0.41 & 0.41 & 0.41 \\
0.65 & 0.65 & 0.65 & \mathbf{1.16} & 0.31 & 0.31 & 0.31 & 0.31 & 0.41 & 0.41 & 0.41 & 0.41 & 0.41 \\
0.40 & 0.40 & 0.40 & 0.40 & \mathbf{1.40} & 0.64 & 0.64 & 0.64 & 0.46 & 0.46 & 0.46 & 0.46 & 0.46 \\
0.40 & 0.40 & 0.39 & 0.40 & 0.89 & \mathbf{1.40} & 0.64 & 0.64 & 0.46 & 0.46 & 0.46 & 0.46 & 0.46 \\
0.39 & 0.40 & 0.39 & 0.39 & 0.89 & 0.89 & \mathbf{1.39} & 0.63 & 0.46 & 0.46 & 0.46 & 0.46 & 0.46 \\
0.39 & 0.39 & 0.39 & 0.39 & 0.89 & 0.89 & 0.88 & \mathbf{1.39} & 0.46 & 0.46 & 0.46 & 0.46 & 0.46 \\
0.63 & 0.63 & 0.62 & 0.62 & 0.77 & 0.77 & 0.77 & 0.76 & \mathbf{1.98} & 0.74 & 0.74 & 0.75 & 0.75 \\
0.63 & 0.63 & 0.63 & 0.63 & 0.77 & 0.77 & 0.77 & 0.77 & 1.48 & \mathbf{2.00} & 0.74 & 0.75 & 0.75 \\
0.62 & 0.63 & 0.62 & 0.62 & 0.77 & 0.77 & 0.76 & 0.76 & 1.47 & 1.48 & \mathbf{1.98} & 0.75 & 0.75 \\
0.63 & 0.63 & 0.63 & 0.63 & 0.78 & 0.78 & 0.77 & 0.77 & 1.49 & 1.49 & 1.49 & \mathbf{2.00} & 0.75 \\
0.63 & 0.63 & 0.63 & 0.63 & 0.77 & 0.77 & 0.77 & 0.77 & 1.48 & 1.49 & 1.48 & 1.50 & \mathbf{1.99}
\end{pmatrix}
$$

The population covariance and correlation matrix associated with small unique variances and small effect sizes with perfect model fit is

$\mathbf{\Sigma_{\Psi_H B_H 0}}$ and $\mathbf{P_{\Psi_H B_H 0}} =$

$$
\begin{pmatrix}
\mathbf{0.75} & 0.87 & 0.86 & 0.86 & 0.46 & 0.46 & 0.46 & 0.46 & 0.57 & 0.57 & 0.57 & 0.57 & 0.57 \\
0.65 & \mathbf{0.76} & 0.86 & 0.86 & 0.46 & 0.46 & 0.46 & 0.46 & 0.57 & 0.57 & 0.57 & 0.57 & 0.57 \\
0.65 & 0.65 & \mathbf{0.76} & 0.86 & 0.46 & 0.45 & 0.45 & 0.45 & 0.57 & 0.57 & 0.57 & 0.57 & 0.57 \\
0.65 & 0.65 & 0.65 & \mathbf{0.76} & 0.45 & 0.45 & 0.45 & 0.45 & 0.57 & 0.57 & 0.57 & 0.57 & 0.57 \\
0.40 & 0.40 & 0.40 & 0.40 & \mathbf{1.00} & 0.90 & 0.90 & 0.89 & 0.61 & 0.61 & 0.61 & 0.61 & 0.61 \\
0.40 & 0.40 & 0.39 & 0.40 & 0.89 & \mathbf{1.00} & 0.89 & 0.89 & 0.61 & 0.61 & 0.61 & 0.61 & 0.61 \\
0.39 & 0.40 & 0.39 & 0.39 & 0.89 & 0.89 & \mathbf{0.99} & 0.89 & 0.61 & 0.61 & 0.61 & 0.61 & 0.61 \\
0.39 & 0.39 & 0.39 & 0.39 & 0.89 & 0.89 & 0.88 & \mathbf{0.99} & 0.61 & 0.61 & 0.61 & 0.61 & 0.61 \\
0.63 & 0.63 & 0.62 & 0.62 & 0.77 & 0.77 & 0.77 & 0.76 & \mathbf{1.58} & 0.93 & 0.93 & 0.93 & 0.94 \\
0.63 & 0.63 & 0.63 & 0.63 & 0.77 & 0.77 & 0.77 & 0.77 & 1.48 & \mathbf{1.60} & 0.93 & 0.93 & 0.93 \\
0.62 & 0.63 & 0.62 & 0.62 & 0.77 & 0.77 & 0.76 & 0.76 & 1.47 & 1.48 & \mathbf{1.58} & 0.93 & 0.93 \\
0.63 & 0.63 & 0.63 & 0.63 & 0.78 & 0.78 & 0.77 & 0.77 & 1.49 & 1.49 & 1.49 & \mathbf{1.60} & 0.94 \\
0.63 & 0.63 & 0.63 & 0.63 & 0.77 & 0.77 & 0.77 & 0.77 & 1.48 & 1.49 & 1.48 & 1.50 & \mathbf{1.59}
\end{pmatrix}
$$

APPENDIX B

The population covariance matrices with model error are presented in the lower triangular matrix, the variances are bold in the matrix diagonal and the population correlation matrices are presented in the upper diagonal (in italics) for the four study conditions. Note that large and small unique variances are denoted by $\mathbf{\Psi}_L$ and $\mathbf{\Psi}_H$, respectively, while small and large structural effects are denoted by $\mathbf{B}_L$ and $\mathbf{B}_H$. Recall that model error was added to the population covariances in Appendix A via the Cudeck and Browne (1992) method and the subscripts G and P denote good ($\epsilon = 0.03$) and poor ($\epsilon = 0.09$) model fit respectively.

The population covariance and correlation matrix associated with large unique variances and small effect sizes with poor model fit is

$\mathbf{\Sigma}_{\mathbf{\Psi}_L \mathbf{B}_L P}$ and $\mathbf{P}_{\mathbf{\Psi}_L \mathbf{B}_L P} =$

$$
\begin{pmatrix}
\mathbf{1.15} & 0.61 & 0.52 & 0.55 & 0.12 & 0.10 & 0.18 & 0.12 & 0.12 & 0.13 & 0.17 & 0.14 & 0.18 \\
0.71 & \mathbf{1.16} & 0.56 & 0.52 & 0.15 & 0.15 & 0.10 & 0.07 & 0.08 & 0.11 & 0.15 & 0.10 & 0.14 \\
0.60 & 0.65 & \mathbf{1.16} & 0.61 & 0.09 & 0.11 & 0.03 & 0.08 & 0.07 & 0.11 & 0.17 & 0.04 & 0.07 \\
0.63 & 0.60 & 0.71 & \mathbf{1.16} & 0.17 & 0.06 & 0.10 & 0.21 & 0.16 & 0.19 & 0.22 & 0.13 & 0.17 \\
0.15 & 0.18 & 0.11 & 0.20 & \mathbf{1.18} & 0.61 & 0.59 & 0.52 & 0.08 & 0.23 & 0.26 & 0.10 & 0.14 \\
0.12 & 0.17 & 0.13 & 0.07 & 0.72 & \mathbf{1.18} & 0.54 & 0.58 & 0.07 & 0.12 & 0.15 & 0.09 & 0.13 \\
0.21 & 0.11 & 0.03 & 0.12 & 0.69 & 0.63 & \mathbf{1.18} & 0.60 & 0.13 & 0.12 & 0.09 & 0.06 & 0.07 \\
0.15 & 0.08 & 0.10 & 0.24 & 0.62 & 0.69 & 0.71 & \mathbf{1.18} & 0.14 & 0.19 & 0.19 & 0.11 & 0.25 \\
0.14 & 0.10 & 0.08 & 0.20 & 0.10 & 0.08 & 0.16 & 0.16 & \mathbf{1.21} & 0.56 & 0.61 & 0.63 & 0.55 \\
0.16 & 0.13 & 0.13 & 0.23 & 0.28 & 0.15 & 0.14 & 0.23 & 0.68 & \mathbf{1.22} & 0.60 & 0.55 & 0.62 \\
0.20 & 0.17 & 0.20 & 0.26 & 0.31 & 0.18 & 0.10 & 0.23 & 0.73 & 0.73 & \mathbf{1.21} & 0.57 & 0.55 \\
0.17 & 0.12 & 0.05 & 0.16 & 0.12 & 0.11 & 0.07 & 0.14 & 0.76 & 0.67 & 0.69 & \mathbf{1.22} & 0.61 \\
0.21 & 0.17 & 0.09 & 0.20 & 0.17 & 0.15 & 0.09 & 0.30 & 0.67 & 0.76 & 0.67 & 0.74 & \mathbf{1.21}
\end{pmatrix}
$$

The population covariance and correlation matrix associated with small unique variances and small effect sizes with good model fit is

$\boldsymbol{\Sigma}_{\boldsymbol{\Psi}_H \mathbf{B}_L G}$ and $\mathbf{P}_{\boldsymbol{\Psi}_H \mathbf{B}_L G} =$

$$
\begin{pmatrix}
\mathbf{0.75} & 0.87 & 0.86 & 0.86 & 0.16 & 0.16 & 0.17 & 0.18 & 0.19 & 0.20 & 0.20 & 0.19 & 0.19 \\
0.66 & \mathbf{0.76} & 0.86 & 0.86 & 0.17 & 0.17 & 0.17 & 0.17 & 0.19 & 0.20 & 0.20 & 0.19 & 0.19 \\
0.65 & 0.65 & \mathbf{0.76} & 0.86 & 0.17 & 0.18 & 0.17 & 0.18 & 0.20 & 0.21 & 0.21 & 0.20 & 0.19 \\
0.65 & 0.65 & 0.65 & \mathbf{0.76} & 0.19 & 0.18 & 0.18 & 0.20 & 0.21 & 0.22 & 0.22 & 0.21 & 0.21 \\
0.13 & 0.13 & 0.13 & 0.14 & \mathbf{0.78} & 0.87 & 0.87 & 0.86 & 0.19 & 0.22 & 0.21 & 0.20 & 0.19 \\
0.13 & 0.13 & 0.14 & 0.14 & 0.68 & \mathbf{0.78} & 0.86 & 0.86 & 0.19 & 0.21 & 0.21 & 0.20 & 0.19 \\
0.13 & 0.13 & 0.13 & 0.14 & 0.68 & 0.67 & \mathbf{0.78} & 0.87 & 0.20 & 0.21 & 0.20 & 0.20 & 0.19 \\
0.13 & 0.13 & 0.14 & 0.16 & 0.67 & 0.68 & 0.67 & \mathbf{0.78} & 0.21 & 0.22 & 0.22 & 0.21 & 0.22 \\
0.15 & 0.15 & 0.16 & 0.17 & 0.15 & 0.16 & 0.16 & 0.17 & \mathbf{0.81} & 0.87 & 0.87 & 0.88 & 0.87 \\
0.16 & 0.16 & 0.17 & 0.18 & 0.17 & 0.17 & 0.17 & 0.18 & 0.71 & \mathbf{0.82} & 0.87 & 0.87 & 0.87 \\
0.16 & 0.16 & 0.17 & 0.17 & 0.17 & 0.17 & 0.16 & 0.17 & 0.71 & 0.71 & \mathbf{0.81} & 0.87 & 0.87 \\
0.15 & 0.15 & 0.16 & 0.17 & 0.16 & 0.16 & 0.16 & 0.17 & 0.71 & 0.71 & 0.71 & \mathbf{0.82} & 0.88 \\
0.15 & 0.15 & 0.15 & 0.16 & 0.15 & 0.16 & 0.15 & 0.17 & 0.71 & 0.72 & 0.71 & 0.72 & \mathbf{0.81}
\end{pmatrix}
$$

The population covariance and correlation matrix associated with small unique variances and small effect sizes with poor model fit is

$\mathbf{\Sigma}_{\mathbf{\Psi}_H \mathbf{B}_L P}$ and $\mathbf{P}_{\mathbf{\Psi}_H \mathbf{B}_L P} =$

$$
\begin{pmatrix}
\mathbf{0.75} & 0.88 & 0.85 & 0.86 & 0.14 & 0.14 & 0.17 & 0.18 & 0.17 & 0.20 & 0.20 & 0.18 & 0.17 \\
0.67 & \mathbf{0.76} & 0.86 & 0.85 & 0.15 & 0.16 & 0.15 & 0.16 & 0.16 & 0.20 & 0.19 & 0.17 & 0.16 \\
0.64 & 0.65 & \mathbf{0.76} & 0.87 & 0.17 & 0.19 & 0.17 & 0.20 & 0.20 & 0.23 & 0.24 & 0.19 & 0.18 \\
0.65 & 0.64 & 0.66 & \mathbf{0.76} & 0.21 & 0.18 & 0.20 & 0.26 & 0.24 & 0.27 & 0.27 & 0.23 & 0.22 \\
0.11 & 0.11 & 0.13 & 0.16 & \mathbf{0.78} & 0.88 & 0.87 & 0.85 & 0.17 & 0.24 & 0.23 & 0.18 & 0.17 \\
0.11 & 0.12 & 0.15 & 0.14 & 0.69 & \mathbf{0.78} & 0.85 & 0.87 & 0.18 & 0.22 & 0.21 & 0.19 & 0.17 \\
0.13 & 0.11 & 0.13 & 0.16 & 0.68 & 0.67 & \mathbf{0.78} & 0.87 & 0.20 & 0.22 & 0.20 & 0.18 & 0.16 \\
0.13 & 0.12 & 0.16 & 0.20 & 0.67 & 0.68 & 0.68 & \mathbf{0.78} & 0.22 & 0.26 & 0.25 & 0.22 & 0.24 \\
0.13 & 0.13 & 0.15 & 0.19 & 0.13 & 0.14 & 0.16 & 0.18 & \mathbf{0.81} & 0.86 & 0.88 & 0.88 & 0.86 \\
0.16 & 0.15 & 0.19 & 0.21 & 0.20 & 0.18 & 0.18 & 0.21 & 0.70 & \mathbf{0.82} & 0.87 & 0.86 & 0.88 \\
0.15 & 0.15 & 0.19 & 0.21 & 0.19 & 0.17 & 0.16 & 0.20 & 0.71 & 0.71 & \mathbf{0.81} & 0.86 & 0.86 \\
0.14 & 0.13 & 0.15 & 0.18 & 0.14 & 0.15 & 0.14 & 0.17 & 0.72 & 0.71 & 0.71 & \mathbf{0.82} & 0.88 \\
0.13 & 0.12 & 0.14 & 0.17 & 0.13 & 0.14 & 0.13 & 0.19 & 0.70 & 0.72 & 0.70 & 0.72 & \mathbf{0.81}
\end{pmatrix}
$$

The population covariance and correlation matrix associated with large unique variances and large effect sizes with good model fit is

$\mathbf{\Sigma}_{\mathbf{\Psi}_L \mathbf{B}_H G}$ and $\mathbf{P}_{\mathbf{\Psi}_L \mathbf{B}_H G} =$

$$
\begin{pmatrix}
\mathbf{1.15} & 0.58 & 0.55 & 0.55 & 0.31 & 0.31 & 0.33 & 0.31 & 0.41 & 0.41 & 0.42 & 0.42 & 0.43 \\
0.67 & \mathbf{1.16} & 0.57 & 0.55 & 0.32 & 0.32 & 0.31 & 0.30 & 0.40 & 0.41 & 0.42 & 0.41 & 0.42 \\
0.64 & 0.65 & \mathbf{1.16} & 0.58 & 0.30 & 0.31 & 0.28 & 0.30 & 0.40 & 0.41 & 0.42 & 0.39 & 0.40 \\
0.64 & 0.63 & 0.67 & \mathbf{1.16} & 0.33 & 0.29 & 0.31 & 0.34 & 0.42 & 0.43 & 0.43 & 0.41 & 0.42 \\
0.40 & 0.41 & 0.39 & 0.42 & \mathbf{1.40} & 0.65 & 0.64 & 0.62 & 0.45 & 0.49 & 0.49 & 0.45 & 0.47 \\
0.39 & 0.41 & 0.40 & 0.37 & 0.91 & \mathbf{1.40} & 0.63 & 0.64 & 0.45 & 0.46 & 0.47 & 0.45 & 0.46 \\
0.42 & 0.39 & 0.36 & 0.39 & 0.90 & 0.88 & \mathbf{1.39} & 0.64 & 0.46 & 0.46 & 0.45 & 0.45 & 0.45 \\
0.40 & 0.38 & 0.38 & 0.43 & 0.86 & 0.89 & 0.90 & \mathbf{1.39} & 0.46 & 0.47 & 0.47 & 0.46 & 0.49 \\
0.62 & 0.61 & 0.60 & 0.64 & 0.75 & 0.74 & 0.76 & 0.76 & \mathbf{1.98} & 0.74 & 0.75 & 0.76 & 0.74 \\
0.63 & 0.62 & 0.62 & 0.65 & 0.81 & 0.77 & 0.76 & 0.79 & 1.47 & \mathbf{2.00} & 0.75 & 0.74 & 0.75 \\
0.64 & 0.63 & 0.64 & 0.66 & 0.82 & 0.78 & 0.75 & 0.79 & 1.48 & 1.48 & \mathbf{1.98} & 0.74 & 0.74 \\
0.64 & 0.62 & 0.59 & 0.63 & 0.76 & 0.76 & 0.74 & 0.76 & 1.51 & 1.48 & 1.48 & \mathbf{2.00} & 0.75 \\
0.65 & 0.63 & 0.60 & 0.64 & 0.78 & 0.77 & 0.75 & 0.81 & 1.47 & 1.50 & 1.47 & 1.51 & \mathbf{1.99}
\end{pmatrix}
$$

The population covariance and correlation matrix associated with large unique variances and large effect sizes with poor model fit is

$\mathbf{\Sigma}_{\Psi_L \mathbf{B}_H P}$ and $\mathbf{P}_{\Psi_L \mathbf{B}_H P} =$

$$
\begin{pmatrix}
\textbf{1.15} & 0.61 & 0.53 & 0.54 & 0.32 & 0.30 & 0.37 & 0.32 & 0.41 & 0.42 & 0.44 & 0.43 & 0.45 \\
0.71 & \textbf{1.16} & 0.57 & 0.52 & 0.34 & 0.34 & 0.30 & 0.27 & 0.37 & 0.40 & 0.42 & 0.39 & 0.42 \\
0.61 & 0.66 & \textbf{1.16} & 0.61 & 0.29 & 0.31 & 0.23 & 0.28 & 0.36 & 0.40 & 0.44 & 0.35 & 0.37 \\
0.62 & 0.60 & 0.71 & \textbf{1.16} & 0.36 & 0.26 & 0.30 & 0.39 & 0.43 & 0.45 & 0.48 & 0.41 & 0.44 \\
0.41 & 0.44 & 0.37 & 0.46 & \textbf{1.40} & 0.66 & 0.65 & 0.59 & 0.42 & 0.53 & 0.55 & 0.43 & 0.47 \\
0.38 & 0.43 & 0.40 & 0.33 & 0.93 & \textbf{1.40} & 0.61 & 0.64 & 0.41 & 0.45 & 0.47 & 0.43 & 0.46 \\
0.47 & 0.37 & 0.29 & 0.38 & 0.91 & 0.86 & \textbf{1.39} & 0.66 & 0.46 & 0.45 & 0.43 & 0.41 & 0.42 \\
0.40 & 0.34 & 0.36 & 0.50 & 0.82 & 0.90 & 0.92 & \textbf{1.39} & 0.46 & 0.50 & 0.50 & 0.45 & 0.54 \\
0.61 & 0.56 & 0.55 & 0.66 & 0.70 & 0.69 & 0.76 & 0.76 & \textbf{1.98} & 0.73 & 0.76 & 0.78 & 0.73 \\
0.63 & 0.60 & 0.60 & 0.69 & 0.89 & 0.76 & 0.75 & 0.83 & 1.45 & \textbf{2.00} & 0.75 & 0.73 & 0.77 \\
0.67 & 0.64 & 0.67 & 0.72 & 0.91 & 0.79 & 0.71 & 0.83 & 1.50 & 1.49 & \textbf{1.98} & 0.73 & 0.72 \\
0.65 & 0.60 & 0.53 & 0.63 & 0.73 & 0.73 & 0.69 & 0.74 & 1.55 & 1.46 & 1.46 & \textbf{2.00} & 0.76 \\
0.68 & 0.64 & 0.56 & 0.66 & 0.78 & 0.76 & 0.70 & 0.90 & 1.45 & 1.53 & 1.44 & 1.52 & \textbf{1.99} \\
\end{pmatrix}
$$

The population covariance and correlation matrix associated with small unique variances and large effect sizes with good model fit is

$\mathbf{\Sigma_{\Psi_H B_H G}}$ and $\mathbf{P_{\Psi_H B_H G}} =$

$$
\begin{pmatrix}
\mathbf{0.75} & 0.87 & 0.86 & 0.86 & 0.45 & 0.45 & 0.46 & 0.46 & 0.57 & 0.57 & 0.57 & 0.57 & 0.57 \\
0.66 & \mathbf{0.76} & 0.86 & 0.86 & 0.45 & 0.45 & 0.45 & 0.45 & 0.56 & 0.57 & 0.57 & 0.57 & 0.56 \\
0.65 & 0.65 & \mathbf{0.76} & 0.86 & 0.45 & 0.46 & 0.45 & 0.46 & 0.57 & 0.58 & 0.58 & 0.57 & 0.57 \\
0.65 & 0.65 & 0.65 & \mathbf{0.76} & 0.46 & 0.46 & 0.46 & 0.48 & 0.58 & 0.59 & 0.59 & 0.58 & 0.58 \\
0.39 & 0.39 & 0.39 & 0.40 & \mathbf{1.00} & 0.90 & 0.90 & 0.89 & 0.61 & 0.62 & 0.62 & 0.61 & 0.61 \\
0.39 & 0.39 & 0.40 & 0.40 & 0.90 & \mathbf{1.00} & 0.89 & 0.89 & 0.61 & 0.62 & 0.61 & 0.61 & 0.61 \\
0.39 & 0.39 & 0.39 & 0.40 & 0.89 & 0.89 & \mathbf{0.99} & 0.89 & 0.61 & 0.61 & 0.61 & 0.61 & 0.60 \\
0.39 & 0.39 & 0.40 & 0.41 & 0.88 & 0.89 & 0.88 & \mathbf{0.99} & 0.61 & 0.62 & 0.62 & 0.61 & 0.62 \\
0.62 & 0.62 & 0.62 & 0.63 & 0.76 & 0.76 & 0.76 & 0.77 & \mathbf{1.58} & 0.93 & 0.93 & 0.94 & 0.93 \\
0.63 & 0.63 & 0.64 & 0.65 & 0.78 & 0.78 & 0.77 & 0.78 & 1.48 & \mathbf{1.60} & 0.93 & 0.93 & 0.94 \\
0.62 & 0.62 & 0.63 & 0.64 & 0.78 & 0.77 & 0.76 & 0.78 & 1.47 & 1.48 & \mathbf{1.58} & 0.93 & 0.93 \\
0.62 & 0.62 & 0.63 & 0.64 & 0.77 & 0.77 & 0.77 & 0.77 & 1.49 & 1.49 & 1.48 & \mathbf{1.60} & 0.94 \\
0.62 & 0.62 & 0.62 & 0.63 & 0.76 & 0.77 & 0.76 & 0.78 & 1.48 & 1.49 & 1.48 & 1.50 & \mathbf{1.59}
\end{pmatrix}
$$

Finally, the population covariance and correlation matrix associated with small unique variances and large effect sizes with poor model fit is

$\Sigma_{\Psi_H \mathbf{B}_H P}$ and $\mathbf{P}_{\Psi_H \mathbf{B}_H P} =$

$$
\begin{pmatrix}
\mathbf{0.75} & 0.89 & 0.85 & 0.86 & 0.42 & 0.43 & 0.45 & 0.46 & 0.55 & 0.57 & 0.57 & 0.56 & 0.55 \\
0.67 & \mathbf{0.76} & 0.86 & 0.85 & 0.43 & 0.44 & 0.43 & 0.44 & 0.54 & 0.57 & 0.57 & 0.55 & 0.54 \\
0.64 & 0.65 & \mathbf{0.76} & 0.87 & 0.45 & 0.47 & 0.45 & 0.48 & 0.57 & 0.59 & 0.60 & 0.56 & 0.56 \\
0.65 & 0.64 & 0.66 & \mathbf{0.76} & 0.48 & 0.46 & 0.48 & 0.52 & 0.60 & 0.62 & 0.62 & 0.59 & 0.58 \\
0.37 & 0.38 & 0.39 & 0.42 & \mathbf{1.00} & 0.90 & 0.90 & 0.88 & 0.59 & 0.64 & 0.63 & 0.60 & 0.59 \\
0.37 & 0.38 & 0.41 & 0.40 & 0.90 & \mathbf{1.00} & 0.88 & 0.89 & 0.60 & 0.62 & 0.62 & 0.60 & 0.59 \\
0.39 & 0.37 & 0.39 & 0.41 & 0.89 & 0.88 & \mathbf{0.99} & 0.90 & 0.61 & 0.62 & 0.61 & 0.60 & 0.59 \\
0.39 & 0.38 & 0.42 & 0.45 & 0.88 & 0.89 & 0.89 & \mathbf{0.99} & 0.62 & 0.65 & 0.64 & 0.62 & 0.63 \\
0.60 & 0.60 & 0.62 & 0.65 & 0.74 & 0.75 & 0.76 & 0.78 & \mathbf{1.58} & 0.93 & 0.94 & 0.94 & 0.93 \\
0.63 & 0.63 & 0.65 & 0.68 & 0.80 & 0.78 & 0.78 & 0.81 & 1.47 & \mathbf{1.60} & 0.93 & 0.93 & 0.94 \\
0.62 & 0.62 & 0.65 & 0.67 & 0.79 & 0.78 & 0.76 & 0.80 & 1.48 & 1.48 & \mathbf{1.58} & 0.93 & 0.93 \\
0.61 & 0.61 & 0.62 & 0.65 & 0.75 & 0.76 & 0.75 & 0.78 & 1.50 & 1.48 & 1.48 & \mathbf{1.60} & 0.94 \\
0.60 & 0.60 & 0.61 & 0.64 & 0.75 & 0.75 & 0.74 & 0.79 & 1.48 & 1.50 & 1.47 & 1.50 & \mathbf{1.59}
\end{pmatrix}
$$

REFERENCES

Agresti, A. (2002). *Categorical data analysis* (2nd. ed.). Hoboken, NJ: John Wiley & Sons.

Akaike, H. (1973). Information theory and an extension of the maximum likelihood principle. In B. N. Petrov & F. Csaki (Eds.), *Proceedings of the second international symposium on information theory*, (pp. 267-281). Budapest: Akadamiai Kiado.

Bollen, K. A. (1989). *Structural equations with latent variables.* New York: John Wiley & Sons.

Brent, R. (1973) *Algorithms for minimization without derivatives.* Englewood Cliffs, NJ: Prentice-Hall.

Browne, M. W. (1984) Asymptotically distribution-free methods for the analysis of covariance structures. *British Journal of Mathematical and Statistical Psychology, 37*, 62-83.

Browne, M. W. & Arminger, G. (1995). Specification and estimation of mean- and covariance-structure models. In G. Arminger, C. C. Clogg, & M. E. Sobel (Eds.), *Handbook of statistical modeling for the social and behavioral sciences* (pp. 311-359). New York: Plenum Press.

Browne, M. W. & Cudeck, R. (1993). Alternative ways of assessing model fit. In K. A. Bollen & S. Long (Eds.), *Testing structural equation models* (pp. 131-161). Newbury Park, CA: Sage.

Browne, M. W., MacCallum, R. C. & Kim, C. T. (2002). When fit indices and residuals are incompatible. *Psychological Methods, 7*, 403-421.

Chen, F., Curran, P. J., Bollen, K. A., Kirby, J. & Paxton, P. (2008). An empirical evaluation of the use of fixed cutoff points in RMSEA test statistic in structural equation models. *Sociological Methods and Research, 36*, 462-494.

Cook, R. D. (1986). Assessment of local influence (with discussion). *Journal of the Royal Statistical Society, Series B, 48*, 133-169.

Cudeck, R. & Browne, M. W. (1992). Constructing a covariance matrix that yields a specified minimizer and a specified minimum discrepancy function value. *Psychometrika, 57*, 357-369.

Dana, J. & Dawes, R. M. (2004). The superiority of simple alternatives to regression for social science predictions. *Journal of Educational and Behavioral Statistics, 29*, 319-331.

duToit, S. H. C. & Cudeck, R. (2009). Estimation of the nonlinear random coefficient model when some random effects are separable. *Psychometrika, 74*, 65-82.

Green, B. F. (1977). Parameter sensitivity in multivariate methods. *Multivariate Behavioral Research, 12*, 263-287.

Koopman, R. F. (1988). On the sensitivity of a composite to its weights. *Psychometrika, 53*, 547-552.

MacCallum, R. C, Browne, M. W., & Lee, T. (2009). *Fungible parameter estimates in structural equation modeling.* Paper presented at the Annual Meeting of the Psychometric Society. Salishan Resort, Oregon.

Meeker, W. Q. & Escobar, L. A. (1995). Teaching about approximate confidence regions based on Maximum Likelihood Estimation. *American Statistician, 49*, 48-53.

Neale, M. C., & Miller, M. B. (1997). The use of likelihood-based confidence intervals in genetic models. *Behavior Genetics, 27*, 113-120.

Pawitan, Y. (2001). *In all likelihood: Statistical modelling and inference using likelihood.* New York: Oxford University Press.

R Development Core Team (2010). *R: A language and environment for statistical computing* [Computer software manual]. Vienna, Austria: R Foundation for Statistical Computing.

Rozeboom, W. W. (1979). Sensitivity of a linear composite of predictor items to differential item weighting. *Psychometrika, 44*, 289-296.

Schmitt, M. T., Branscombe, N. R., Kobrynowicz, D., & Owen, S. (2002). Perceiving discrimination against one's gender group has different implications for well-being in women and men. *Personality and Social Psychology Bulletin, 28*, 197-210.

Schwartz, G. (1978). Estimating the dimension of a model. *Annals of Statistics, 6*, 461-464.

Steiger, J. H., & Lind, J. C. (1980). *Statistically-based tests for the number of common factors.* Paper presented at the Annual Meeting of the Psychometric Society. Iowa City.

Stryhn, H. & Christensen, J. (2003). *Confidence intervals by the profile likelihood method, with applications in veterinary epidemiology.* Paper presented at the Proceedings of the 10th International Symposia on Veterinary Epidemiology and Economics. Vina del Mar, Chile.

Tucker, L. R., Koopman, R. F. & Linn, R. L. (1969). Evaluation of factor analytic research procedures by means of simulated correlation matrices. *Psychometrika, 34*, 421-459.

Tucker, L. R., & Lewis, C. (1973). The reliability coefficient for maximum likelihood factor analysis. *Psychometrika, 38*, 1-10.

Venzon, D. J., & Moolgavkar, S. H. (1988). A method for computing profile-likelihood-based confidence intervals. *Journal of the Royal Statistical Society, Series C, 37*, 87-94.

Wainer, H. (1976). Estimating coefficients in linear models: It don't make no nevermind. *Psychological Bulletin, 83*, 213-217.

Wainer, H. (1978). On the sensitivity of regression and regressors. *Psychological Bulletin, 85*, 267-273.

Waller, N. G. (2008). Fungible weights in multiple regression. *Psychometrika, 73*, 691-703.

Waller, N. G., & Jones, J. A. (2009). Locating the extrema of fungible regression weights. *Psychometrika, 74*, 589-602.